COMPARISON OF PHABSIM AND 2-D MODELING OF HABITAT FOR STEELHEAD AND FALL-RUN CHINOOK SALMON SPAWNING IN THE LOWER AMERICAN RIVER

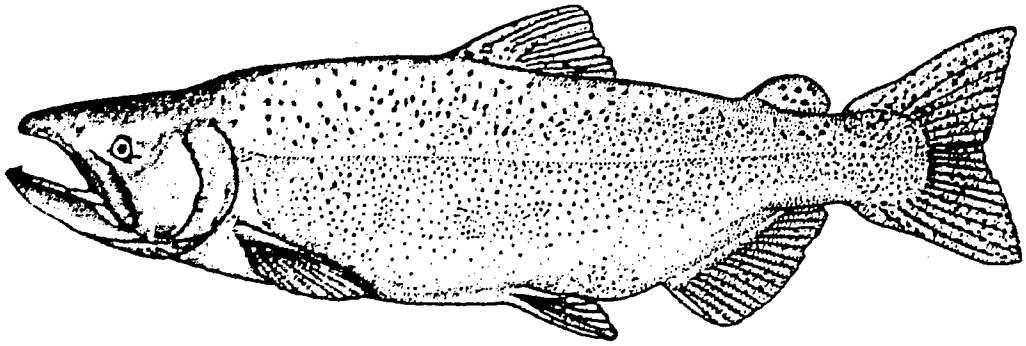

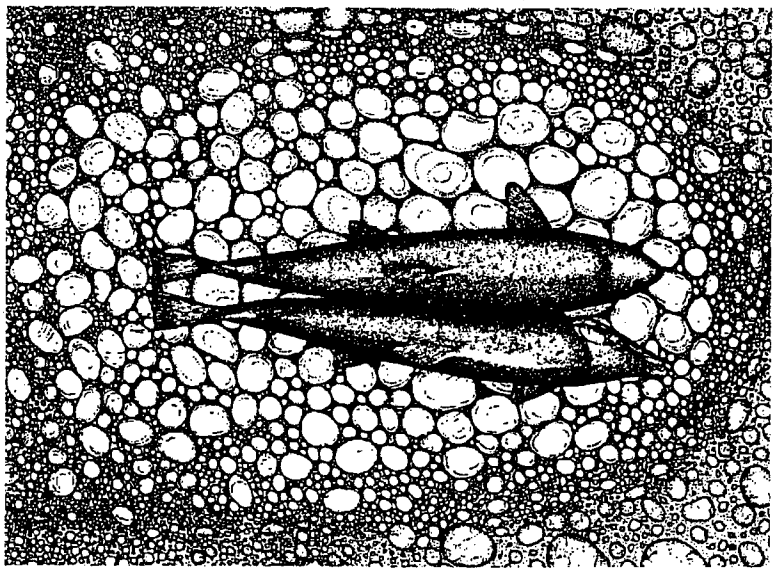

U. S. Fish and Wildlife Service
Sacramento Fish and Wildlife Office
2800 Cottage Way, Room W-2605
Sacramento, CA 95825

Prepared by staff of
The Energy Planning and Instream Flow Branch

CVPIA INSTREAM FLOW INVESTIGATIONS
LOWER AMERICAN RIVER PHABSIM AND 2-D HABITAT MODELING

PREFACE

The following is the last report for the U. S. Fish and Wildlife Service's studies on the Lower American River, part of the Central Valley Project Improvement Act (CVPIA) Instream Flow Investigations, a 7-year effort which began in February, 1995. Title 34, Section 3406(b)(1)(B) of the CVPIA, P.L. 102-575, requires the Secretary of the Interior to determine instream flow needs for anadromous fish for all Central Valley Project controlled streams and rivers, based on recommendations of the U. S. Fish and Wildlife Service after consultation with the California Department of Fish and Game (CDFG). The purpose of these investigations are to provide scientific information to the U. S. Fish and Wildlife Service Central Valley Project Improvement Act Program to be used to develop such recommendations for Central Valley rivers.

To those who are interested, comments and information regarding this report are welcomed. Written comments or information can be submitted to:

Mark Gard, Senior Biologist
Energy Planning and Instream Flow Branch
U.S. Fish and Wildlife Service
Sacramento Fish and Wildlife Office
2800 Cottage Way, Room W-2605
Sacramento, CA 95825

ACKNOWLEDGMENTS

The field work for this study was conducted by Ed Ballard, Susan Boring, Mark Gard, John Kelly, Jason Kent, Justin Ly and Rick Williams. Data analysis and report preparation were performed by Ed Ballard, Mark Gard and John Kelly. Funding was provided by the Central Valley Project Improvement Act.

INTRODUCTION

In response to substantial declines in anadromous fish populations, the Central Valley Project Improvement Act requires the doubling of the natural production of anadromous fish stocks, including the four races of chinook salmon (fall, late-fall, winter, and spring runs), steelhead, and white and green sturgeon. For the Lower American River, the Central Valley Project Improvement Act Anadromous Doubling Plan calls for October through February (during fall-run chinook salmon spawning) flows at the H Street Bridge ranging from 1750 cfs in critically dry years to 2500 cfs in wet years (U. S. Fish and Wildlife Service 1995). In December 1994, the U. S. Fish and Wildlife Service prepared a study proposal to identify the instream flow requirements for anadromous fish in certain streams within the Central Valley of California, including the Lower American River. The purpose of this study was to produce models predicting the availability of physical habitat in the Lower American River for fall-run chinook salmon and steelhead spawning over a range of stream flows.

The original study was a one year effort which culminated in a March 27, 1996 report detailing the methods and results of that effort. The 1996 report was submitted to CDFG for enclosure in their final report on the Lower American River. Subsequently, questions arose as to which of the chinook salmon spawning habitat suitability criteria (HSC) used in the March 27, 1996 report would be transferable to the Lower American River. As a result, additional field work was conducted in FY97, culminating in a supplemental report submitted to CDFG on February 11, 1997. As a result of substantial changes in the Lower American River study sites from severe storms in January 1997, a second round of habitat data collection and modeling was begun in April 1998. Five sites were re-modeled with both the Physical Habitat Simulation System (PHABSIM) and two dimensional (2-D) modeling. Data collection for this effort was completed by February 1999, with data analysis from that work resulting in this report. The results of this study are intended to support or revise the flow recommendations mentioned above.

METHODS

Background

In January 1997, 115,000 cfs flood releases were made into the Lower American River. Considerable morphological changes occurred in many areas of the river including some of the sites used in the March 1996 study. As a result of these changes, CDFG requested that we collect additional hydraulic and structural data, and develop new spawning habitat models for the river. We decided to run both PHABSIM and the 2-dimensional modeling program River2D developed at the University of Alberta, Edmonton, Alberta (Steffler and Blackburn 2001). This model is currently being used by the USGS office in Fort Collins, Colorado for habitat studies.

Models used

PHABSIM is the Physical Habitat Simulation component of the Instream Flow Incremental Methodology (IFIM). It is the collection of one dimensional hydraulic and habitat models which can be used to predict the relationship between physical habitat availability, expressed as Weighted Useable Area (WUA), and streamflow over a range of river discharges. PHABSIM extrapolates from cells on each transect to represent a length of stream. Depths are computed from a stage-discharge relationship for each transect and the bed elevation of each cell. Velocities are simulated in PHABSIM using an empirical method based on Manning's n values (computed from measured depths and velocities), depths, and a velocity adjustment factor.

Similar to one-dimensional PHABSIM, the 2-D model uses as inputs the bed topography and substrate of a site, the water surface elevation at the bottom of the site, and HSC, to predict the amount of habitat present in the site. However, the 2-D model avoids problems of transect placement, common to PHABSIM, since the entire site can be modeled. The 2-D model also has the potential to model depths and velocities in complex channels over a range of flows more accurately than PHABSIM because it takes into account upstream and downstream bed topography and bed roughness, and explicitly uses mechanistic processes (conservation of mass and momentum), rather than Manning's n and an empirical velocity adjustment factor. Other advantages of 2-D modeling are that it can explicitly handle complex habitats, including transverse flows, across-channel variation in water surface elevations, and flow contractions/expansions. The model scale of resolution can be adjusted to correspond to the scale of microhabitat use data with depths and velocities produced on a continuous basis, rather than in cells extrapolated from transects. The 2-D model does a better job of representing patchy microhabitat features, such as gravel patches. The data can be collected with a stratified sampling scheme, with higher intensity sampling in areas with more complex or more quickly varying microhabitat features, and lower intensity sampling in areas with uniformly varying bed topography and uniform substrate. Bed topography and substrate mapping data can be collected at a very low flow, with the only data needed at high flow being water surface elevations at the top and bottom of the site and flow and randomly sampled velocities for validation purposes. In addition, alternative habitat suitability criteria, such as measures of habitat diversity, can be used when coupled with additional software. In contrast, standard HSC and WUA (as used in this report) are the same for both models.

Study Site Selection

Sites were selected based on CDFG aerial photos of fall 1997 chinook salmon redds in the Lower American River. The five areas with the highest concentration of redds were chosen as sites (Table 1). Each site was evaluated based on morphological and channel characteristics which facilitate the development of reliable hydraulic models. Also noted were riverbank and floodplain characteristics (e.g. steep, heavily vegetated berms or gradually sloping cobble benches) which might affect our ability to collect the necessary data to build these models.

Table 1
Sites Selected for Modeling Chinook Salmon Spawning

Site Name	Number of PHABSIM Transects	Length of Site (ft)
Sailor Bar	4	1,553
Above Sunrise	7	2,590
Sunrise	7	3,103
El Manto	2	754
Rossmoor	7	3,442

Transect Placement

A total of 27 PHABSIM transects were placed in the five study sites in April 1998. At each site, transects were located such that they crossed the areas most heavily used by spawning fall-run chinook salmon in 1997. Transect head and tail pins were marked on each river bank above the 12,000 cfs water surface level using rebar driven into the ground and/or lag bolts placed in stumps. Survey flagging was used to mark the locations of each pin. See U. S. Fish and Wildlife Service 2000 for location of sites and transects.

The downstream-most PHABSIM transect was used as the bottom of the site, to provide water surface elevations (WSELs) as an input to the 2-D model. The upstream-most PHABSIM transect was used as the top of the site. To calibrate the 2-D model, bed roughnesses are adjusted until the WSEL at the top of the site matches the WSEL measured at the upstream-most transect. Measured WSELs at the bottom and top of the site were used to calibrate the 2-D model, while PHABSIM-simulated WSELs at the bottom of the site were used in the 2-D model for simulated flows.

Hydraulic and Structural Data Collection

Vertical benchmarks were established at each site to serve as the reference elevations to which all elevations (streambed and water surface) were tied. Vertical benchmarks consisted of lag bolts driven into trees. In addition, horizontal benchmarks (rebar driven into the ground) were established at each site to serve as reference locations to which all horizontal locations (northings and eastings) were tied.

Details on the hydraulic and structural data collection for the PHABSIM transects are given in U. S. Fish and Wildlife Service 2000.

The upstream-most and downstream-most PHABSIM transects at each site were used as the boundaries for 2-D modeling. In between these transects, the following data were collected: 1) bed elevation; 2) horizontal location (northing and easting, relative to horizontal benchmarks); and 3) substrate. These parameters were collected at sufficient points to characterize the bed topography and substrate of the site. The PHABSIM transects within the sites were used as an additional data source to characterize the bed topography and substrate of the sites.

Two techniques were used to collect the data within the site: 1) for areas that were dry or shallow (less than three feet), bed elevation and horizontal location of individual points were obtained using a total station and a stadia rod and prism, while the substrate was visually assessed at each point; and 2) in portions of the site with depths greater than three feet, a jet boat equipped with a Broad-Band Acoustic Doppler Current Profiler (ADCP), manufactured by RD Instruments, was used in concert with the total station to obtain bed elevation and horizontal location. Specifically, the ADCP was run across the channel at 50 to 150 foot intervals, with the initial and final horizontal location of each run recorded by the total station. Water surface elevations (WSELs) were measured along the longitudinal gradient of the site using differential leveling, with the longitudinal distance measured with an electronic distance meter.

Velocities at each point measured by the ADCP were used to validate the 2-D model. Velocity data collected for the PHABSIM transects were used to validate the velocities predicted for shallow areas within a site.

For the collection of substrate data on the ADCP runs, the initial and final locations of each ADCP run were located and marked with buoys using the previously measured horizontal angles and slope distances. An underwater video system and an electronic distance meter were then used to determine the substrate along the course of each run so that values could be assigned to each point collected by the ADCP. The underwater video equipment consisted of two waterproof remote cameras mounted on an aluminum frame with two 30 lb lead bombs. One camera was mounted facing forward, depressed at a 45° angle from the horizontal, and the second camera was mounted such that it faced directly down at a 90° angle from the horizontal. The camera mounted at a 45° angle was used for distinguishing changes in substrate size classes, while the camera mounted at 90° was used for assessing substrate size. The frame was attached to a cable/winch assembly, while a separate cable from the remote cameras was connected to two TV monitors on the boat. The two monitors were used by the winch operator to distinguish changes in substrate size classes and determine the substrate size. Substrates were visually assessed (using a calibrated grid[1] on the monitor connected to the 90° camera

[1] The grid was calibrated so that, when the camera frame was one foot off the bottom, the smallest grid corresponded to a two-inch substrate, the next largest grid corresponded to a four-inch substrate, etc.

for the deep water substrates) for the dominant particle size range (e.g., range of 2-4"). Table 2 gives the substrate codes and size classes used in this study. At each change in substrate size class, the distance from the start of the ADCP run was measured using the electronic distance meter. The number of data points collected for each site is given in Table 3.

Table 2
Substrate Descriptors, Codes and Initial Bed Roughness Values

Code	Type	Particle Size (inches)	Bed Roughness (m)
0.1	Sand/Silt	< 0.1	0.05
1	Small Gravel	0.1 - 1	0.1
1.2	Medium Gravel	1 - 2	0.2
1.3	Medium/Large Gravel	1 - 3	0.25
2.3	Large Gravel	2 - 3	0.3
2.4	Gravel/Cobble	2 - 4	0.4
3.4	Small Cobble	3 - 4	0.45
3.5	Small Cobble	3 - 5	0.5
4.6	Medium Cobble	4 - 6	0.65
6.8	Large Cobble	6 - 8	0.9
8	Large Cobble	8 - 12	1.25
9	Bedrock	> 12	0.05
10	Boulder	> 12	1.4

Biological Validation Data Collection

Surveys for shallow and deep fall-run chinook salmon redds were conducted December 14-17, 1998 to collect depth, velocity, and substrate data. Redds in shallow water were located on foot. All active redds (those not covered with periphyton growth) within a given site were measured. Data for shallow redds were collected from an area adjacent to the redd which was judged to have a similar depth and velocity as was present at the redd location prior to redd construction. This location was generally two to four feet upstream of the pit of the redd; however, it was sometimes necessary to make

Table 3
Number of Data points Collected for Each Site

Site	Points on Transects	Points Between Transects Collected with Total Station	Points Between Transects Collected with ADCP
Sailor Bar	293	58	466
Above Sunrise	368	232	410
Sunrise	521	368	451
El Manto	65	40	112
Rossmoor	431	411	558

measurements at a 45 degree angle upstream, to the side, or behind the pit. The data were almost always collected within six feet of the pit of the redd. Depth to the nearest 0.1 ft and average water column velocity to the nearest 0.01 ft/s were measured with a top-setting wading rod equipped with either a Marsh-McBirney^{R} model 2000 or Price AA velocity meter. Substrate was visually assessed on the same scale used in the hydraulic modeling (Table 2). Substrate embeddedness data were not collected because the substrate adjacent to all of the redds sampled was predominantly unembedded. Location of redds in deep water was accomplished using a jet boat equipped with the previously described underwater video system. When searching for redds in this manner, one conducts a series of parallel upstream runs through the site. After locating a redd in deep water, the boat was held stationary directly over the redd. Substrate size was measured using the size grid on the underwater video display monitor, while water depth and average column velocity were measured using the ADCP. Horizontal location of all redds, shallow and deep, was recorded by sighting from the total station to a stadia rod and prism. All data were entered into spreadsheets.

A total of 101 redds were sampled at the Sailor Bar site, and a total of 89 shallow redds were sampled at the Above Sunrise Site[2]. A total of 15 deep redds were observed at the Sailor Bar site. No deep water redds were observed at the Above Sunrise site. Visibility at this site was marginal (around 3 feet) during the search for deep redds, which may have affected the number of redds located. Furthermore, the surveys were conducted during the latter part of the fall-run chinook salmon spawning season. Many of the redds constructed earlier in the season were likely already recolonized with algae, making recognition difficult. Flows were relatively constant, averaging 3087 cfs ± 5%, from November 11 to December 17, 1998.

[2] Time constraints limited sampling effort to these two sites.

Hydraulic Model Construction and Calibration

Details on the hydraulic model construction and calibration of the PHABSIM transects are given in U. S. Fish and Wildlife Service 2000.

ASCII files of the raw data from each ADCP run were produced using the Playback feature of the Transect program[3]. Each raw data ASCII file was then imported into RHABSIM (Riverine Habitat Simulation) Version 2.0[4] to produce the bed elevations, average water column velocities, and stations (distance along the ADCP run). RHABSIM was then used to output a second ASCII file containing this data. The second ASCII file was input into a QuattroPro spreadsheet. We defined a statistic (R) to provide a quality control check of the velocity measured by the ADCP at a given station n, where $R = Vel_n/(Vel_{n-1} + Vel_{n+1})/2$ at station n[5]. R was calculated for each velocity where Vel_n, Vel_{n-1} and Vel_{n+1} were all greater than 1 ft/s for each ADCP data set. Based on data collected using a Price AA velocity meter during our March 1996 Lower American River study, the acceptable range of R was set at 0.5-1.6. The velocities with R values less than 0.5 or greater than 1.6 were deleted from each ADCP data set[6]. The values that failed this test and the tests in footnote 6 were considered outliers or artifacts of the sampling process and were discarded because they would skew the reported values inappropriately.

The procedure to determine the WSEL of each run was as follows: 1) a longitudinal WSEL profile of the site was computed from the measured WSELs and measured longitudinal distances; and 2) the initial and final locations of each run were used to determine the longitudinal location of each run, so that the WSEL of each run could be determined from the WSEL profile. The bed elevation of each point along each run was calculated as the difference between the WSEL of the run and the depth at each point. The distance along each ADCP run, in concert with initial and final horizontal locations, was

---

[3] The Transect program is the software used to receive, record and process data from the ADCP (RD Instruments 1995).

[4] RHABSIM (Payne and Associates 1998) is a software package which includes the features of PHABSIM, and also has the capability of converting the raw data from ADCP runs into bed elevations, average water column velocities and stations.

[5] n - 1 refers to the station immediately before station n and n + 1 refers to the station immediately after station n.

[6] We also deleted velocities where Vel_n was less than 1.00 ft/s and Vel_{n-1} and Vel_{n+1} were greater than 2.00 ft/s, and where Vel_n had one sign (negative or positive) and Vel_{n-1} and Vel_{n+1} had the opposite sign (when the absolute value of all three velocities were greater than 1.00 ft/s); these criteria were also based on the March 1996 dataset.

used to compute the horizontal location of each point. The station (position) along each PHABSIM transect, in concert with the horizontal locations of the headpins and tailpins of the transects, was used to compute the horizontal location of each vertical of the PHABSIM transects. The ADCP run positions and the PHABSIM transect positions were referenced to the same horizontal and vertical benchmarks described earlier.

A table of substrate ranges/values was created to determine the substrate for each point along each ADCP run (e.g, if the substrate size class was 2-4" on a run from station 50 to 70, all of the verticals with station values between 50 and 70 were given a substrate coding of 2.4).

The data from the ADCP runs were combined in Quattropro with the dry/shallow total station data and the PHABSIM transect data to create the input files (bed and substrate) for the 2-D modeling program. The bed files contain the horizontal location (northing and easting), bed elevation and initial bed roughness value for each point, while the substrate files contain the horizontal location, bed elevation and substrate code for each point. An artificial extension one channel-width-long was added upstream of the top of the site to enable the flow to be distributed by the model when it reached the study area. The initial bed roughness value for each point was determined from the substrate code for that point and the corresponding bed roughness value in Table 2. The bed roughness values in Table 2 were computed as five times the average particle size[7]. The bed and substrate files were exported from Quattropro as ASCII files.

A utility program, R2D_BED (Steffler 2001b), was used to define the study area boundary and to refine the raw topographical data TIN (triangulated irregular network) by defining breaklines[8] going up the channel along features such as thalwegs, tops of bars and bottoms of banks. Breaklines were also added connecting the ends of the ADCP runs, the deepest points of the dry/shallow total station data, and along lines of constant elevation. The bed topography of the sites is shown in Appendix A.

An additional utility program, R2D_MESH (Steffler 2001a), was used to define the inflow and outflow boundaries and create the finite element computational mesh for the River2D model. R2D_MESH uses the final bed files as an input. The first stage in creating the computational mesh was to define mesh

---

[7] Five times the average particle size is approximately the same as 2 to 3 times the d85 particle size, which was suggested by Peter Steffler (personal communication) for the initial bed roughness values.

[8] Breaklines are a feature of the R2D_Bed program which force the TIN of the bed nodes to linearly interpolate bed elevation and bed roughness values between the nodes on each breakline and force the TIN to fall on the breaklines (Steffler 2001b).

breaklines[9] which coincided with the final bed file breaklines. Additional mesh breaklines were then added between the initial mesh breaklines, and then additional nodes were added as needed to improve the fit between the mesh and the final bed file and to improve the quality of the mesh, as measured by the Quality Index (QI) value. An ideal mesh (all equilateral triangles) would have a QI of 1.0. A QI value of at least 0.2 is considered acceptable (Steffler 2001a). The QI is a measure of how much the least equilateral mesh element deviates from an equilateral triangle. As shown in Appendix B, the meshes for all sites had QI values of at least 0.3. In addition, the difference in bed elevation between the mesh and final bed file was less than 0.1 feet (0.03 m) for most of the area of all sites. The percentage of the original bed nodes for which the mesh differed by less than 0.1 feet (0.03 m) from the elevation of the original bed nodes ranged from 71.9% to 98.8% (Appendix B). In most cases, the areas of the mesh where there was greater than a 0.1 feet (0.03 m) difference between the mesh and final bed file were in steep areas; in these areas, the mesh would be within 0.1 (0.03 m) feet vertically of the bed file within one foot (0.3 m) horizontally of the bed file location. Given that we had a one-foot (0.3 m) horizontal level of accuracy, such areas would have an adequate fit of the mesh to the bed file. The final step with the R2D_MESH software was to generate the computational (cdg) files.

The cdg files were opened in the RIVER2D software, where the computational bed topography mesh was used together with the WSEL at the bottom of the site, the flow entering the site, and the bed roughnesses of the computational mesh elements to compute the depths, velocities and WSELs throughout the site. The basis for the current form of RIVER2D is given in Ghanem et al (1995). The model was run to steady state at the highest flow for which WSELs were measured, and the WSELs predicted by RIVER2D at the upstream end of the site were compared to the WSELs measured at the top transect. The bed roughnesses of the computational mesh elements were then modified by multiplying them by a constant bed roughness multiplier (BR Mult) until the WSELs predicted by RIVER2D at the upstream end of the site matched the WSELs measured at the top transect. For sites with PHABSIM transects within the sites, the bed roughnesses downstream of each transect were also modified by multiplying them by a constant BR Mult so that the WSELs predicted by RIVER2D matched the WSELs measured at these transects[10].

---

[9] Mesh breaklines are a feature of the R2D_MESH program which force edges of the computation mesh elements to fall on the mesh breaklines and force the TIN of the computational mesh to linearly interpolate the bed elevation and bed roughness values of mesh nodes between the nodes at the end of each breakline segment (Steffler 2001a). A better fit between the bed and mesh TINs is achieved by having the mesh and bed breaklines coincide.

[10] Different BR Mults were used for different transects and for different split channels of transects.

A stable solution will generally have a solution change (Sol Δ) of less than 0.00001 and a net outflow (Net Q) of less than one percent (Steffler and Blackburn 2001). In addition, solutions for low gradient streams should usually have a maximum Froude Number (Max F) of less than one[11]. Finally, the WSEL predicted by the 2-D model should be within 0.10 feet (0.031 m) of the WSEL measured at the upstream transect[12]. The calibrated cdg files all had a solution change of less than 0.00001, but the calibrated cdg file for two of the five sites had a net Q of greater than 1% (Appendix B). We considered these sites to have a stable solution since the net Q was not changing and the net Q in both cases was still less than 2%. The calibrated cdg file for the Sailor Bar site had a maximum Froude Number greater than one (Appendix B); however, we considered this solution to be acceptable since the Froude Number was only greater than one at a few nodes, with the vast majority of the site having Froude Numbers less than one.

For the most part, the calibrated cdg files had WSELs that were within 0.10 feet (0.031 m) of the measured WSELs (see Appendix B for WSEL calibration statistics). However, the calibrated cdg files commonly had WSELs that varied by more than 0.10 feet (0.031 m) across a transect. This resulted in differences of more than 0.10 feet (0.031 m) between the measured and predicted WSELs for the following transects: Sailor Bar XS 2 LC, XS 3 LC, XS 3 RC; Above Sunrise XS 2 RC, XS 6; Sunrise XS 2 RMC, XS 7; and Rossmoor XS 2 LC, XS 2 RC, XS 3. This is consistent with our measurements of WSELs on the transects, where we often found differences of greater than 0.10 feet (0.031 m) , up to as much as 0.3 feet (0.09 m) , between the two banks of the transects. For the above transects, the predicted WSELs near the water's edge, where the WSELs were measured, were all within 0.10 feet (0.031 m) of the measured WSELs. Accordingly, we concluded that the calibration of these transects was acceptable. In other cases (Above Sunrise XS 4, XS 5; Sunrise XS 3, XS5; and Rossmoor XS 4), we were able to get the predicted WSEL near the water's edge on one bank within 0.10 feet (0.031 m) of the measured WSEL, but were unable to get the predicted WSEL near the water's edge on the other bank within 0.10 feet (0.031 m) of the measured WSEL. Since varying the BR Mult across a transect does not generally work to calibrate WSELs, we viewed the calibration in these cases as acceptable because the difference between observed and predicted WSL was similar to the variation in WSL measurements obtained on opposite sides of the channel. The calibration problems for these cases are likely due to some feature of topography that we missed in our data collection; for example, there was a pipe (for which we did not obtain topography data) upstream of Rossmoor XS 4 which depressed the WSEL on the right bank. For Sailor Bar XS 4, the predicted WSEL on the right bank was still considerably higher than the measured WSEL even with a BR Mult of

---

[11] This criteria is based on the assumption that flow in low gradient streams is usually subcritical, where the Froude number is less than one (Peter Steffler, personal communication).

[12] We have selected this standard because it is a standard used for PHABSIM (U. S. Fish and Wildlife Service 2000).

0.01; we judged the calibration of this transect to be acceptable since the average predicted WSEL for the right channel was within 0.10 feet (0.031 m) of the measured WSEL. For Above Sunrise XS 3, we were limited in our ability to calibrate this transect because it was on a split channel; when we lowered the BR Mult below 0.8, the predicted WSEL actually increased due to increased flow down the split channel with a lower bed roughness. We concluded that the calibration for this transect was acceptable since the BR Mult used produced the closest WSELs to the measured WSELs; in addition, for this transect there were significant differences in measured WSELs across the transect, adding to the difficulty in calibrating this transect. For Sunrise XS 2 SC, we concluded that the calibration was adequate since the average predicted WSEL was within 0.10 feet (0.031 m) of the measured WSEL, even though the predicted WSEL near the water's edge differed by more than 0.10 feet (0.031 m) from the measured WSEL. For Sunrise XS 6, the predicted WSEL on the left bank was more than 0.10 feet (0.031 m) higher than the measured WSEL, while the predicted WSEL on the left bank was more than 0.10 feet (0.031 m) lower than the measured WSEL. We selected the BR Mult for this transect as the best overall for the transect, since the average difference between the predicted and measured WSEL was less than 0.10 feet (0.031 m). The most likely explanation for the difference between the predicted and measured WSELs for this transect was that the measurements for the two banks at the calibration flow had been reversed, and thus that the performance of the 2-D model was adequate. Based on the above discussion, we concluded that the WSEL calibration of the sites was acceptable.

Velocity validation is the final step in the preparation of the hydraulic models for use in habitat simulation. Velocities predicted by RIVER2D were compared with measured velocities to determine the accuracy of the model's predictions of mean water column velocities. See Appendix C for velocity validation statistics. Although there was a strong correlation between predicted and measured velocities, there were significant differences between individual measured and predicted velocities. As shown in the figures in Appendix C, we attribute most of the differences between measured and predicted velocities to noise in the measured velocity measurements; specifically, for the transects, the simulated velocities typically fell within the range of the measured velocities of the three or more ADCP runs made on each transect. In addition, the velocities simulated by the 2-D model differed from the measured velocities by the same magnitude as for velocities simulated by PHABSIM from velocity sets collected at higher flows (Appendix C). Another possible explanation for cases where the 2-D model overpredicted velocities is that the measured velocities were the component of the velocity in the downstream direction, while the velocities predicted by the 2-D model were the absolute magnitude of the velocity. For areas with transverse flow, this would result in the 2-D model appearing to overpredict velocities even if it was actually accurately predicting the velocities. The 2-D model integrates effects from the surrounding elements at each point. Thus, point measurements of velocity can differ from simulated values simply due to the local area integration that takes place. As a result, the area integration effect noted above will produce somewhat smoother lateral velocity profiles than the observations. However, there were several cases where the difference between measured and predicted velocities could not be attributed to the above causes.

For Sailor Bar, simulated velocities tended to be higher than measured velocities on the south side of the channel, and for the upper portion of the site, were lower than measured velocities on the north side of the channel (Appendix C). We attribute this to the effect of the velocity distribution at the upstream boundary of the site. River2D distributes velocities across the upstream boundary in proportion to depth, so that the fastest velocities are at the thalweg, which was near the south bank near the top of Sailor Bar. In contrast, the measured velocities showed that the fastest velocities at the top of the site were actually in the middle of the channel. The bed topography above the Sailor Bar site was such that the highest velocities were in the middle of the channel rather than at the thalweg. Since we did not measure the bed topography above the site, River2D was unable to properly distribute the flow across the top of the site. This problem could have been overcome by changing the bed topography at the upstream boundary so that River2D reproduced the velocity distribution at the top of the site; ie by having the thalweg in the middle of the extended channel. The topography would have then gradually transitioned going downstream from the upstream boundary to the measured bed topography at the top of the site.

For Above Sunrise, the simulated velocities on the south side of transect one were higher than the measured velocities, while the simulated velocities on the south side of transects three and five were lower than the measured velocities (Appendix C). In addition, for the northern split channel, the simulated velocities were lower than the measured velocities on the south side of this split channel but higher than the measured velocities on the north side of this split channel. We attribute the errors in the velocities in the north split channel (including transect five) to some aspect of the bed topography between transects five and six which we did not capture in our data collection, and which altered the flow distribution in the northern split channel. Similarly, the errors in the simulated velocities for transects one and three are also likely due to aspects of the bed topography of the sites that we did not capture in our data collection. For Sunrise, simulated velocities were lower than measured velocities in most of the right main channel of transect one, and were higher than the measured velocities on the south side of transects three and seven. The errors in velocities for transects one and three are likely due to aspects of the bed topography of the site that were not captured in our data collection, while the errors in velocities for transect seven were likely due to the same reasons as for Sailor Bar. For El Manto, simulated velocities were higher than measured near the east bank of transect one, but lower than measured near both banks of transect two. The errors in velocities for transect one are likely due to aspects of the bed topography of the site that were not captured in our data collection, while the errors in velocities for transect two were likely due to the same reasons as for Sailor Bar. Although, as discussed above, there were errors in simulated velocities, we concluded that the velocity simulation was adequate, given the data limitations.

The flow and downstream WSEL in the calibrated cdg file were changed to simulate the hydrodynamics of the sites at the simulation flows (1,000 cfs to 3,000 cfs by 200 cfs increments, 3,000 cfs to 9,800 cfs by 400 cfs increments, and 9,800 cfs to 11,000 cfs by 600 cfs increments). The cdg file for each flow contained the WSEL predicted by PHABSIM at the downstream transect at that

flow. Each discharge was run in RIVER2D to steady state. Again, a stable solution will generally have a Sol Δ of less than 0.00001 and a Net Q of less than one percent. In addition, solutions should usually have a Max F of less than one. The production cdg files all had a solution change of less than 0.00001, but the net Q was greater than 1% for ten flows for Sailor Bar, for the next to lowest flow for Above Sunrise, for seven of the lower flows (less than 3400 cfs) for Sunrise, and for the six highest flows and one lower flow for Rossmoor (Appendix D). We still considered these sites to have a stable solution since the net Q was not changing and the net Q in all cases was still less than 5.1%. In comparison, the accepted level of accuracy for USGS gages is generally 5%. Thus, the difference between the flows at the upstream and downstream boundary (net Q) is within the same range as the accuracy for USGS gages, and is thus acceptable. The maximum Froude Number was greater than one for all of the simulated flows for Sailor Bar, for the 25 lowest simulated flows for Above Sunrise, for 24 out of 30 simulated flows for Sunrise and for 25 out of 30 simulated flows for Rossmoor (Appendix D); however, we considered these production runs to be acceptable since the Froude Number was only greater than one at a few nodes, with the vast majority of the area within the site having Froude Numbers less than one.

Habitat Suitability Curves

Habitat suitability curves (HSC or HSI Curves) are used within both PHABSIM and 2-D habitat modeling to translate hydraulic and structural elements of rivers into indices of habitat quality (Bovee 1994). Two sets of HSC were used in this study, one for fall-run chinook salmon spawning and one for steelhead trout spawning (U. S. Fish and Wildlife Service 2000). Both sets of criteria were site-specific, developed from redd measurements on the Lower American River. The redd measurement were made in 1996 for fall-run chinook and in 1992 for steelhead.

Habitat Simulation

The final step in the process was to simulate available habitat for each site. Preference curve files were created containing the digitized HSC in U. S. Fish and Wildlife Service 2000. RIVER2D was used with the final cdg files, the substrate file and the preference curve files to compute WUA for each site over the desired range of flows (1,000 cfs to 3,000 cfs by 200 cfs increments, 3,000 cfs to 9,800 cfs by 400 cfs increments, and 9,800 cfs to 11,000 cfs by 600 cfs increments). The WUA values calculated for each site and criteria set are contained in Appendix E. The WUA values for the sites were added together to produce the total WUA.

Biological Validation

We compared the combined habitat suitability predicted by PHABSIM and RIVER2D at each redd location in the Sailor Bar and Above Sunrise sites. We ran the PHABSIM and RIVER2D models at 3087 cfs to determine the combined habitat suitability in each PHABSIM cell and at individual points

for RIVER2D for the average discharge from November 11 to December 17, 1998. We used the horizontal location measured for each redd to determine which PHABSIM cell each redd was in and to determine the location of each redd in the RIVER2D sites. We used a random number generator to select 211 locations without redds in the Sailor Bar site and to select 286 locations without redds in the Above Sunrise site[13]. Locations were eliminated that: 1) were less than three feet from a previously-selected location; 2) were less than three feet from a redd location; and 3) were not located in the wetted part of the site. We used Mann-Whitney tests (Zar 1984) to determine whether the compound suitability predicted by PHABSIM and RIVER2D was significantly higher at redd locations versus locations where redds were absent.

RESULTS

Habitat Simulation

The flow-habitat relationships for fall-run chinook salmon and steelhead are shown in Figures 1 and 2. For fall-run chinook salmon, the 2-D model predicts the highest WUA at a higher flow than for PHABSIM, predicts higher WUA than PHABSIM for flows in the range of 4,000 to 6,000 cfs, and predicts lower WUA than PHABSIM for flows above 6,000 cfs. For steelhead, the 2-D model does not exhibit the spike in WUA that PHABSIM predicts around 5,000 cfs. This spike was caused by switching from the low-flow to the high-flow PHABSIM deck for Above Sunrise transects six and seven (U. S. Fish and Wildlife Service 2000). In contrast, the 2-D model more accurately reflected the change in distribution of flow across the channel with increased flow, and thus did not show this same spike. Overall, the habitat-flow relationships predicted by PHABSIM and the 2-D model were essentially the same. The differences between the models can largely be attributed to the two methods of filling in the space between transects, assumed uniform extrapolation and explicit simulation. However, when the habitat-flow relationships for each site (shown in Appendix E) are examined, there were significant differences in the flow-habitat relationships for some sites and criteria. While the flow-habitat relationships predicted by PHABSIM and the 2-D model were nearly identical for some sites and criteria (such as Rossmoor for chinook salmon spawning), the flow-habitat relationships predicted by PHABSIM and the 2-D model were quite different for other sites and criteria (such as Sailor Bar for chinook salmon and steelhead spawning and Sunrise for chinook salmon spawning).

[13] These were the same numbers as the number of PHABSIM cells without redds in each site.

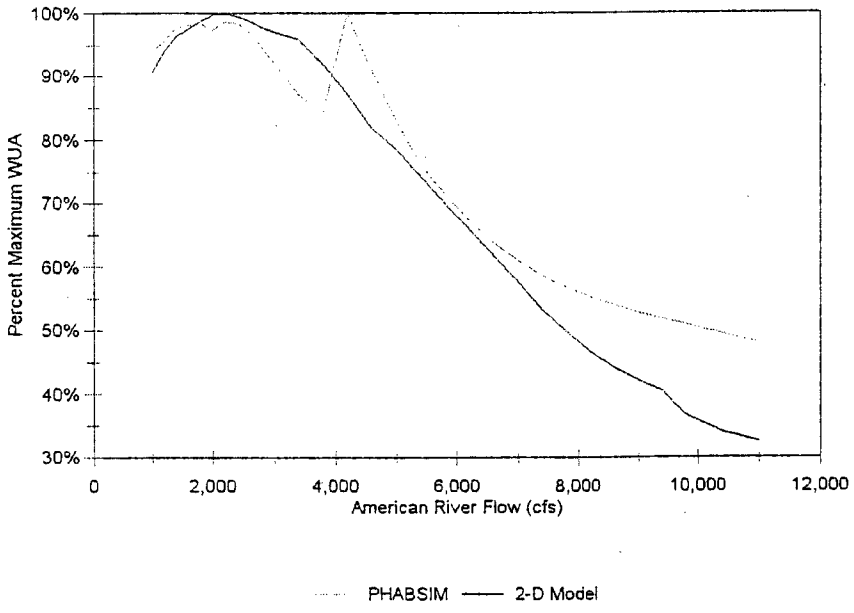

Figure 1
Fall-run chinook salmon flow-habitat relationships

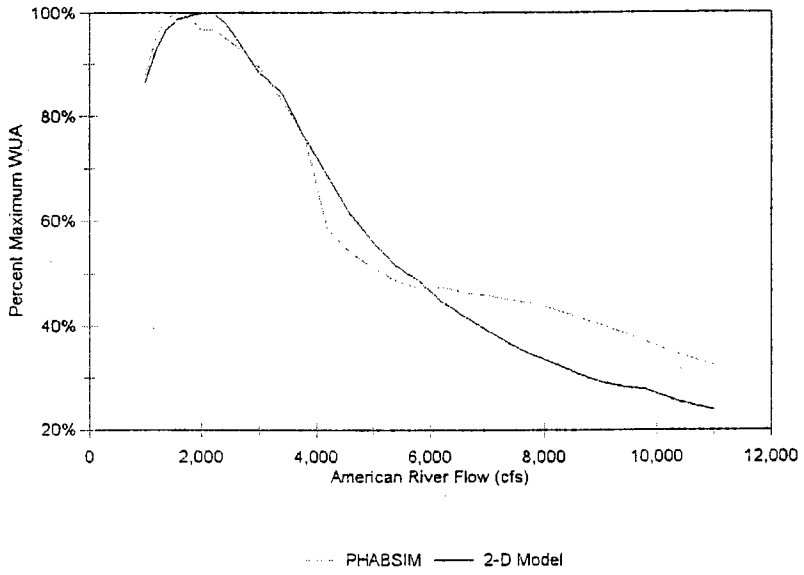

Figure 2
Steelhead flow-habitat relationships

Biological Validation

The distribution of the redd measurement depths and velocities, relative to the fall-run chinook salmon criteria, are shown in Figures 3 and 4. In general, the redd measurements in 1998 were somewhat slower and shallower than the 1996 redd measurements that were used to develop the habitat suitability criteria. We attribute this to the 1998 data being biased toward shallower redds as a result of lower visibility (i.e. the lack of deep redds at Above Sunrise). Deeper redds tend to have somewhat higher velocities.

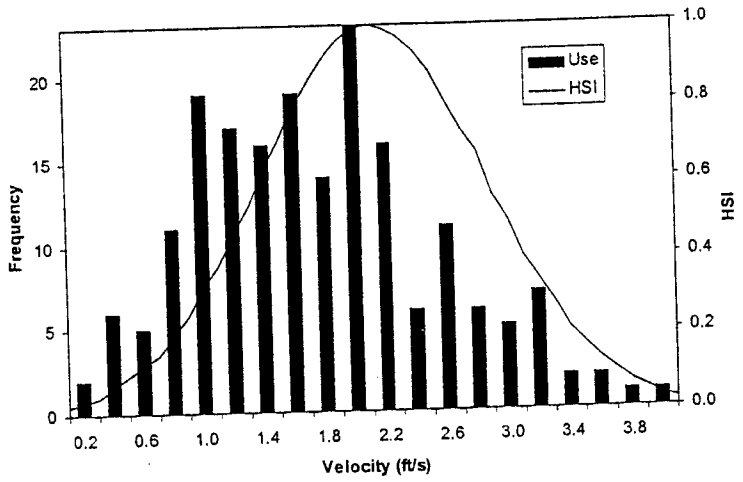

Figure 3
Velocity Distribution of 1998 Redds and Fall-run Criteria

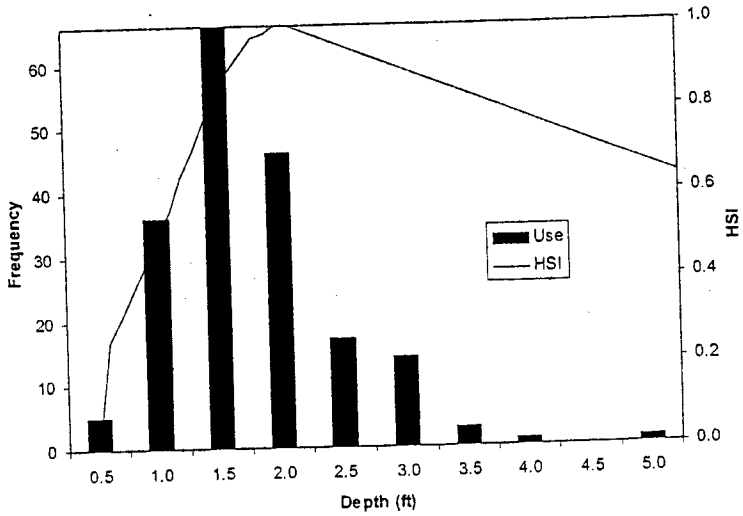

Figure 4
Depth Distribution of 1998 Redds and Fall-run Criteria

There were a total of 103 PHABSIM cells with redds and 497 wetted cells without redds for the Sailor Bar and Above Sunrise sites. The combined habitat suitability was significantly higher for cells with redds (median = 0.2343) than for cells without redds (median = 0.0099), based on the Mann-Whitney U test (p = 0.003). Thirty six percent of the PHABSIM cells with redds had a combined suitability of zero. The frequency distribution of combined habitat suitability for cells with redds is shown in Figure 5, while the frequency distribution of combined habitat suitability for cells without redds is shown in Figure 6. The frequency distribution of combined habitat suitability based on the velocities, depths and substrates measured at the redd locations is shown in Figure 7.

As shown in Figure 7, four of the redds measured had a combined suitability of zero, based on the measured depth, velocity and substrate. This occurred because these redds had characteristics that fell outside of the range of redds measured in 1996 that were used to develop the habitat suitability criteria. Specifically, the shallowest depth for the redds measured in 1996 was 0.6 feet, and thus depths less than 0.6 feet had a suitability of zero. In contrast, the measured depths of three of the redds in 1998 were less than 0.6 feet (two had a depth of 0.4 feet and one had a depth of 0.5 feet). In addition, none of the redds measured in 1996 had substrate of 0.1 to 1 inches (substrate code 1), and thus substrate code 1 had a suitability of zero. In contrast, the fourth redd in 1998 with a combined suitability of zero had a substrate code of 1.

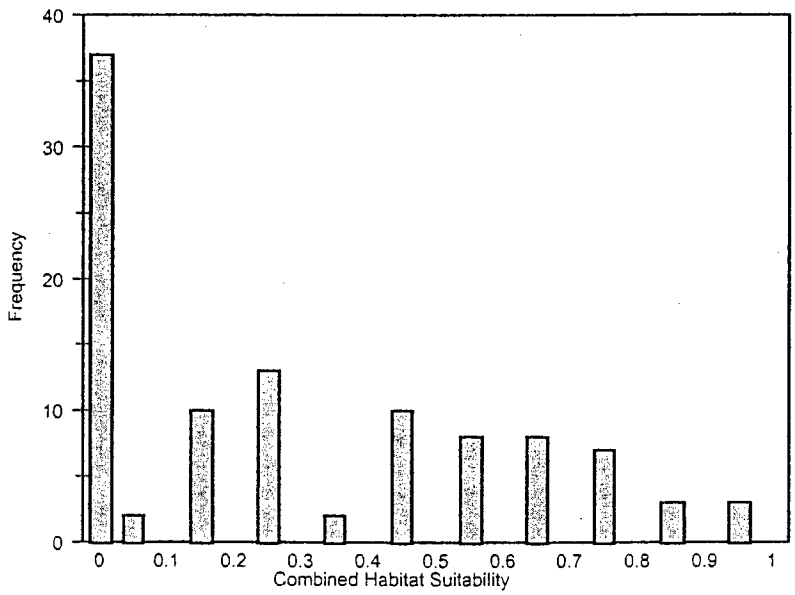

Figure 5
Combined Habitat Suitability of PHABSIM Cells with Redds

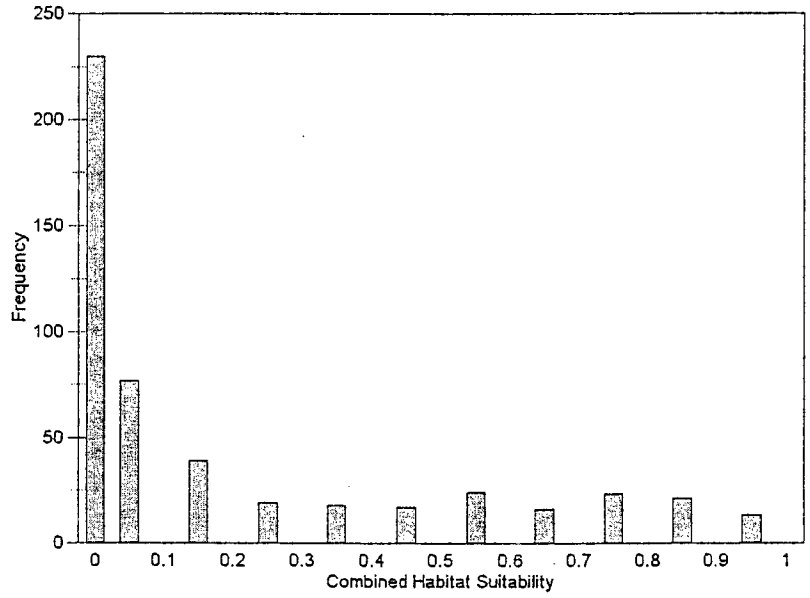

Figure 6
Combined Habitat Suitability for PHABSIM Cells Without Redds

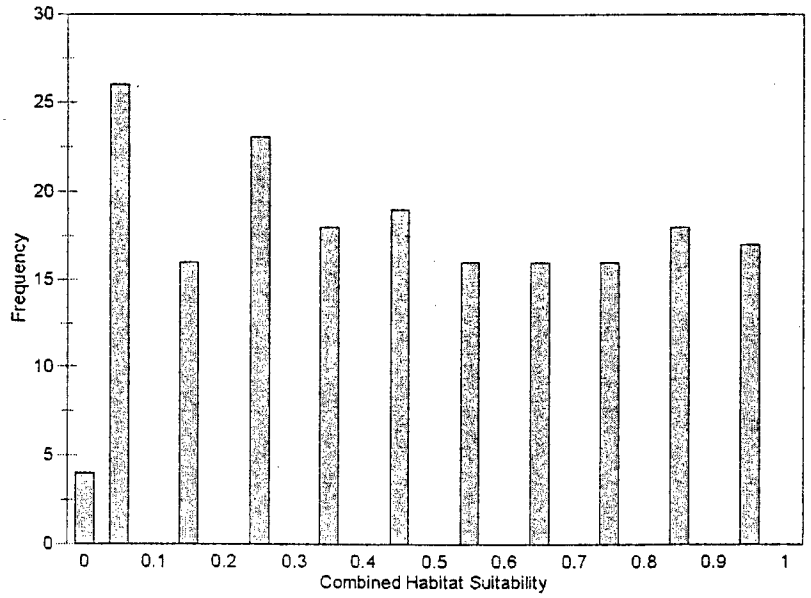

Figure 7
Combined Habitat Suitability of Redd Measurement Data

Of the 190 redds measured, four redds were upstream of the sites and an additional redd was outside of the boundary of the Above Sunrise Site. Thus, we had a total of 185 locations with redds and 497 locations without redds for Above Sunrise and Sailor Bar. The combined habitat suitability predicted by the 2-D model was significantly higher for locations with redds (median = 0.04) than for cells without redds (median = 0.0), based on the Mann-Whitney U test ($p = 0.000003$). The frequency distribution of combined habitat suitability predicted by the 2-D model for locations with redds is shown in Figure 8, while the frequency distribution of combined habitat suitability for locations without redds is shown in Figure 9. The location of redds relative to the distribution of combined suitability is shown in Appendix F.

Of the 61 redd locations that the 2-D model predicted had a combined suitability of zero (33%), 52 had a combined suitability of zero due to the predicted substrate being too small (substrate codes 0 and 1) or too large (substrate codes 4.6 and 6.8), five had a combined suitability of zero because the location was predicted to be dry by the 2-D model, three had a combined suitability of zero because the predicted velocity was too fast (greater than 4.3 ft/s), and one had a combined suitability of zero because the predicted velocity was too slow (velocity of 0 ft/s). The 2-D model predicts substrate at a given location by the substrate at the nearest point in the substrate file. It appears based upon our substrate data that substrate varies more laterally (across the channel) than longitudinally (upstream and downstream). To test whether this supposition could be used to improve the performance of the 2-D model, we created a test substrate file for Above Sunrise in which we added longitudinal breaklines to

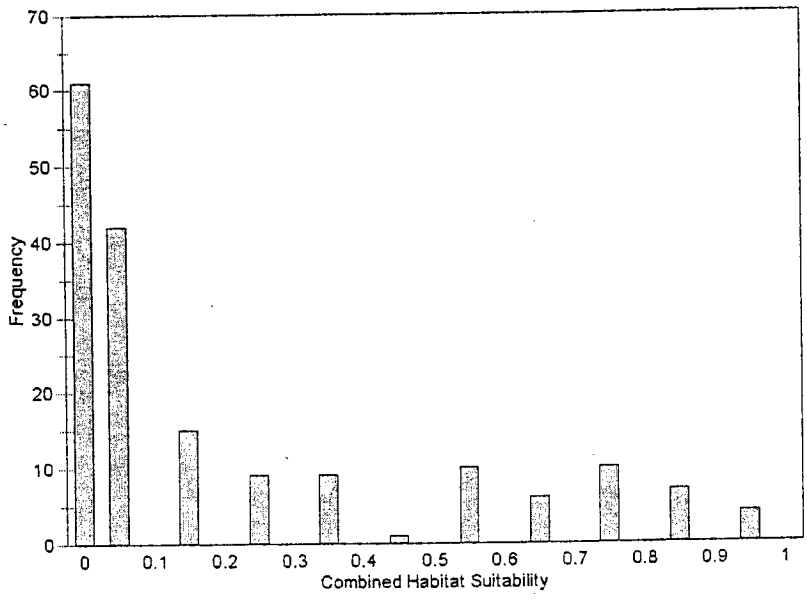

Figure 8
Combined Habitat Suitability for 2-D Model Locations With Redds

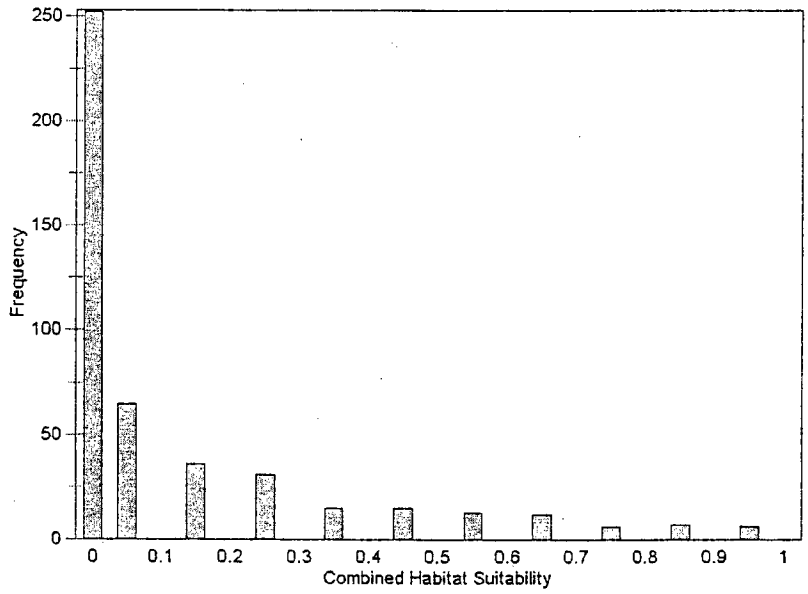

Figure 9
Combined Habitat Suitability for 2-D Model Locations Without Redds

force the 2-D model to predict substrate at a given location based on the nearest longitudinal point where we collected substrate data. This decreased the number of redds with predicted substrate suitability of zero from 22 to 13. The WUA predicted using the test substrate file differed little from the WUA predicted using the original substrate file. An increased density of substrate data would have been required to further improve the ability of the 2-D model to predict the substrate, and thus the combined suitability, of redd locations. However, this would likely had little effect on the resulting flow-habitat relationship. Specifically, flow-habitat relationships are not very sensitive to substrate data, since the substrate does not change with flow. The only effect of substrate data on flow-habitat relationships is when the depths and velocities in areas with suitable substrates differ from the depths and velocities in areas with unsuitable substrates. For example, if the substrates are suitable in the thalweg (where the highest depths and velocities typically are found) but unsuitable in the remaining portion of the channel, the peak WUA will be at a lower flow than if the substrates are unsuitable in the thalweg but suitable in the remaining portion of the channel.

The errors of the 2-D model for the redds that had a predicted combined suitability of zero due to the predicted velocity being too low or too high can be attributed to the same reasons discussed above for errors in simulated velocities. The prediction by the 2-D model that redd locations were dry can be attributed to either: 1) the model underpredicting the WSELs in the site at the flow at which redd data was collected; or 2) to longitudinal curvature in the bed topography which was not captured by the data

collection, for redds that were located near the water's edge. As shown in Figure 10, the 2-D model underpredicted the WSELs in the site at the flow at which redd data was collected for the Above Sunrise site, where four of the five redd locations which were predicted to be dry were located. This suggests that it may be necessary to vary the BR Mult with flow to get an accurate prediction of WSELs. Overall, we conclude that the 2-D model did a slightly better job of predicting the combined suitability of redd locations, based on the percentage of locations/cells with zero suitability and the p-values for the Mann-Whitney U tests.

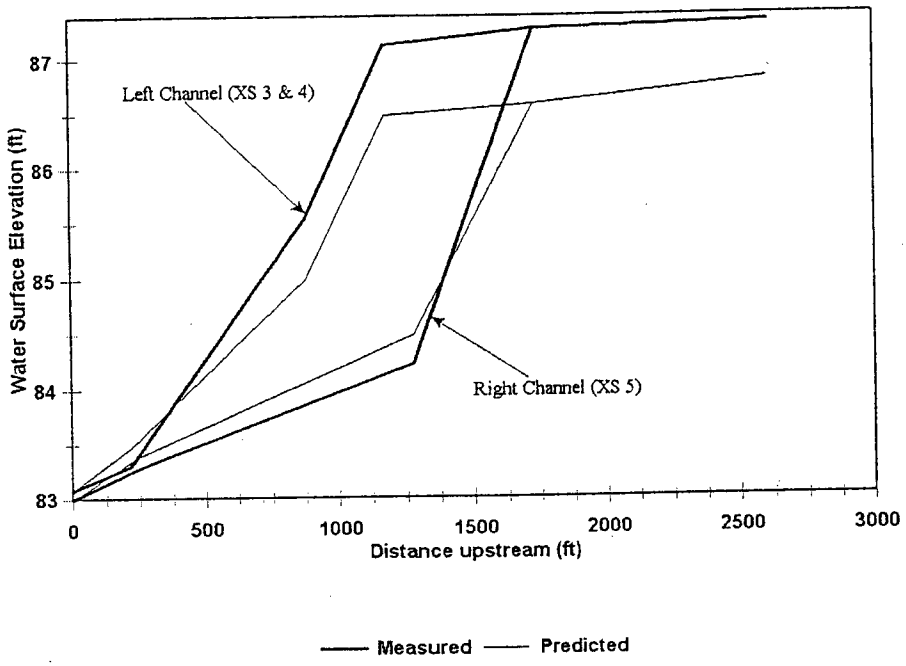

Figure 10
Above Sunrise WSELs at Redd Data Collection Flow

REFERENCES

Bovee, K. D. 1986. Development and evaluation of habitat suitability criteria for use in the Instream Flow Incremental Methodology. Instream Flow Information Paper 21. U. S. Fish and Wildlife Service Biological Report 86(7). 235 pp.

Bovee, K. D. 1994. Data collection procedures for the physical habitat simulation system. National Biological Service, Fort Collins, CO. 322 pp.

Ghanem, A., P. Steffler, F. Hicks and C. Katopodis. 1995. Two-dimensional modeling of flow in aquatic habitats. Water Resources Engineering Report 95-S1, Department of Civil Engineering, University of Alberta, Edmonton, Alberta. March 1995.

Milhous, R. T., M. A. Updike and D. M. Schneider. 1989. Physical habitat simulation system reference manual - version II. Instream Flow Information Paper No. 26. U. S. Fish and Wildlife Service Biological Report 89(16).

Payne and Associates. 1998. Users manual: RHABSIM 2.0 Riverine habitat simulation software for DOS and Windows. Thomas R. Payne and Associates, Arcata, CA 166 pp.

RD Instruments. 1995. Direct reading and self-contained broadband acoustic doppler current profiler technical manual. RD Instruments, San Diego, CA.

Steffler, P. 2001a. R2D_Mesh - mesh generation program for River2D two dimensional depth averaged finite element hydrodynamic model - version 2.01. User's manual. University of Alberta, Edmonton, Alberta. 22 pp. http://bertram.civil.ualberta.ca/download.htm

Steffler, P. 2001b. River2D_Bed. Bed topography file editor - version 1.23. User's manual. University of Alberta, Edmonton, Alberta. 24 pp. http://bertram.civil.ualberta.ca/download.htm

Steffler, P. and J. Blackburn. 2001. River2D: Two-dimensional depth averaged model of river hydrodynamics and fish habitat. Introduction to depth averaged modeling and user's manual. University of Alberta, Edmonton, Alberta. 88 pp. http://bertram.civil.ualberta.ca/download.htm

Trihey, E. W. and Wegner, D. L. 1981. Field data collection procedures for use with the physical habitat simulation system of the Instream Flow Group, U. S. Fish and Wildlife Service, National Ecology Research Center, Fort Collins, CO. 151 pp.

U. S. Fish and Wildlife Service. 1995. Working paper on restoration needs: habitat restoration actions to double natural production of anadromous fish in the Central Valley of California. Volume 1. May 9, 1995. Prepared for the U. S. Fish and Wildlife Service under the direction of the Anadromous Fish Restoration Program Core Group. Stockton, CA.

U. S. Fish and Wildlife Service. 2000. Effects of the January 1997 flood on flow-habitat relationships for steelhead and fall-run chinook salmon spawning in the Lower American River. Sacramento, CA: U.S. Fish and Wildlife Service.

Zar, J. H. 1984. Biostatistical Analysis, Second Edition. Englewood Cliffs, NJ: Prentice-Hall, Inc.

APPENDIX A
BED TOPOGRAPHY OF STUDY SITES

SAILOR BAR STUDY SITE

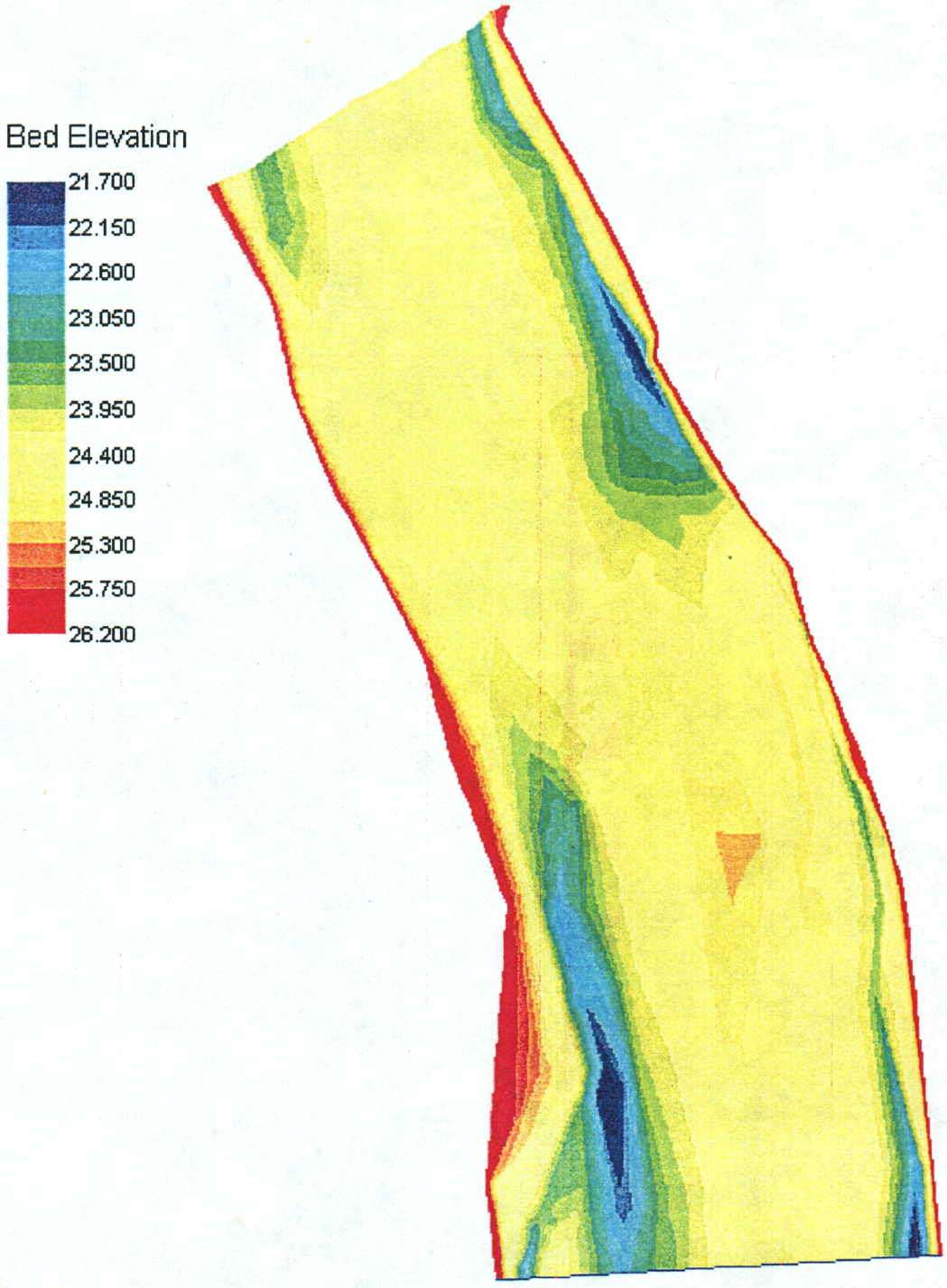

Units of Bed Elevation are meters.

ABOVE SUNRISE STUDY SITE

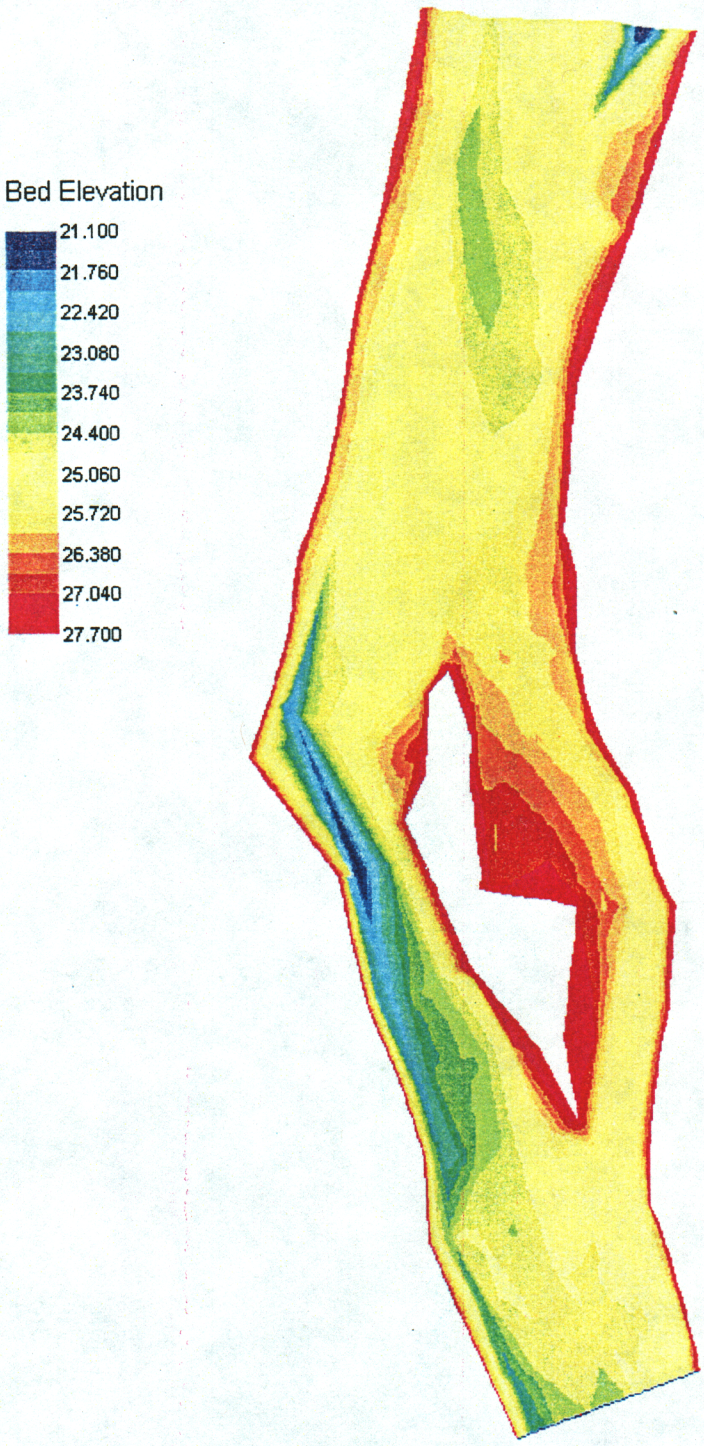

Units of Bed Elevation are meters.

SUNRISE STUDY SITE

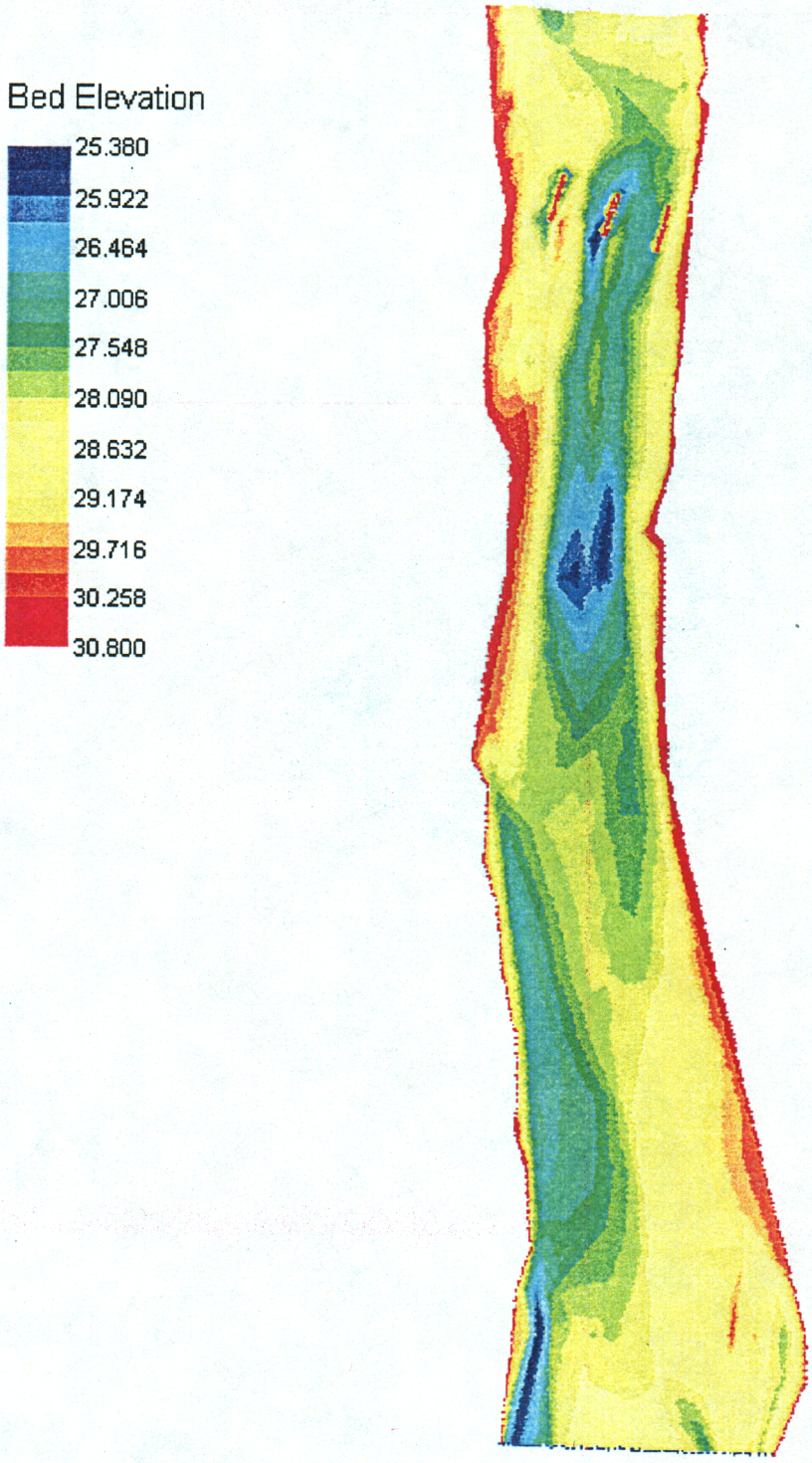

Units of Bed Elevation are meters.

EL MANTO STUDY SITE

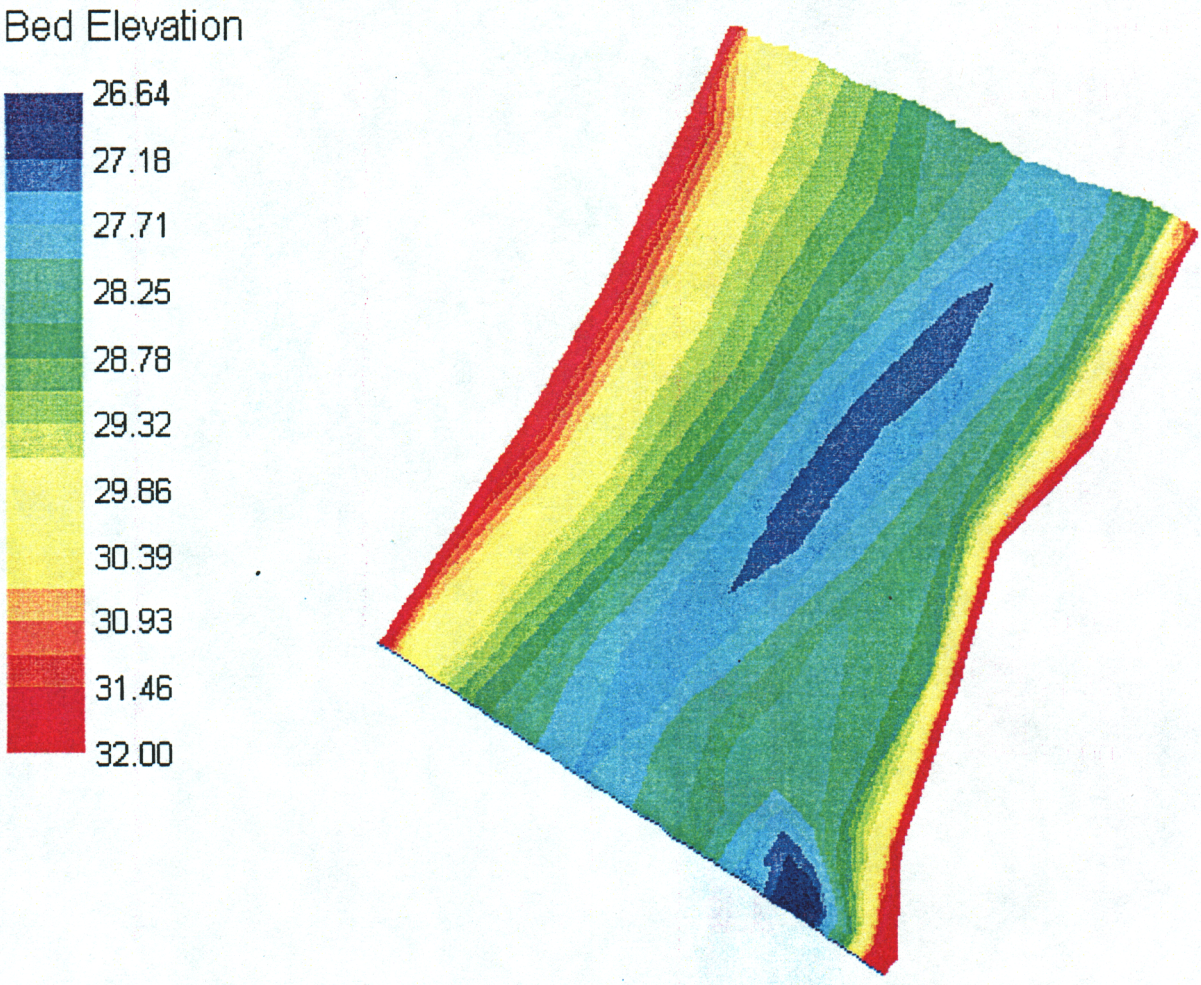

Units of Bed Elevation are meters.

ROSSMOOR STUDY SITE

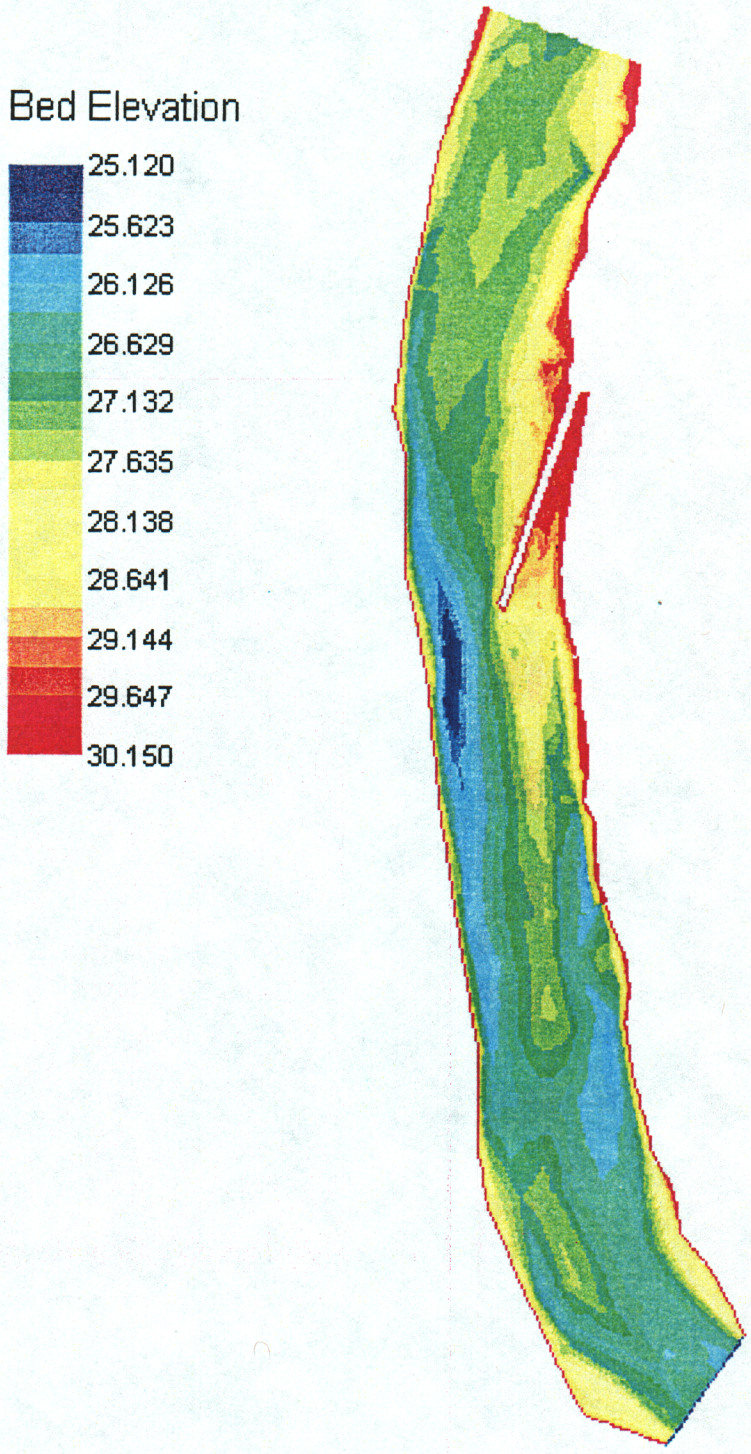

Units of Bed Elevation are meters.

APPENDIX B
WSEL CALIBRATION

Calibration Statistics

Site Name	% Nodes within 0.1'	Nodes	QI	Net Q	Sol Δ	Max F
Sailor Bar	77.6%	9443	0.34	1.9%	.000002	1.27
Above Sunrise	71.9%	11095	0.30	0.2%	<.000001	0.95
Sunrise	72.0%	11442	0.32	0.8%	.000005	0.98
El Manto	98.8%	4758	0.37	0.7%	<.000001	0.73
Rossmoor	71.9%	12223	0.30	1.7%	<.000001	0.96

Sailor Bar Site

		Difference (measured vs. pred. WSELs)		
XSEC	BR Mult	Average	Standard Deviation	Maximum
2 LC	0.5	0.07	0.04	0.18
2 LB	0.5	0.05	0.02	0.10
2 RC	0.45	0.03	0.03	0.07
3 LC	7	0.10	0.004	0.11
3 LB	7	0.10	0.002	0.10
3 RC	1.2	0.03	0.07	0.11
3 RB	1.2	0.02	0.04	0.09
4 LC	8	0.05	0.01	0.07
4 RC	0.01	0.09	0.20	0.60
4 RB	0.01	0.29	0.20	0.60

Above Sunrise Site

XSEC	BR Mult	Difference (measured vs. pred. WSELs) Average	Standard Deviation	Maximum
2 LC	8	0.04	0.03	0.10
2 RC	0.3	0.08	0.07	0.17
2 RB	0.3	0.07	0.01	0.08
3	0.8	0.22	0.18	0.55
4	0.6	0.32	0.07	0.40
4 LB	0.6	0.10	0.005	0.10
4 RB	0.6	0.16	0	0.16
5	N/A	0.01	0.35	0.61
5 LB	0.01	0.42	0.23	0.61
5 RB	13	0.01	0.04	0.07
6	N/A	0.11	0.07	0.21
6 LB	2	0.06	0.01	0.10
6 RB	0.1	0.09	0.01	0.10
7	0.1	0.01	0.02	0.04

Sunrise Site

XSEC	BR Mult	Difference (measured vs. pred. WSELs) Average	Standard Deviation	Maximum
2 LMC	0.7	—	—	---
2 RMC	0.7	0.22	0.05	0.28
RB 2 RMC	0.7	0.10	0	0.10
2 SC	3	0.09	0.19	0.27
RB 2 SC	3	0.22	0	0.22
3	0.01	0.09	0.02	0.13
3 LB	0.01	0.11	0.01	0.12
3 RB	0.01	0.05	0.02	0.10
4	0.5	0.03	0.01	0.06
5	0.3	0.04	0.08	0.15
5 LB	0.3	0.11	0.004	0.11
5 RB	0.3	0.09	0.01	0.10
6	1	0.08	0.05	0.23
6 LB	1	0.10	0.06	0.23
6 RB	1	0.10	0.03	0.15
7	3	0.13	0.09	0.27
7 LB	3	0.05	0.02	0.10
7 RB	3	0.08	0.01	0.09

El Manto Site

XSEC	BR Mult	Difference (measured vs. pred. WSELs) Average	Standard Deviation	Maximum
2	1.15	0.01	0.05	0.09

Rossmoor Site

XSEC	BR Mult	Difference (measured vs. pred. WSELs) Average	Standard Deviation	Maximum
2 LC	0.95	0.03	0.05	0.15
2 LB	0.95	0.02	0.04	0.10
2 RC	0.9	0.17	0.11	0.31
2 RB	0.9	0.02	0.04	0.08
3	0.1	0.01	0.03	0.11
3 LB	0.1	0.01	0.03	0.10
3 RB	0.1	0.02	0.03	0.07
4	N/A	0.07	0.11	0.29
4 LB	0.1	0.07	0.02	0.10
4 RB	0.01	0.44	0.08	0.53
5	0.1	0.02	0.03	0.06
6	0.3	0.04	0.03	0.09
7	0.7	0.001	0.04	0.10

APPENDIX C
VELOCITY VALIDATION STATISTICS

Measured Velocities less than 3 ft/s

Site Name	Difference (measured vs. pred. velocities, ft/s) Average	Standard Deviation	Maximum
Sailor Bar	2.06	1.75	7.97
Above Sunrise	0.83	0.85	4.95
Sunrise	0.87	0.73	3.23
El Manto	1.16	1.04	3.97
Rossmoor	1.03	0.81	4.08

Measured Velocities greater than 3 ft/s

Site Name	Percent Difference (measured vs. pred. velocities) Average	Standard Deviation	Maximum
Sailor Bar	38%	36%	326%
Above Sunrise	27%	24%	130%
Sunrise	17%	17%	118%
El Manto	24%	15%	78%
Rossmoor	22%	18%	93%

All differences were calculated as the absolute value of the difference between the measured and simulated velocity.

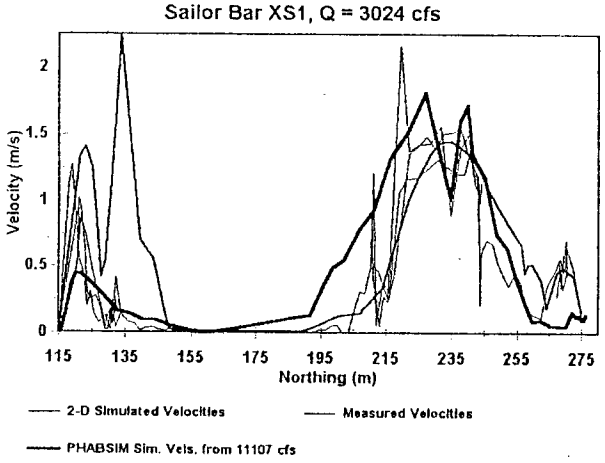
Sailor Bar XS1, Q = 3024 cfs
Velocity (m/s)
Northing (m)
2-D Simulated Velocities
Measured Velocities
PHABSIM Sim. Vels. from 11107 cfs

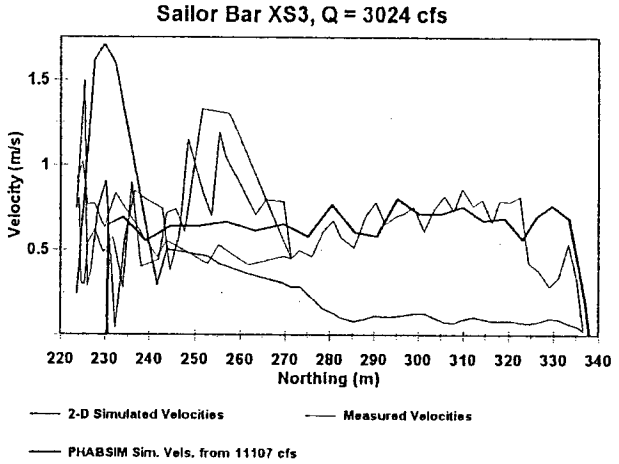
Sailor Bar XS3, Q = 3024 cfs
Velocity (m/s)
Northing (m)
2-D Simulated Velocities
Measured Velocities
PHABSIM Sim. Vels. from 11107 cfs

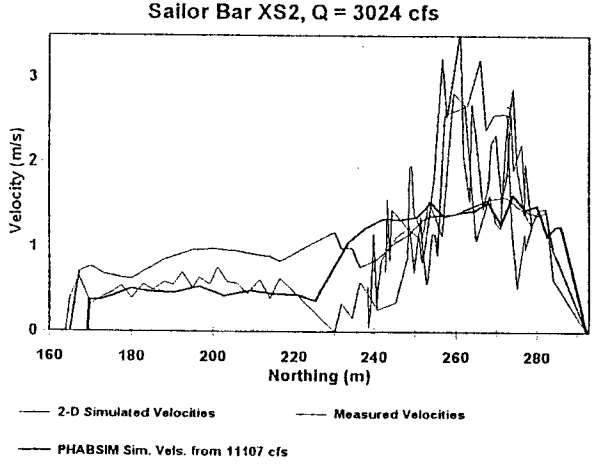
Sailor Bar XS2, Q = 3024 cfs
Velocity (m/s)
Northing (m)
2-D Simulated Velocities
Measured Velocities
PHABSIM Sim. Vels. from 11107 cfs

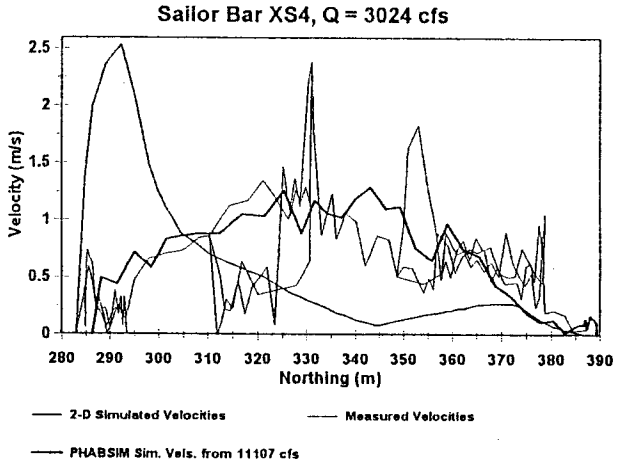
Sailor Bar XS4, Q = 3024 cfs
Velocity (m/s)
Northing (m)
2-D Simulated Velocities
Measured Velocities
PHABSIM Sim. Vels. from 11107 cfs

Sailor Bar

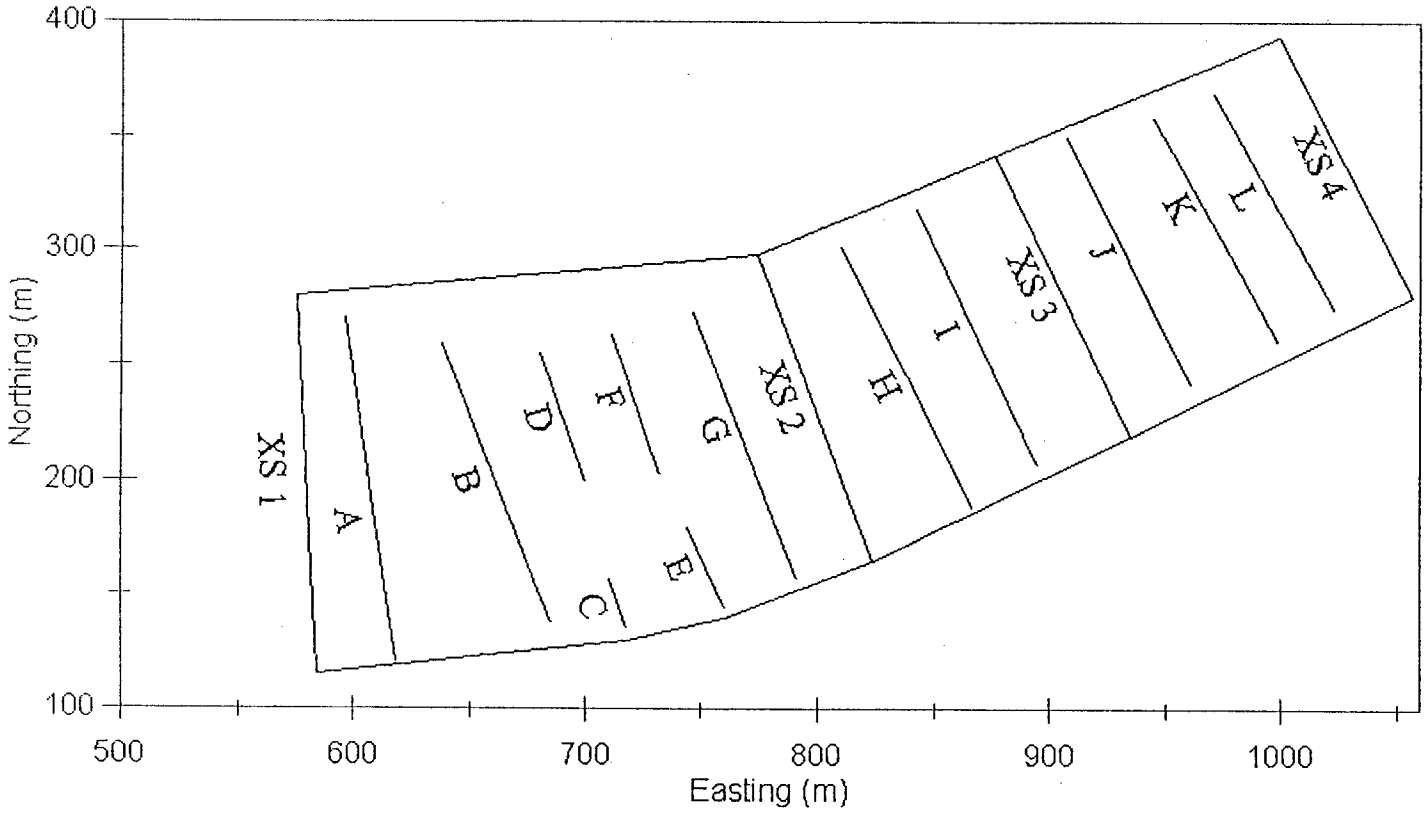
400
300
200
100
Northing (m)
500
600
700
800
900
1000
Easting (m)
XS 1
A
B
C
D
E
F
G
XS 2
H
I
XS 3
J
K
L
XS 4

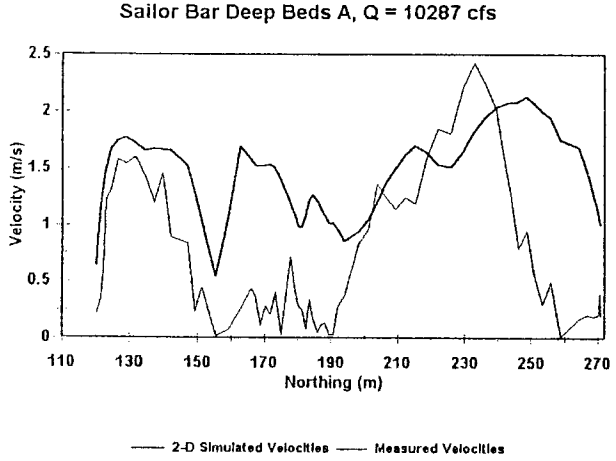
Sailor Bar Deep Beds A, Q = 10287 cfs
Velocity (m/s)
2.5
2
1.5
1
0.5
0
110 130 150 170 190 210 230 250 270
Northing (m)
2-D Simulated Velocities
Measured Velocities

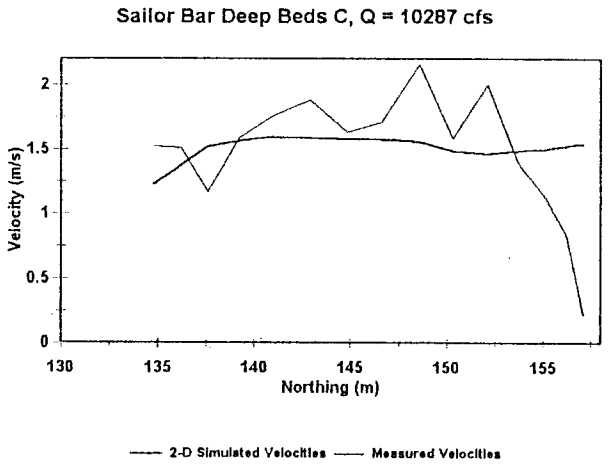
Sailor Bar Deep Beds C, Q = 10287 cfs
Velocity (m/s)
2
1.5
1
0.5
0
130 135 140 145 150 155
Northing (m)
2-D Simulated Velocities
Measured Velocities

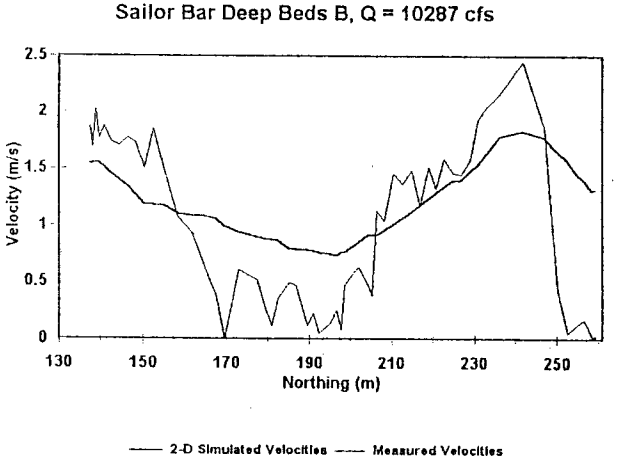
Sailor Bar Deep Beds B, Q = 10287 cfs
Velocity (m/s)
2.5
2
1.5
1
0.5
0
130 150 170 190 210 230 250
Northing (m)
2-D Simulated Velocities
Measured Velocities

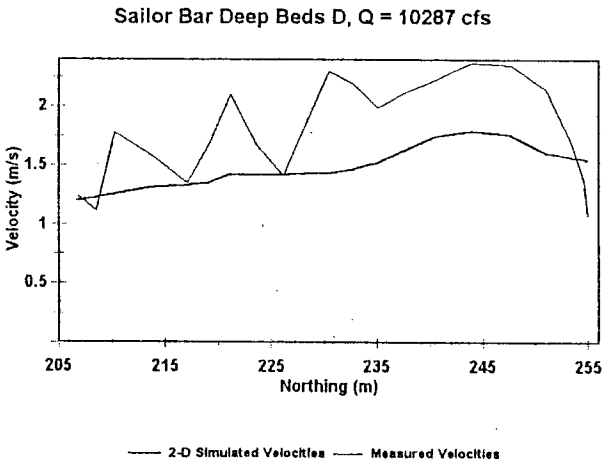
Sailor Bar Deep Beds D, Q = 10287 cfs
Velocity (m/s)
2
1.5
1
0.5
205 215 225 235 245 255
Northing (m)
2-D Simulated Velocities
Measured Velocities

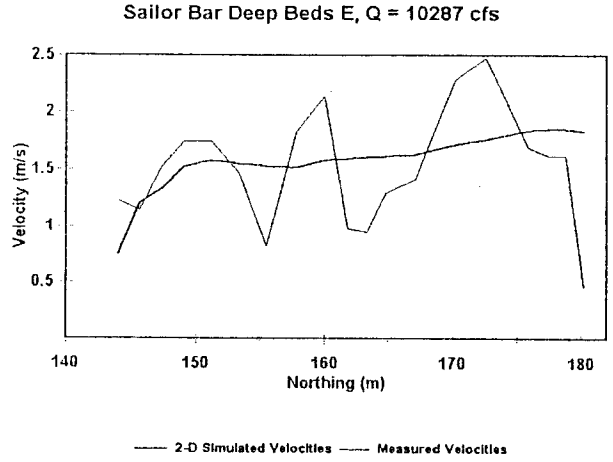
Sailor Bar Deep Beds E, Q = 10287 cfs
Velocity (m/s)
2.5
2
1.5
1
0.5
140
150
160
170
180
Northing (m)
2-D Simulated Velocities
Measured Velocities

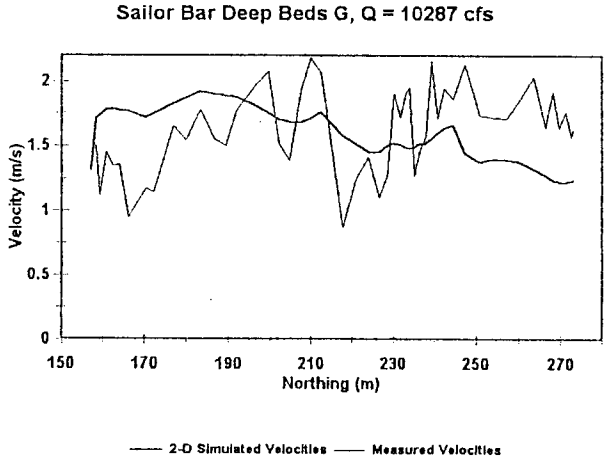
Sailor Bar Deep Beds G, Q = 10287 cfs
Velocity (m/s)
2
1.5
1
0.5
0
150
170
190
210
230
250
270
Northing (m)
2-D Simulated Velocities
Measured Velocities

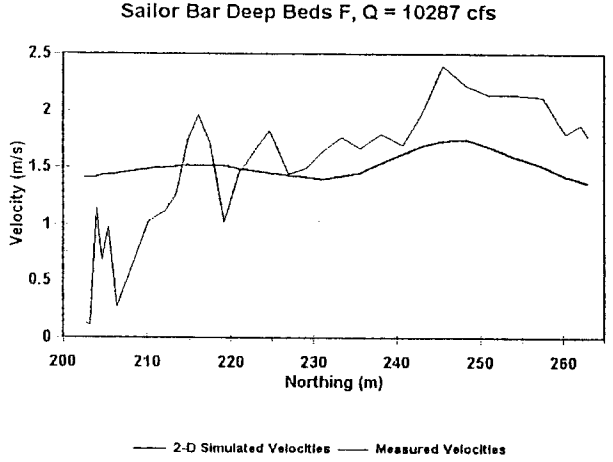
Sailor Bar Deep Beds F, Q = 10287 cfs
Velocity (m/s)
2.5
2
1.5
1
0.5
0
200
210
220
230
240
250
260
Northing (m)
2-D Simulated Velocities
Measured Velocities

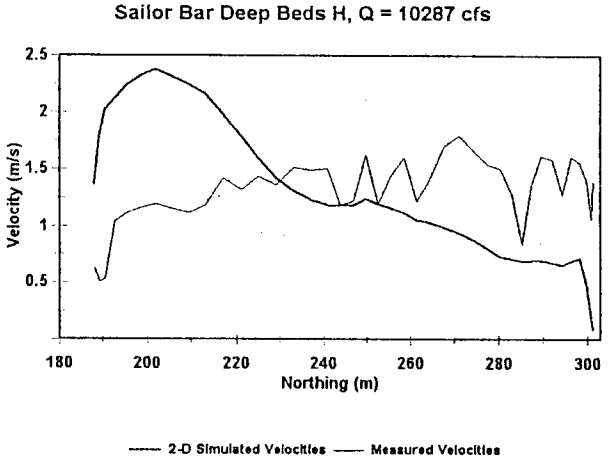
Sailor Bar Deep Beds H, Q = 10287 cfs
Velocity (m/s)
2.5
2
1.5
1
0.5
180
200
220
240
260
280
300
Northing (m)
2-D Simulated Velocities
Measured Velocities

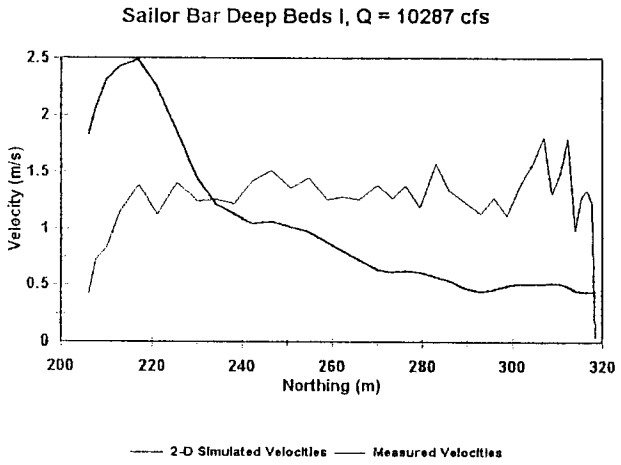
Sailor Bar Deep Beds I, Q = 10287 cfs
Velocity (m/s)
Northing (m)
2-D Simulated Velocities
Measured Velocities

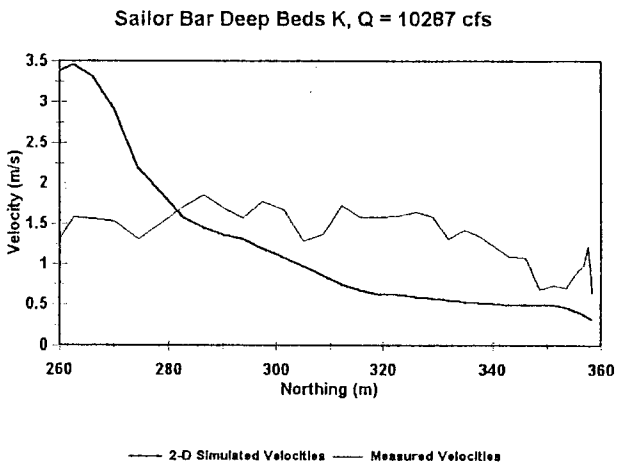
Sailor Bar Deep Beds K, Q = 10287 cfs
Velocity (m/s)
Northing (m)
2-D Simulated Velocities
Measured Velocities

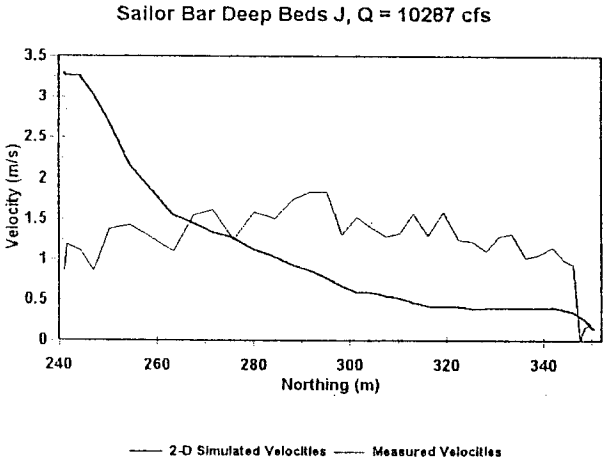
Sailor Bar Deep Beds J, Q = 10287 cfs
Velocity (m/s)
Northing (m)
2-D Simulated Velocities
Measured Velocities

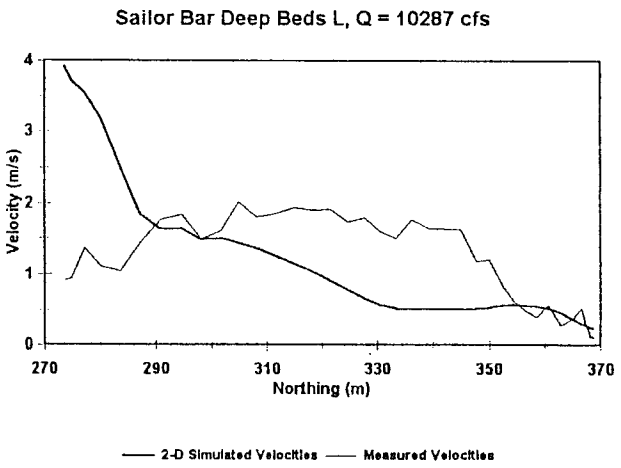
Sailor Bar Deep Beds L, Q = 10287 cfs
Velocity (m/s)
Northing (m)
2-D Simulated Velocities
Measured Velocities

Sailor Bar

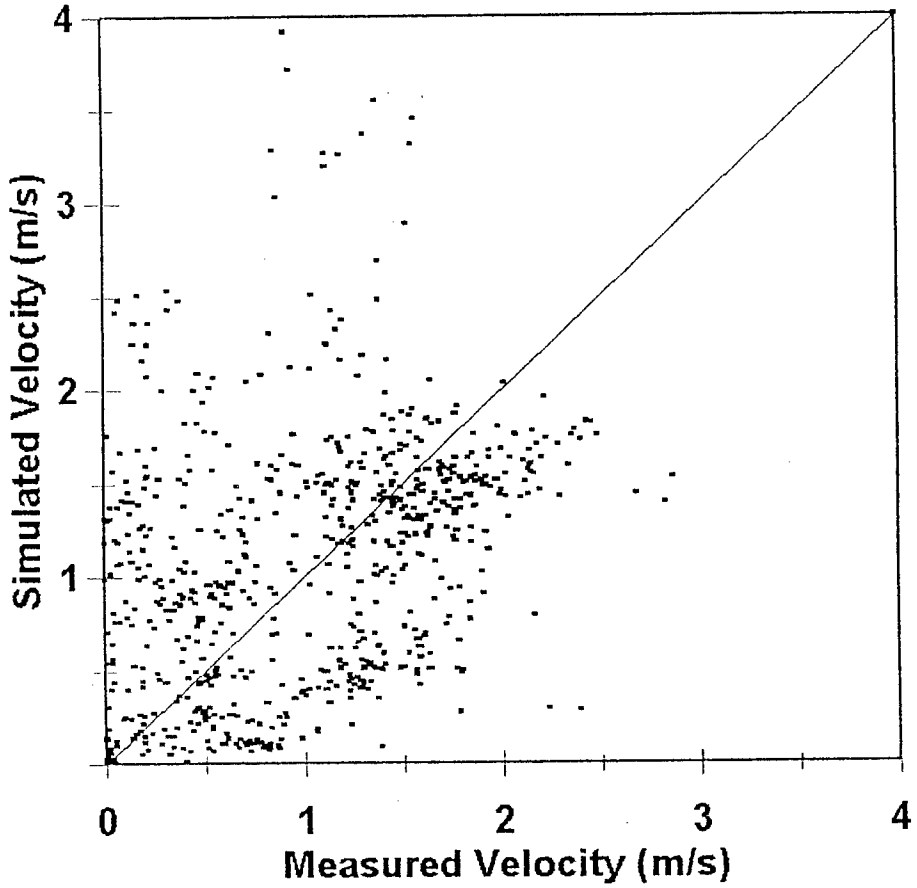

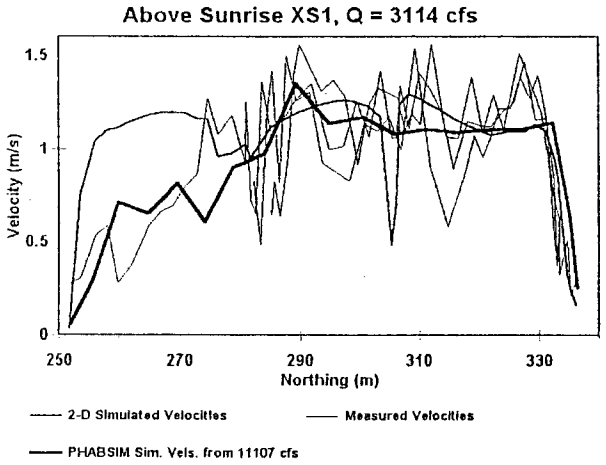
Above Sunrise XS1, Q = 3114 cfs
Velocity (m/s)
Northing (m)
2-D Simulated Velocities
Measured Velocities
PHABSIM Sim. Vels. from 11107 cfs

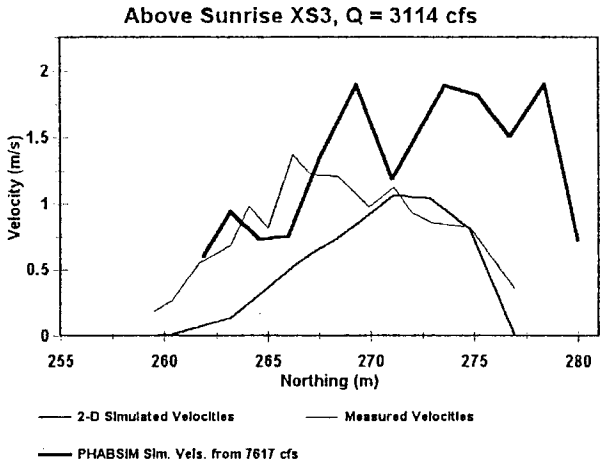
Above Sunrise XS3, Q = 3114 cfs
Velocity (m/s)
Northing (m)
2-D Simulated Velocities
Measured Velocities
PHABSIM Sim. Vels. from 7617 cfs

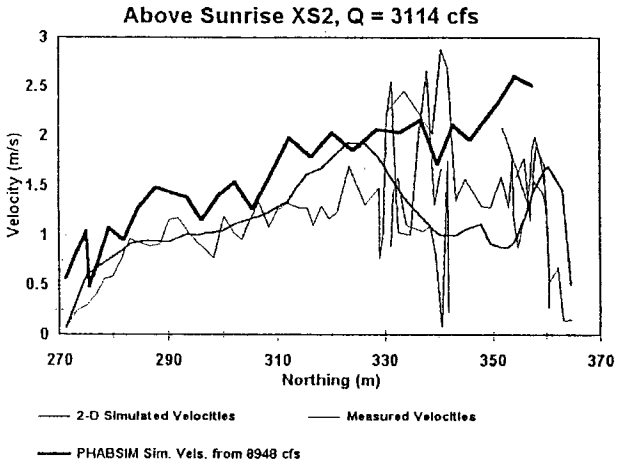
Above Sunrise XS2, Q = 3114 cfs
Velocity (m/s)
Northing (m)
2-D Simulated Velocities
Measured Velocities
PHABSIM Sim. Vels. from 8948 cfs

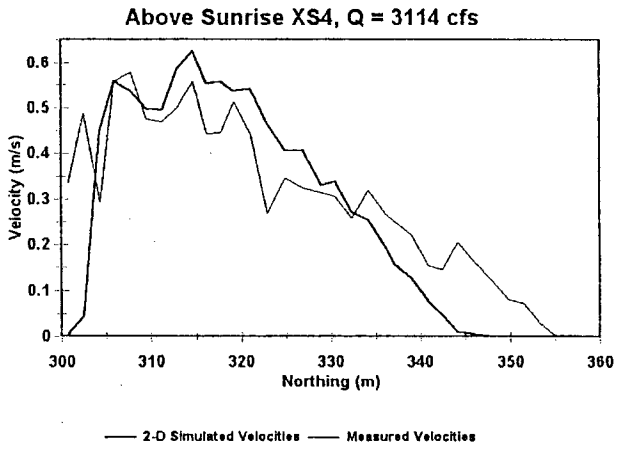
Above Sunrise XS4, Q = 3114 cfs
Velocity (m/s)
Northing (m)
2-D Simulated Velocities
Measured Velocities

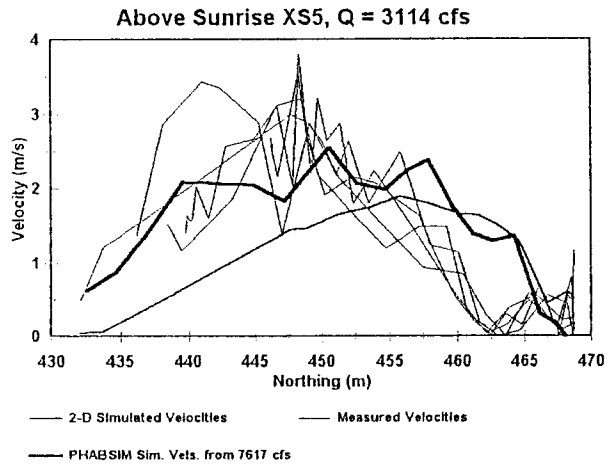
Above Sunrise XS5, Q = 3114 cfs
Velocity (m/s)
Northing (m)
2-D Simulated Velocities
Measured Velocities
PHABSIM Sim. Vels. from 7617 cfs

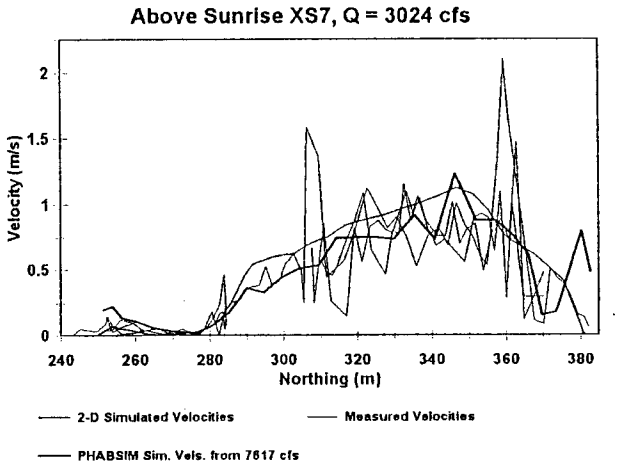
Above Sunrise XS7, Q = 3024 cfs
Velocity (m/s)
Northing (m)
2-D Simulated Velocities
Measured Velocities
PHABSIM Sim. Vels. from 7617 cfs

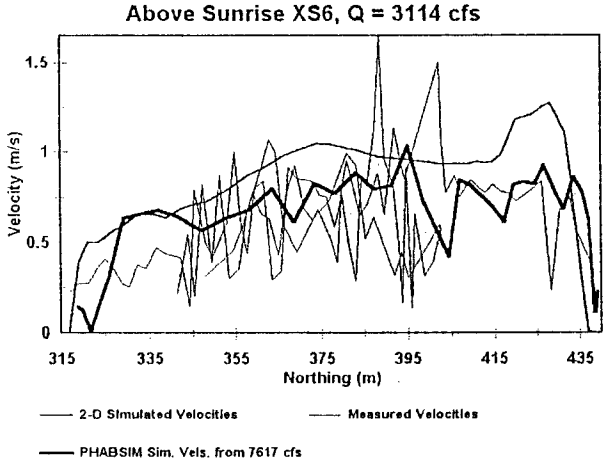
Above Sunrise XS6, Q = 3114 cfs
Velocity (m/s)
Northing (m)
2-D Simulated Velocities
Measured Velocities
PHABSIM Sim. Vels. from 7617 cfs

Above Sunrise

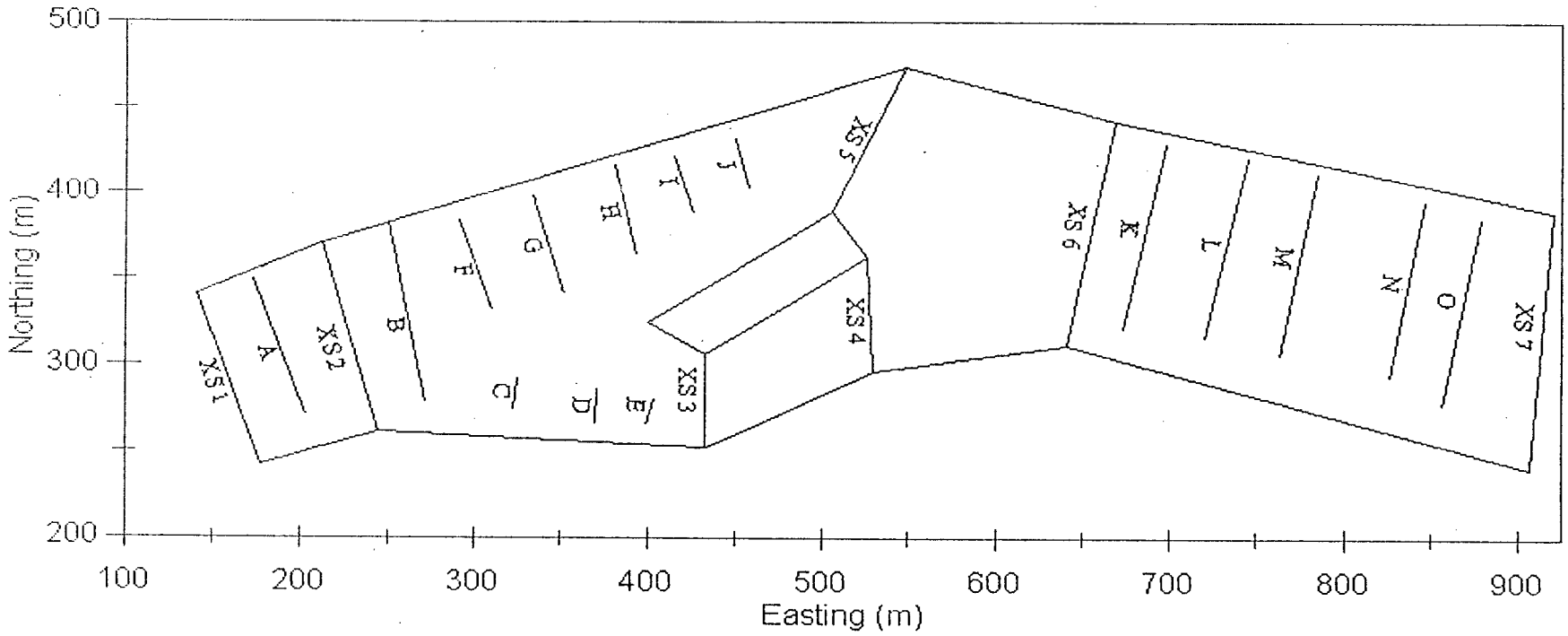

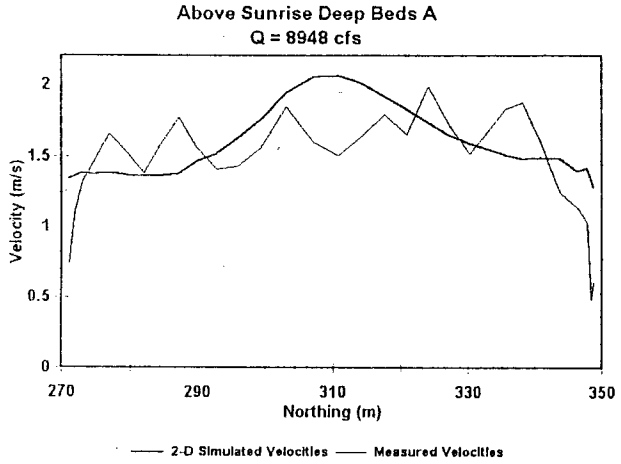
Above Sunrise Deep Beds A
Q = 8948 cfs
Velocity (m/s)
0
0.5
1
1.5
2
270
290
310
330
350
Northing (m)
2-D Simulated Velocities
Measured Velocities

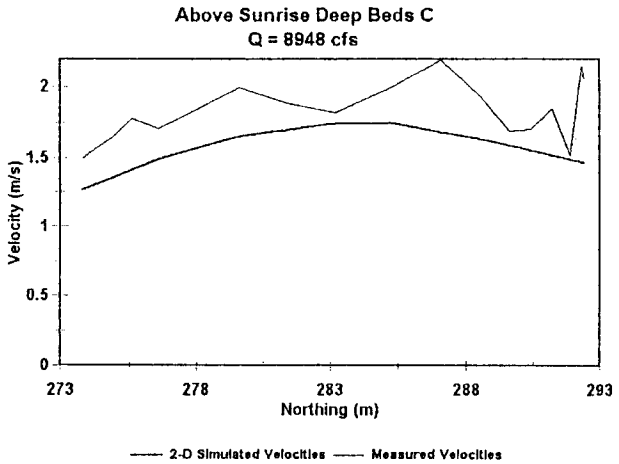
Above Sunrise Deep Beds C
Q = 8948 cfs
Velocity (m/s)
0
0.5
1
1.5
2
273
278
283
288
293
Northing (m)
2-D Simulated Velocities
Measured Velocities

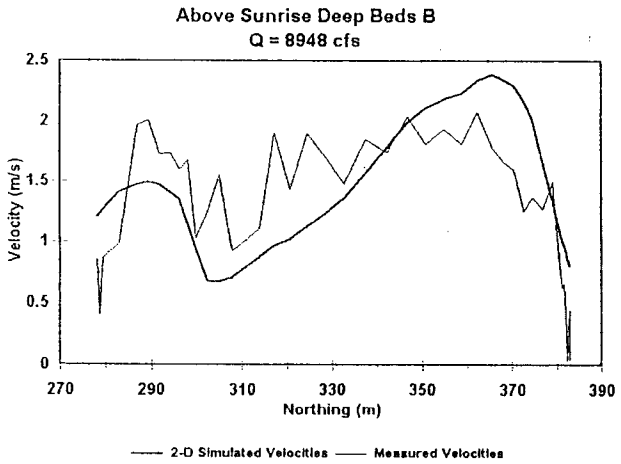
Above Sunrise Deep Beds B
Q = 8948 cfs
Velocity (m/s)
0
0.5
1
1.5
2
2.5
270
290
310
330
350
370
390
Northing (m)
2-D Simulated Velocities
Measured Velocities

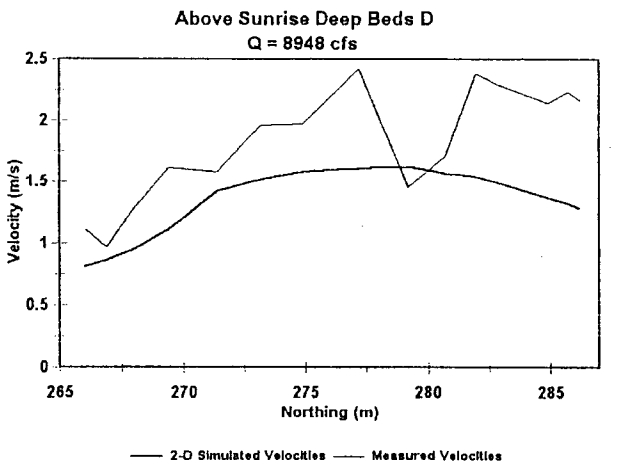
Above Sunrise Deep Beds D
Q = 8948 cfs
Velocity (m/s)
0
0.5
1
1.5
2
2.5
265
270
275
280
285
Northing (m)
2-D Simulated Velocities
Measured Velocities

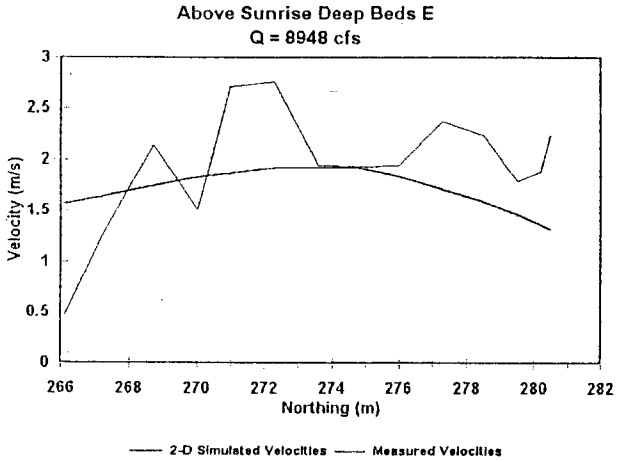
Above Sunrise Deep Beds E
Q = 8948 cfs
Velocity (m/s)
Northing (m)
2-D Simulated Velocities
Measured Velocities

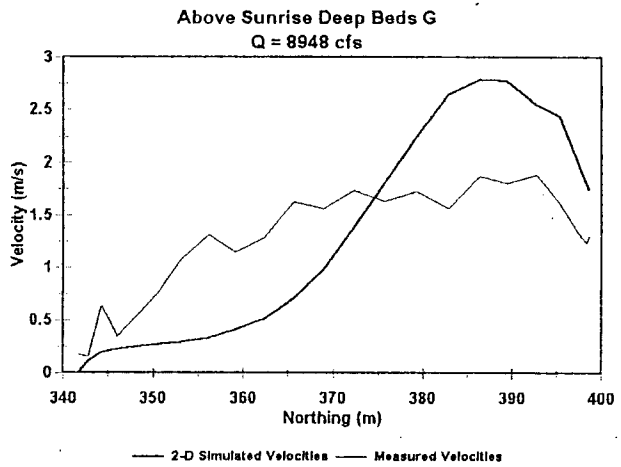
Above Sunrise Deep Beds G
Q = 8948 cfs
Velocity (m/s)
Northing (m)
2-D Simulated Velocities
Measured Velocities

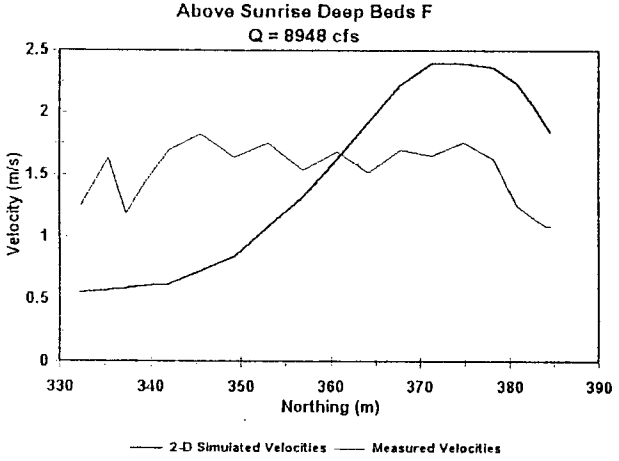
Above Sunrise Deep Beds F
Q = 8948 cfs
Velocity (m/s)
Northing (m)
2-D Simulated Velocities
Measured Velocities

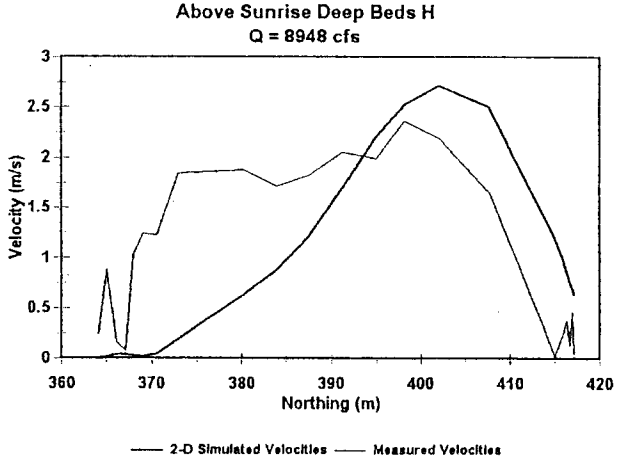
Above Sunrise Deep Beds H
Q = 8948 cfs
Velocity (m/s)
Northing (m)
2-D Simulated Velocities
Measured Velocities

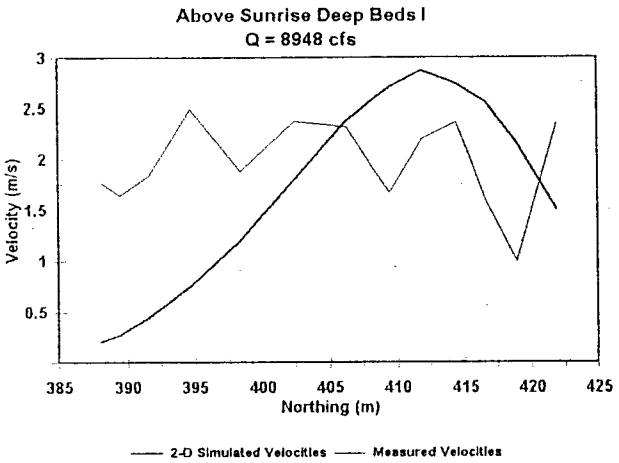
Above Sunrise Deep Beds I
Q = 8948 cfs
Velocity (m/s)
Northing (m)
2-D Simulated Velocities
Measured Velocities

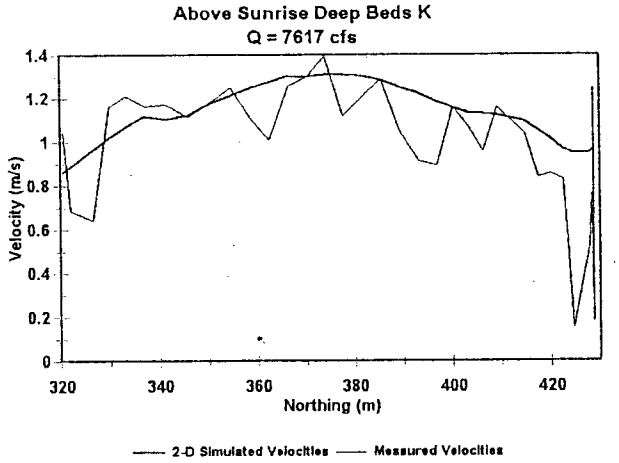
Above Sunrise Deep Beds K
Q = 7617 cfs
Velocity (m/s)
Northing (m)
2-D Simulated Velocities
Measured Velocities

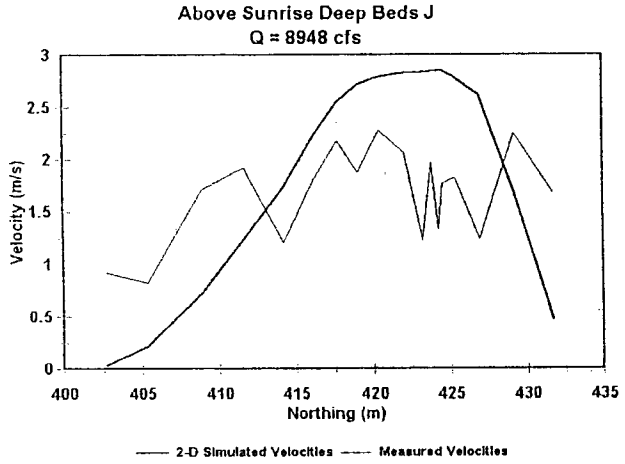
Above Sunrise Deep Beds J
Q = 8948 cfs
Velocity (m/s)
Northing (m)
2-D Simulated Velocities
Measured Velocities

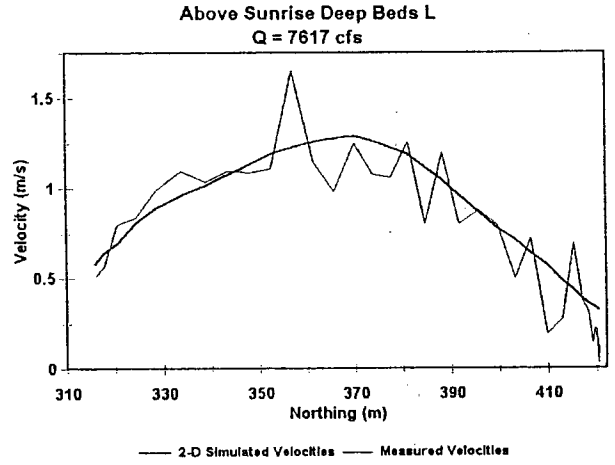
Above Sunrise Deep Beds L
Q = 7617 cfs
Velocity (m/s)
Northing (m)
2-D Simulated Velocities
Measured Velocities

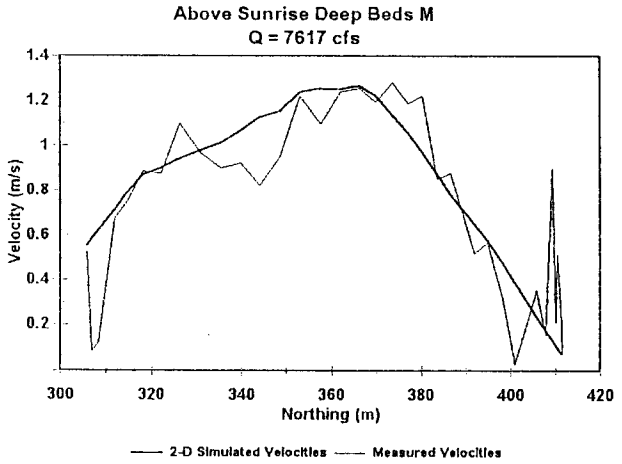
Above Sunrise Deep Beds M
Q = 7617 cfs
Velocity (m/s)
1.4
1.2
1
0.8
0.6
0.4
0.2
300
320
340
360
380
400
420
Northing (m)
2-D Simulated Velocities
Measured Velocities

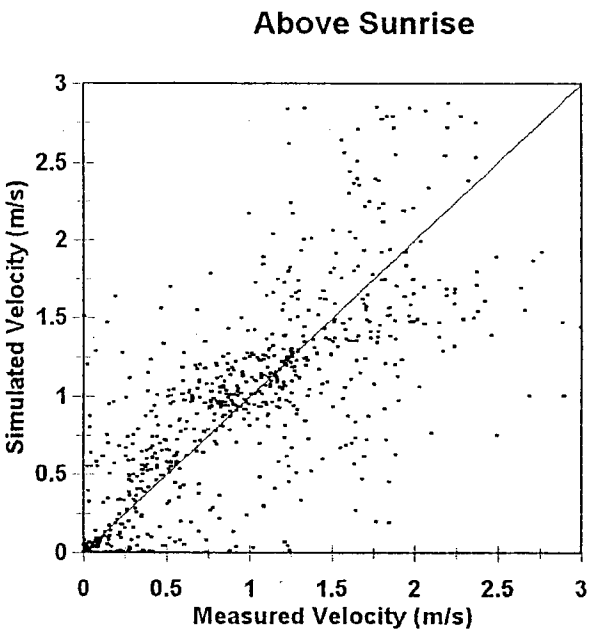
Above Sunrise
Simulated Velocity (m/s)
3
2.5
2
1.5
1
0.5
0
0
0.5
1
1.5
2
2.5
3
Measured Velocity (m/s)

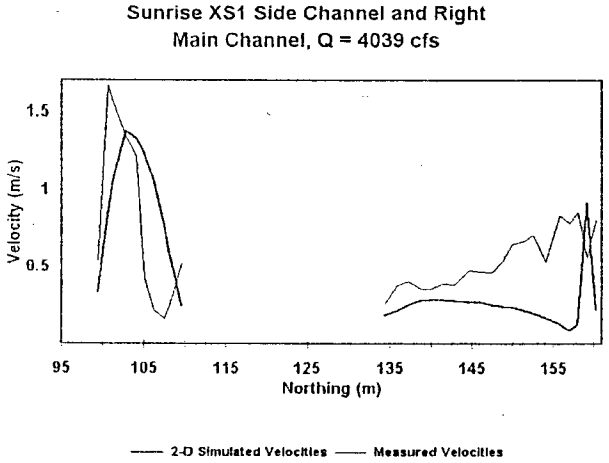
Sunrise XS1 Side Channel and Right Main Channel, Q = 4039 cfs
Velocity (m/s)
1.5
1
0.5
95
105
115
125
135
145
155
Northing (m)
2-D Simulated Velocities
Measured Velocities

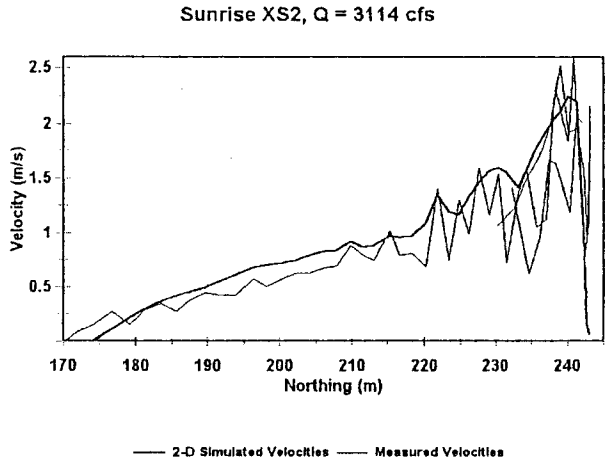
Sunrise XS2, Q = 3114 cfs
Velocity (m/s)
2.5
2
1.5
1
0.5
170
180
190
200
210
220
230
240
Northing (m)
2-D Simulated Velocities
Measured Velocities

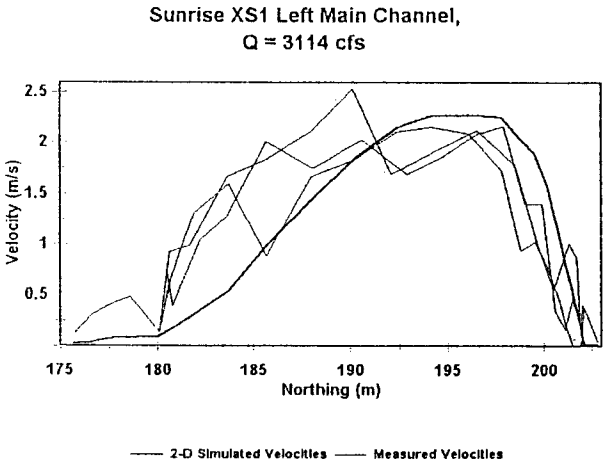
Sunrise XS1 Left Main Channel, Q = 3114 cfs
Velocity (m/s)
2.5
2
1.5
1
0.5
175
180
185
190
195
200
Northing (m)
2-D Simulated Velocities
Measured Velocities

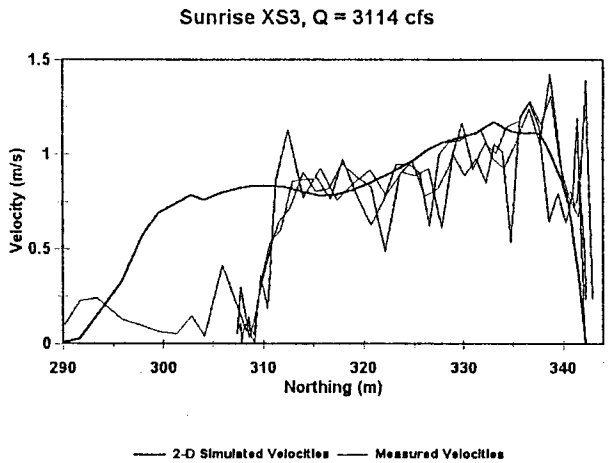
Sunrise XS3, Q = 3114 cfs
Velocity (m/s)
1.5
1
0.5
0
290
300
310
320
330
340
Northing (m)
2-D Simulated Velocities
Measured Velocities

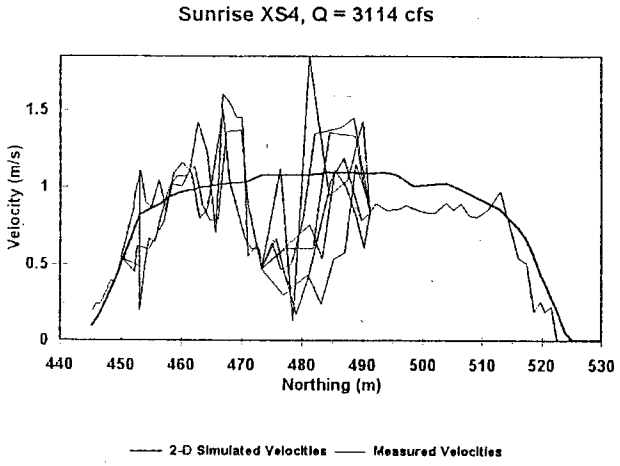
Sunrise XS4, Q = 3114 cfs
Velocity (m/s)
0
0.5
1
1.5
440
450
460
470
480
490
500
510
520
530
Northing (m)
2-D Simulated Velocities
Measured Velocities

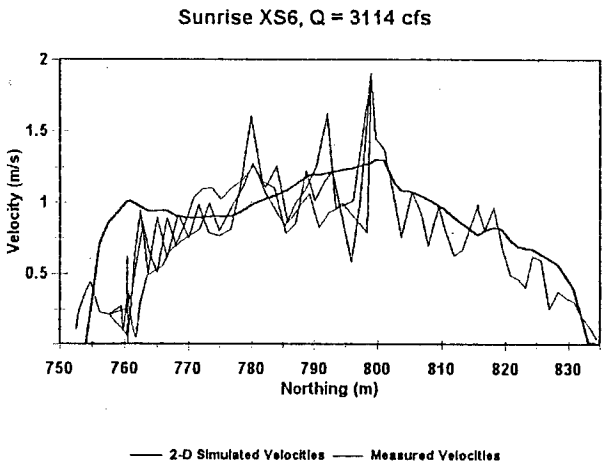
Sunrise XS6, Q = 3114 cfs
Velocity (m/s)
0.5
1
1.5
2
750
760
770
780
790
800
810
820
830
Northing (m)
2-D Simulated Velocities
Measured Velocities

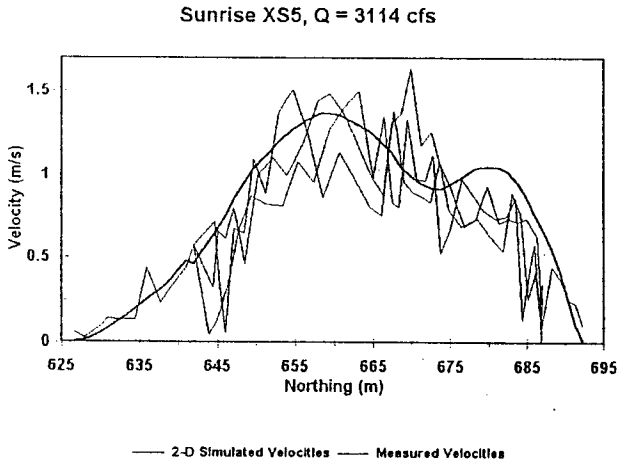
Sunrise XS5, Q = 3114 cfs
Velocity (m/s)
0
0.5
1
1.5
625
635
645
655
665
675
685
695
Northing (m)
2-D Simulated Velocities
Measured Velocities

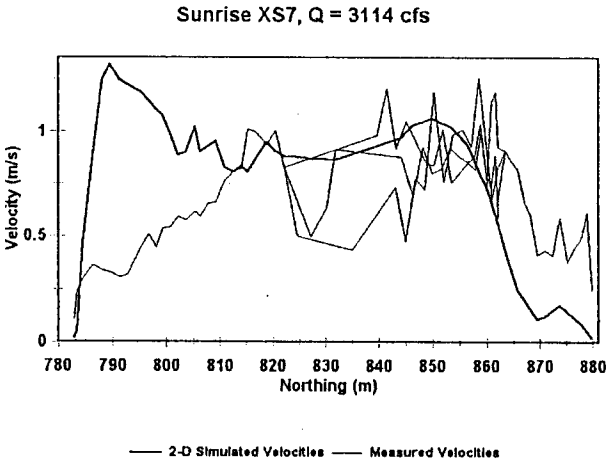
Sunrise XS7, Q = 3114 cfs
Velocity (m/s)
0
0.5
1
780
790
800
810
820
830
840
850
860
870
880
Northing (m)
2-D Simulated Velocities
Measured Velocities

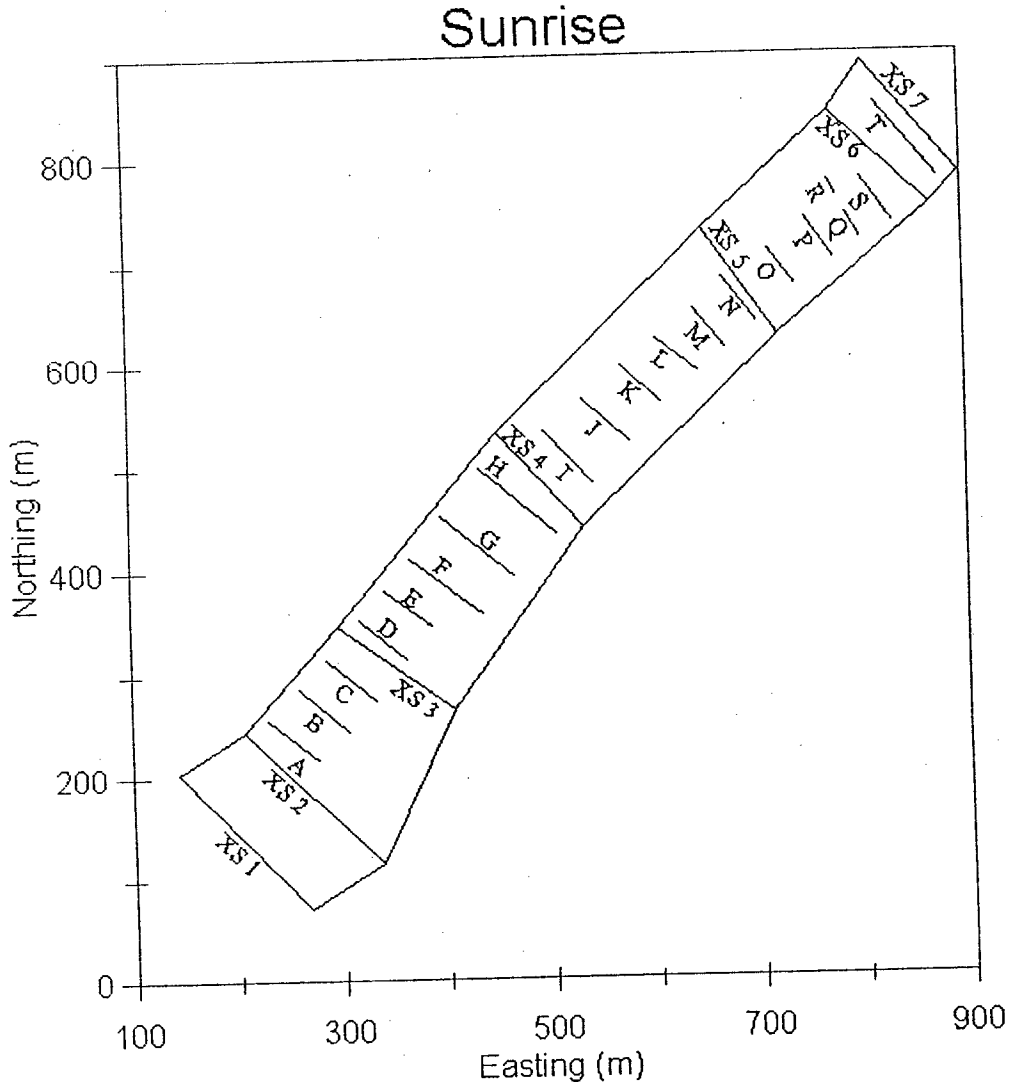
Sunrise
Northing (m)
0
200
400
600
800
100
300
500
700
900
Easting (m)
XS1
XS2
XS3
XS4
XS5
XS6
XS7
A
B
C
D
E
F
G
H
I
J
K
L
M
N
O
P
Q
R
S
T

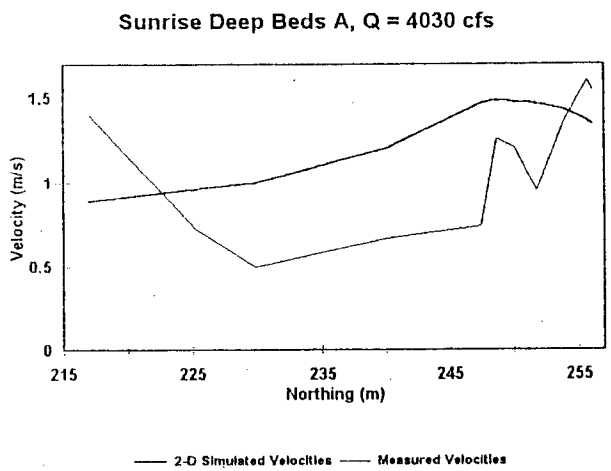
Sunrise Deep Beds A, Q = 4030 cfs
Velocity (m/s)
1.5
1
0.5
0
215
225
235
245
255
Northing (m)
2-D Simulated Velocities
Measured Velocities

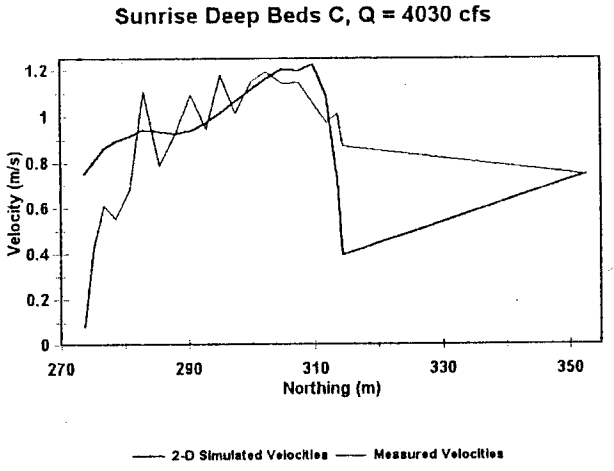
Sunrise Deep Beds C, Q = 4030 cfs
Velocity (m/s)
1.2
1
0.8
0.6
0.4
0.2
0
270
290
310
330
350
Northing (m)
2-D Simulated Velocities
Measured Velocities

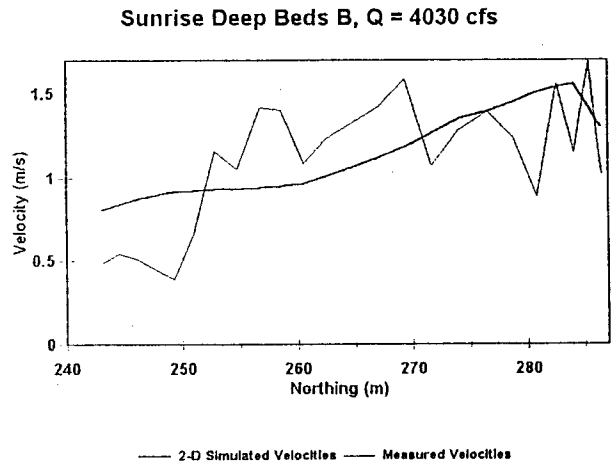
Sunrise Deep Beds B, Q = 4030 cfs
Velocity (m/s)
1.5
1
0.5
0
240
250
260
270
280
Northing (m)
2-D Simulated Velocities
Measured Velocities

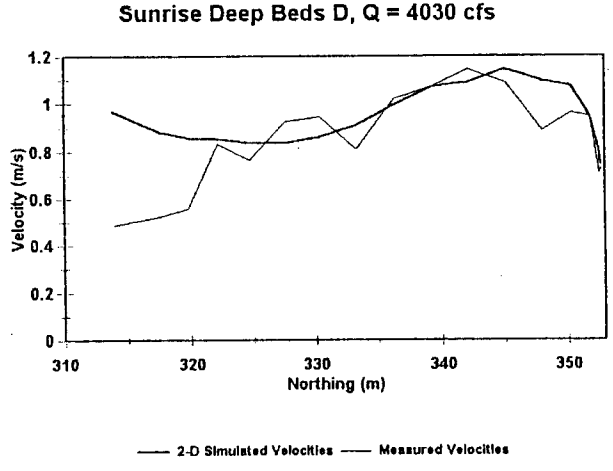
Sunrise Deep Beds D, Q = 4030 cfs
Velocity (m/s)
1.2
1
0.8
0.6
0.4
0.2
0
310
320
330
340
350
Northing (m)
2-D Simulated Velocities
Measured Velocities

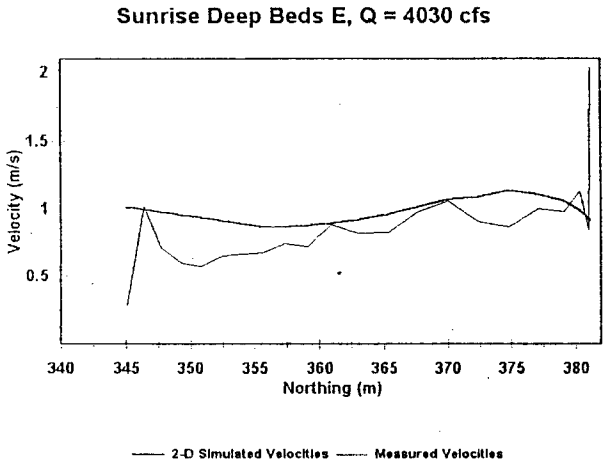
Sunrise Deep Beds E, Q = 4030 cfs
Velocity (m/s)
2
1.5
1
0.5
340
345
350
355
360
365
370
375
380
Northing (m)
2-D Simulated Velocities
Measured Velocities

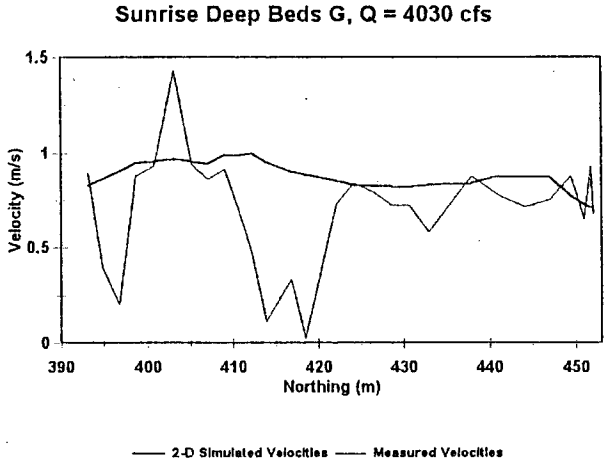
Sunrise Deep Beds G, Q = 4030 cfs
Velocity (m/s)
1.5
1
0.5
0
390
400
410
420
430
440
450
Northing (m)
2-D Simulated Velocities
Measured Velocities

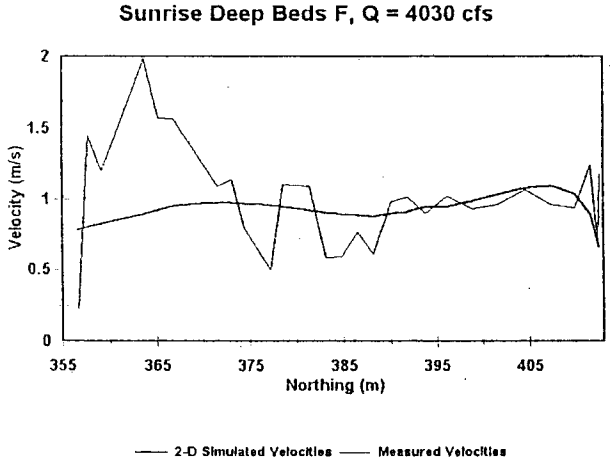
Sunrise Deep Beds F, Q = 4030 cfs
Velocity (m/s)
2
1.5
1
0.5
0
355
365
375
385
395
405
Northing (m)
2-D Simulated Velocities
Measured Velocities

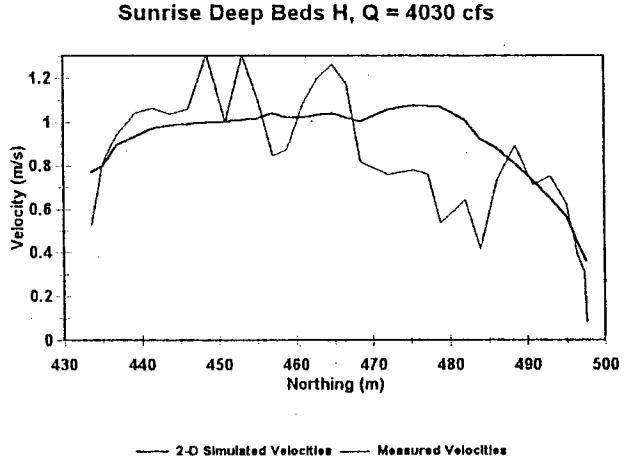
Sunrise Deep Beds H, Q = 4030 cfs
Velocity (m/s)
1.2
1
0.8
0.6
0.4
0.2
0
430
440
450
460
470
480
490
500
Northing (m)
2-D Simulated Velocities
Measured Velocities

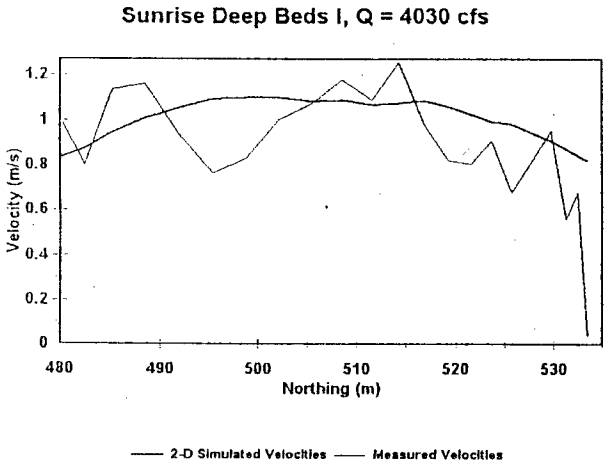
Sunrise Deep Beds I, Q = 4030 cfs
Velocity (m/s)
1.2
1
0.8
0.6
0.4
0.2
0
480
490
500
510
520
530
Northing (m)
2-D Simulated Velocities
Measured Velocities

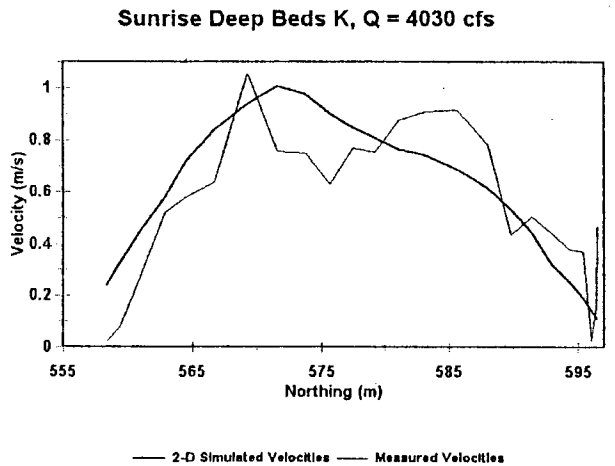
Sunrise Deep Beds K, Q = 4030 cfs
Velocity (m/s)
1
0.8
0.6
0.4
0.2
0
555
565
575
585
595
Northing (m)
2-D Simulated Velocities
Measured Velocities

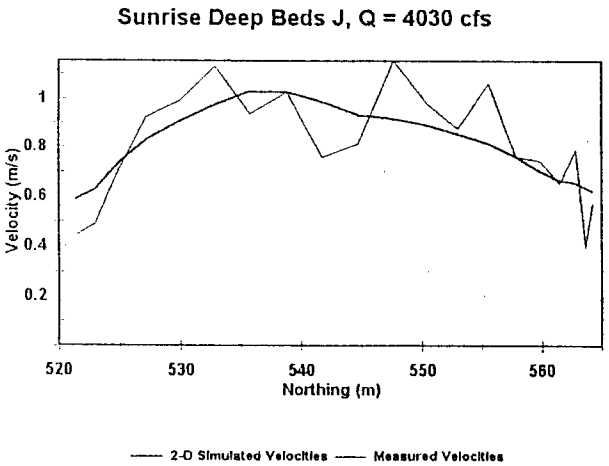
Sunrise Deep Beds J, Q = 4030 cfs
Velocity (m/s)
1
0.8
0.6
0.4
0.2
520
530
540
550
560
Northing (m)
2-D Simulated Velocities
Measured Velocities

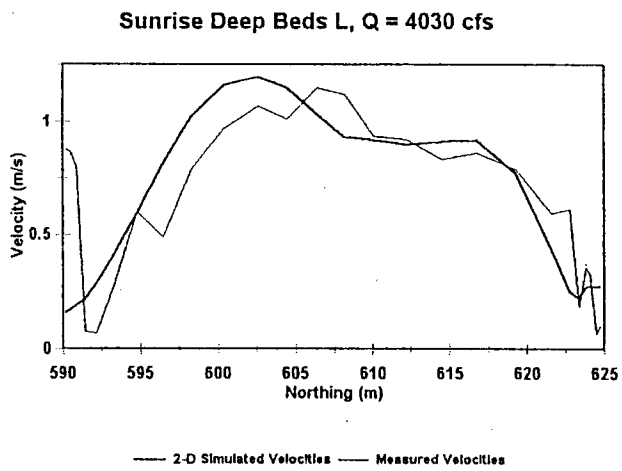
Sunrise Deep Beds L, Q = 4030 cfs
Velocity (m/s)
1
0.5
0
590
595
600
605
610
615
620
625
Northing (m)
2-D Simulated Velocities
Measured Velocities

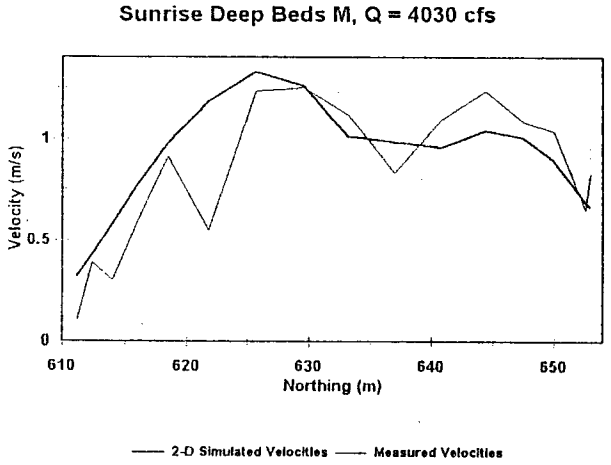
Sunrise Deep Beds M, Q = 4030 cfs
Velocity (m/s)
0
0.5
1
610
620
630
640
650
Northing (m)
2-D Simulated Velocities
Measured Velocities

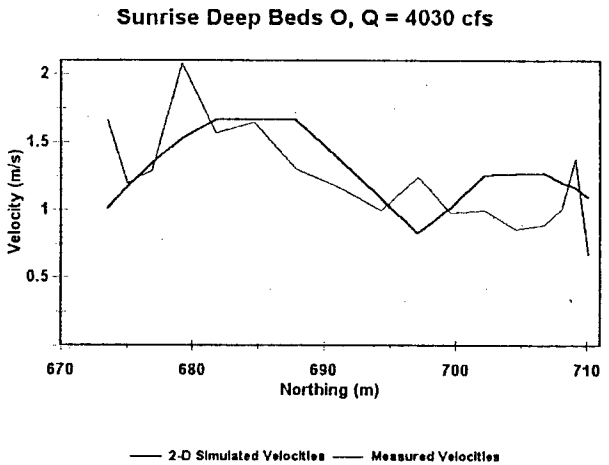
Sunrise Deep Beds O, Q = 4030 cfs
Velocity (m/s)
0.5
1
1.5
2
670
680
690
700
710
Northing (m)
2-D Simulated Velocities
Measured Velocities

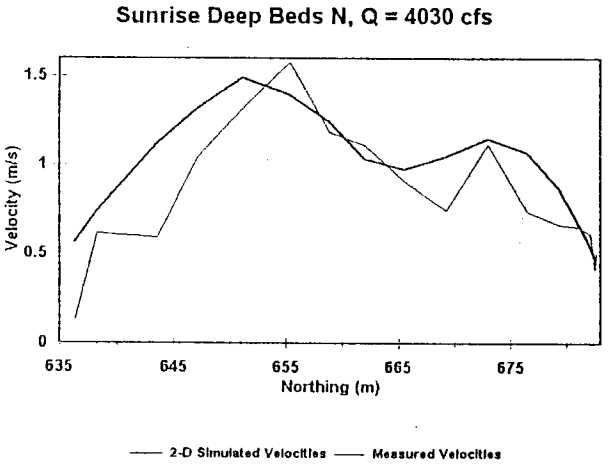
Sunrise Deep Beds N, Q = 4030 cfs
Velocity (m/s)
0
0.5
1
1.5
635
645
655
665
675
Northing (m)
2-D Simulated Velocities
Measured Velocities

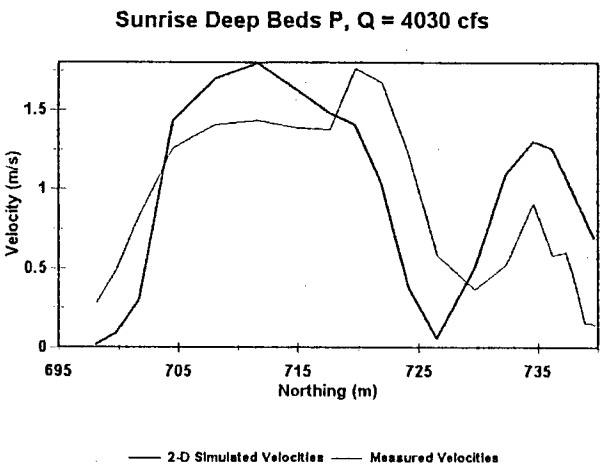
Sunrise Deep Beds P, Q = 4030 cfs
Velocity (m/s)
0
0.5
1
1.5
695
705
715
725
735
Northing (m)
2-D Simulated Velocities
Measured Velocities

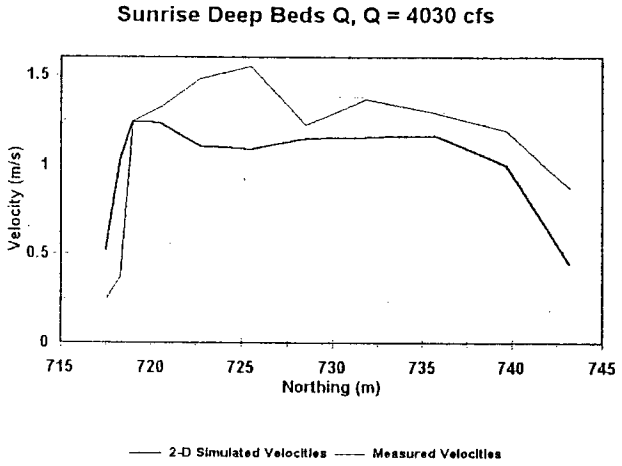
Sunrise Deep Beds Q, Q = 4030 cfs
Velocity (m/s)
1.5
1
0.5
0
715
720
725
730
735
740
745
Northing (m)
2-D Simulated Velocities
Measured Velocities

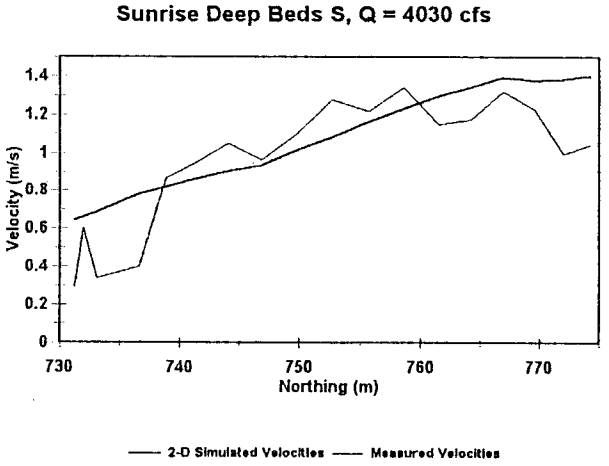
Sunrise Deep Beds S, Q = 4030 cfs
Velocity (m/s)
1.4
1.2
1
0.8
0.6
0.4
0.2
0
730
740
750
760
770
Northing (m)
2-D Simulated Velocities
Measured Velocities

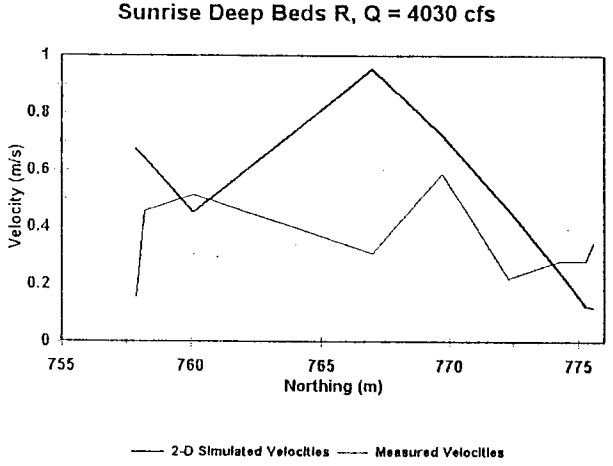
Sunrise Deep Beds R, Q = 4030 cfs
Velocity (m/s)
1
0.8
0.6
0.4
0.2
0
755
760
765
770
775
Northing (m)
2-D Simulated Velocities
Measured Velocities

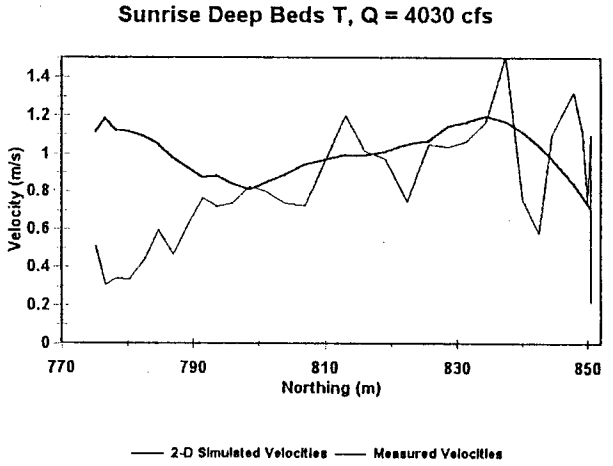
Sunrise Deep Beds T, Q = 4030 cfs
Velocity (m/s)
1.4
1.2
1
0.8
0.6
0.4
0.2
0
770
790
810
830
850
Northing (m)
2-D Simulated Velocities
Measured Velocities

Sunrise

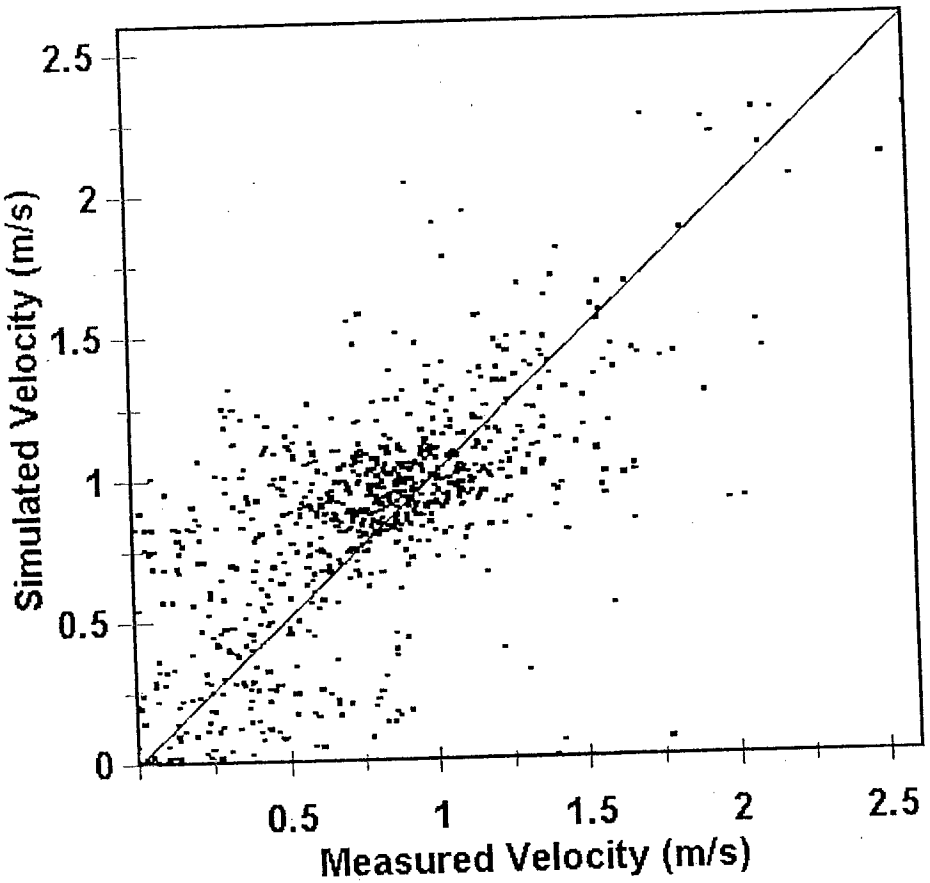
2.5
2
1.5
1
0.5
0
Simulated Velocity (m/s)
0.5
1
1.5
2
2.5
Measured Velocity (m/s)

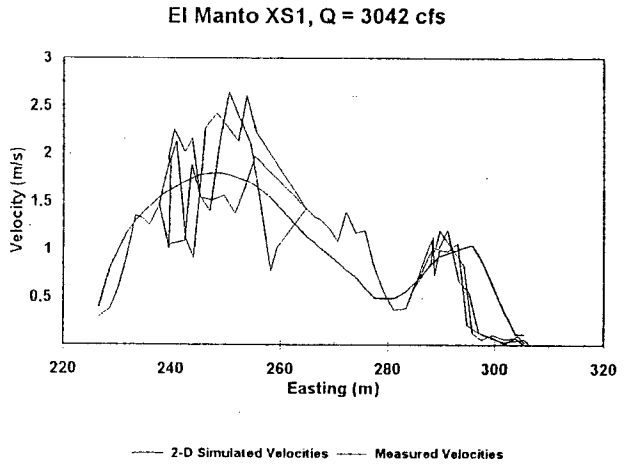
El Manto XS1, Q = 3042 cfs
Velocity (m/s)
Easting (m)
2-D Simulated Velocities
Measured Velocities

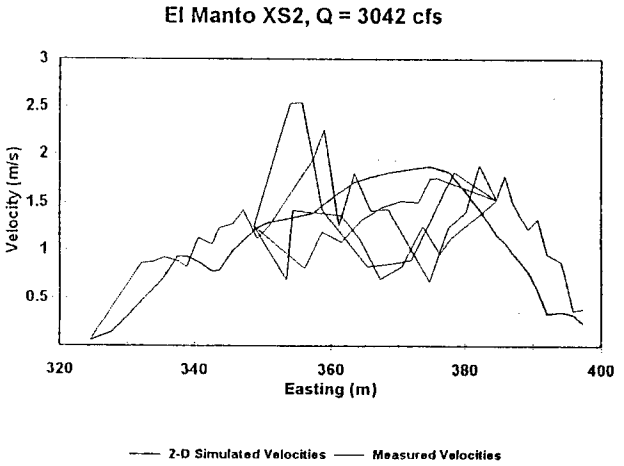
El Manto XS2, Q = 3042 cfs
Velocity (m/s)
Easting (m)
2-D Simulated Velocities
Measured Velocities

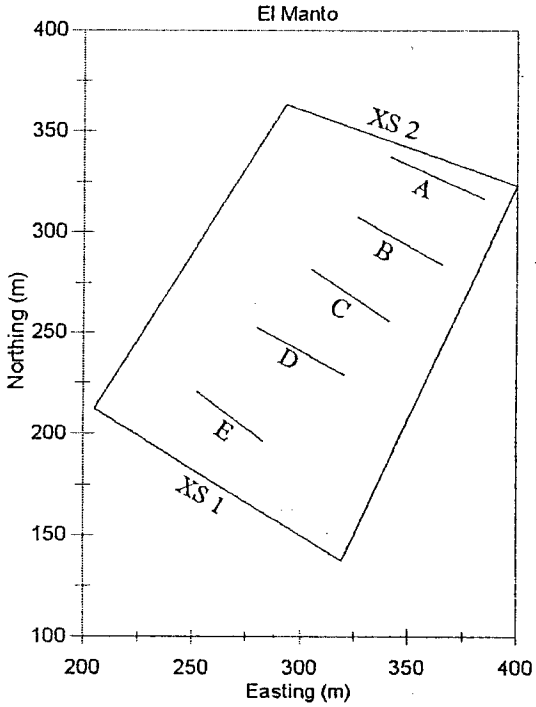
El Manto
XS 2
XS 1
A
B
C
D
E
Northing (m)
Easting (m)

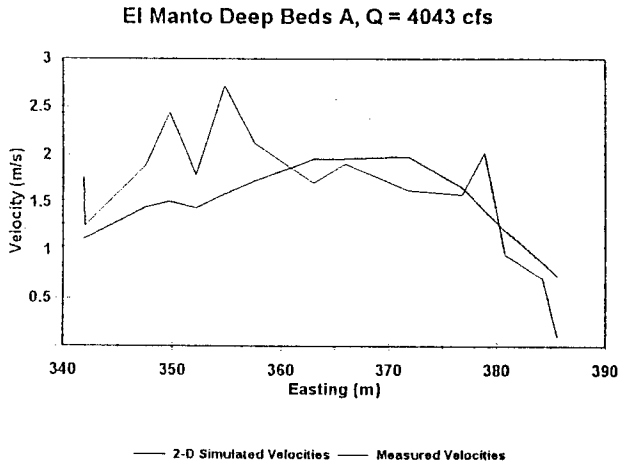
El Manto Deep Beds A, Q = 4043 cfs
Velocity (m/s)
Easting (m)
2-D Simulated Velocities
Measured Velocities

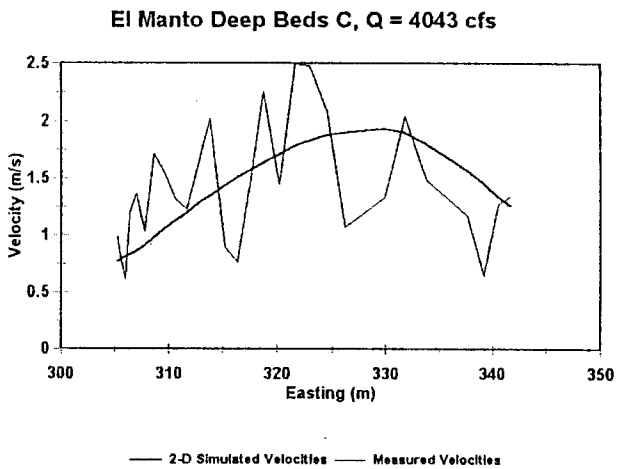
El Manto Deep Beds C, Q = 4043 cfs
Velocity (m/s)
Easting (m)
2-D Simulated Velocities
Measured Velocities

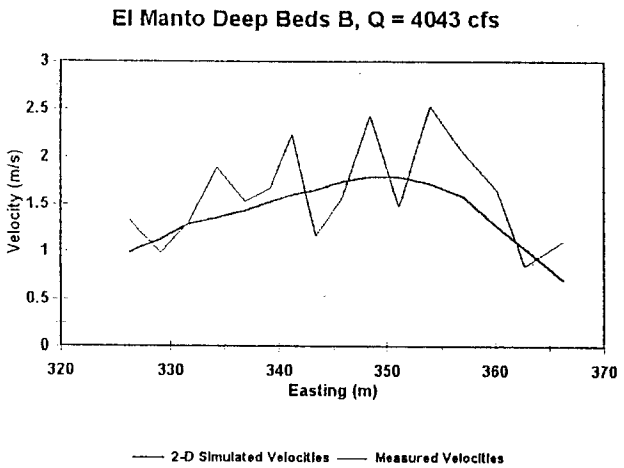
El Manto Deep Beds B, Q = 4043 cfs
Velocity (m/s)
Easting (m)
2-D Simulated Velocities
Measured Velocities

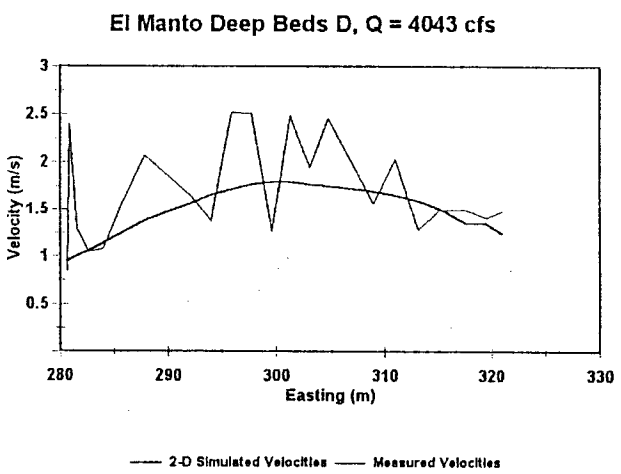
El Manto Deep Beds D, Q = 4043 cfs
Velocity (m/s)
Easting (m)
2-D Simulated Velocities
Measured Velocities

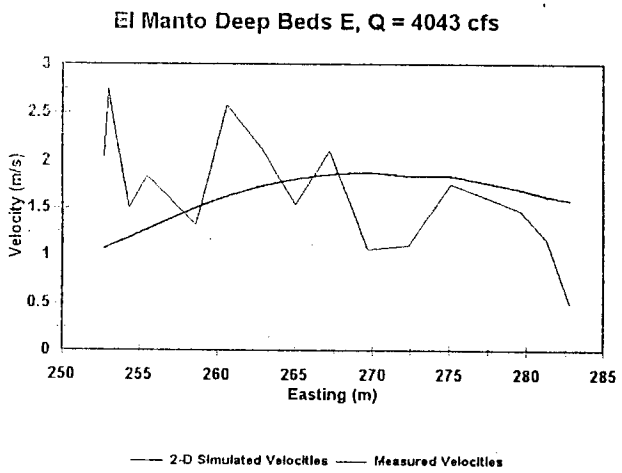
El Manto Deep Beds E, Q = 4043 cfs
Velocity (m/s)
Easting (m)
2-D Simulated Velocities
Measured Velocities

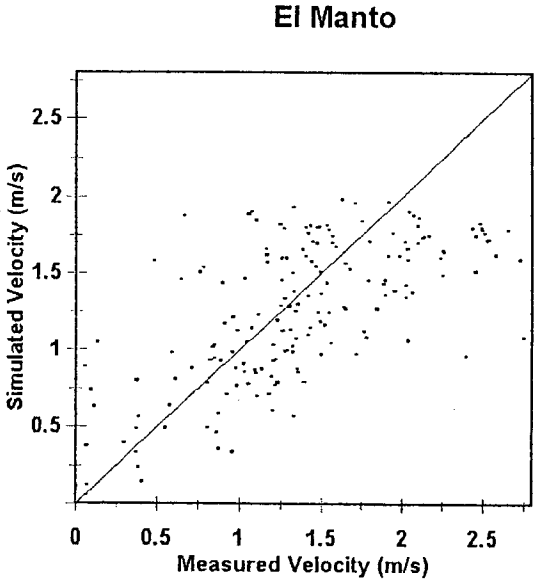
El Manto
Simulated Velocity (m/s)
Measured Velocity (m/s)

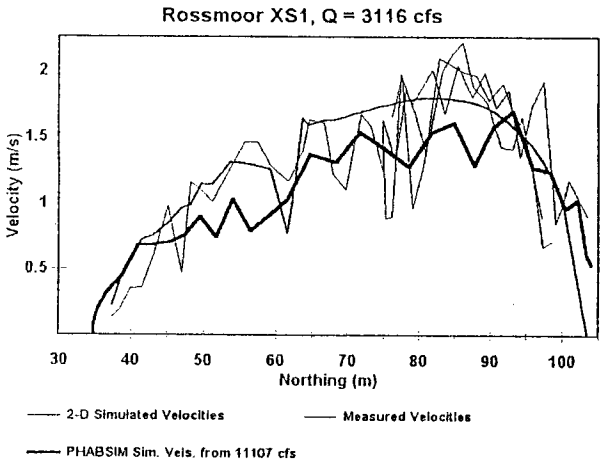
Rossmoor XS1, Q = 3116 cfs
Velocity (m/s)
Northing (m)
2-D Simulated Velocities
Measured Velocities
PHABSIM Sim. Vels. from 11107 cfs

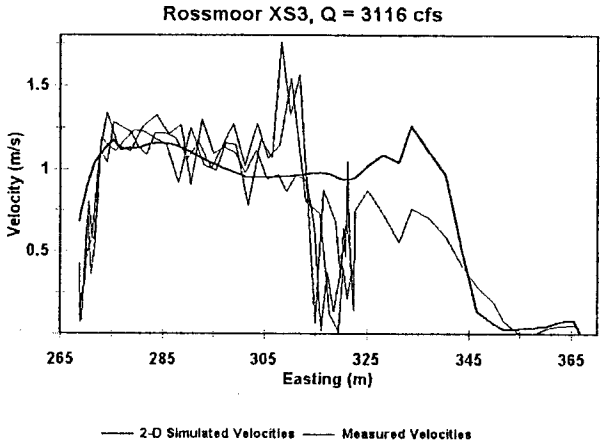
Rossmoor XS3, Q = 3116 cfs
Velocity (m/s)
Easting (m)
2-D Simulated Velocities
Measured Velocities

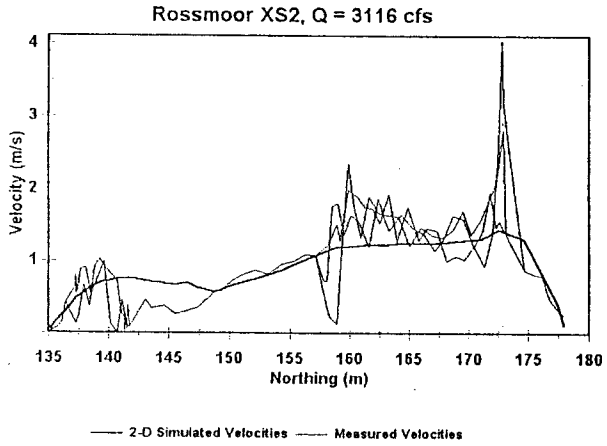
Rossmoor XS2, Q = 3116 cfs
Velocity (m/s)
Northing (m)
2-D Simulated Velocities
Measured Velocities

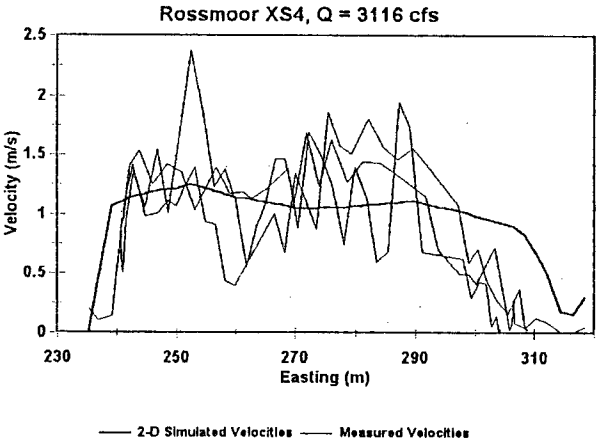
Rossmoor XS4, Q = 3116 cfs
Velocity (m/s)
Easting (m)
2-D Simulated Velocities
Measured Velocities

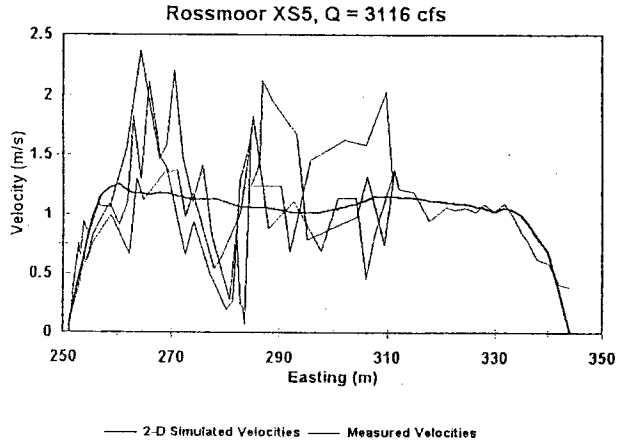
Rossmoor XS5, Q = 3116 cfs
Velocity (m/s)
2.5
2
1.5
1
0.5
0
250
270
290
310
330
350
Easting (m)
2-D Simulated Velocities
Measured Velocities

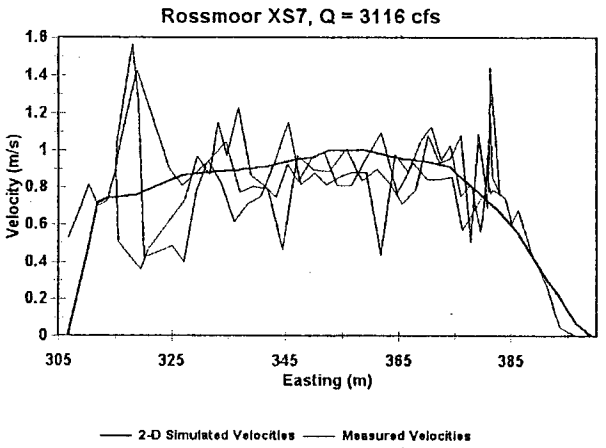
Rossmoor XS7, Q = 3116 cfs
Velocity (m/s)
1.8
1.4
1.2
1
0.8
0.6
0.4
0.2
0
305
325
345
365
385
Easting (m)
2-D Simulated Velocities
Measured Velocities

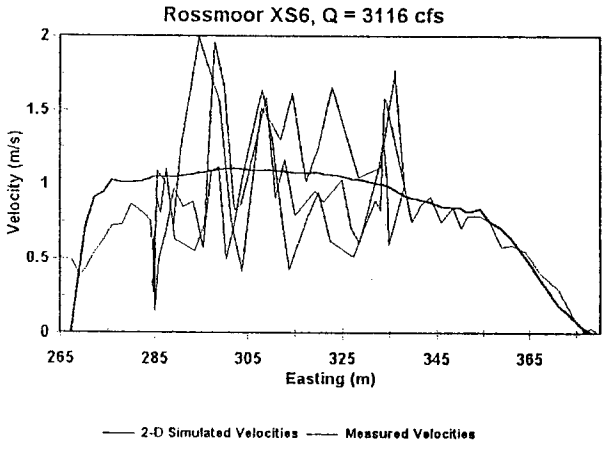
Rossmoor XS6, Q = 3116 cfs
Velocity (m/s)
2
1.5
1
0.5
0
265
285
305
325
345
365
Easting (m)
2-D Simulated Velocities
Measured Velocities

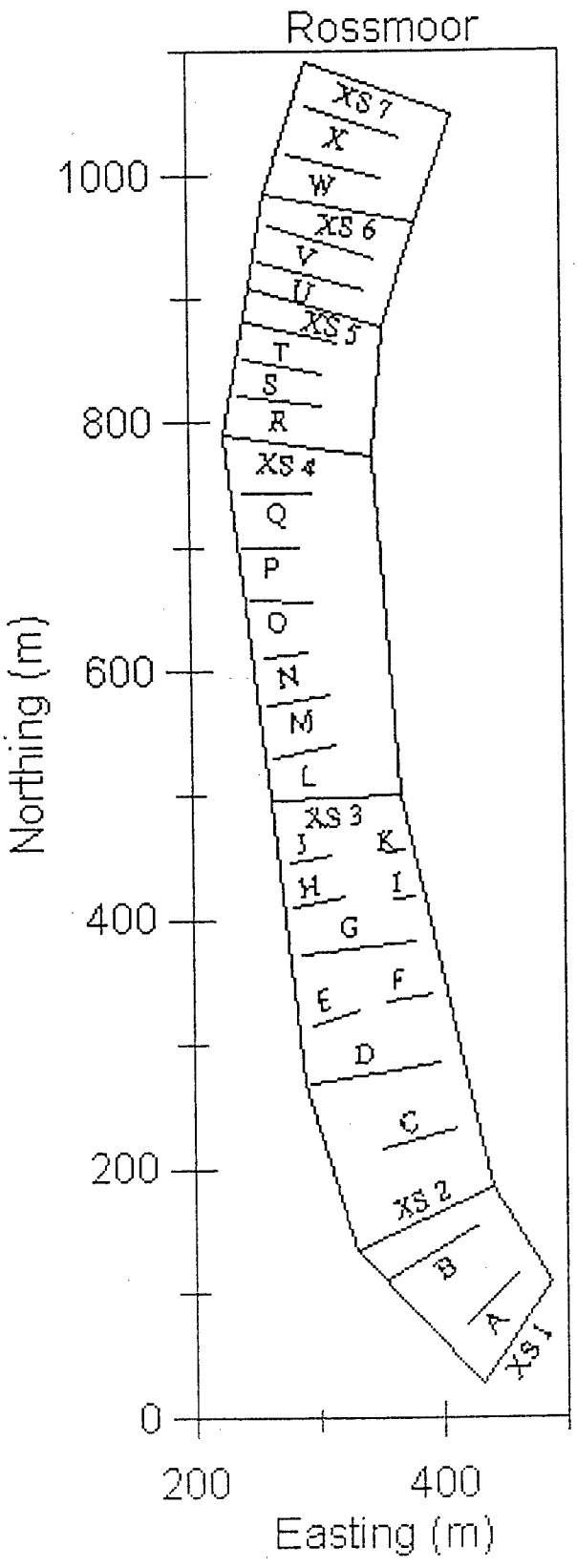
Rossmoor
XS 7
X
W
XS 6
V
U
XS 5
T
S
R
XS 4
Q
P
O
N
M
L
XS 3
J
K
H
I
G
E
F
D
C
XS 2
B
A
XS 1
1000
800
600
400
200
0
Northing (m)
200
400
Easting (m)

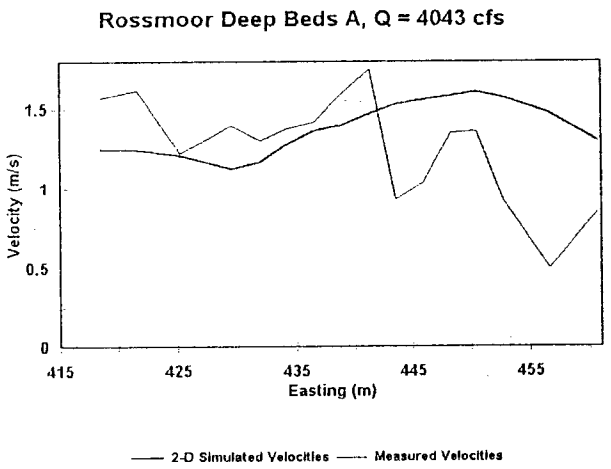
Rossmoor Deep Beds A, Q = 4043 cfs
Velocity (m/s)
0
0.5
1
1.5
415
425
435
445
455
Easting (m)
2-D Simulated Velocities
Measured Velocities

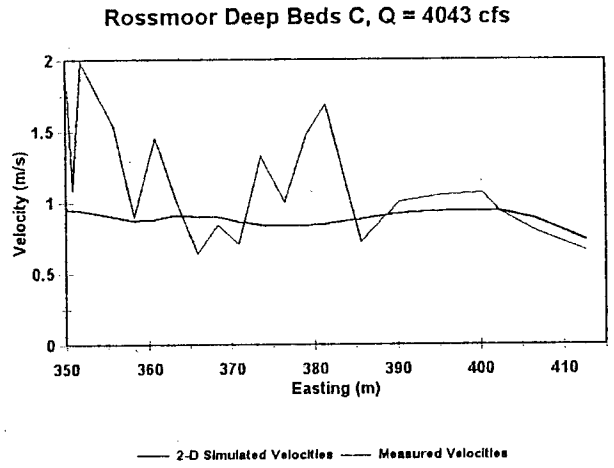
Rossmoor Deep Beds C, Q = 4043 cfs
Velocity (m/s)
0
0.5
1
1.5
2
350
360
370
380
390
400
410
Easting (m)
2-D Simulated Velocities
Measured Velocities

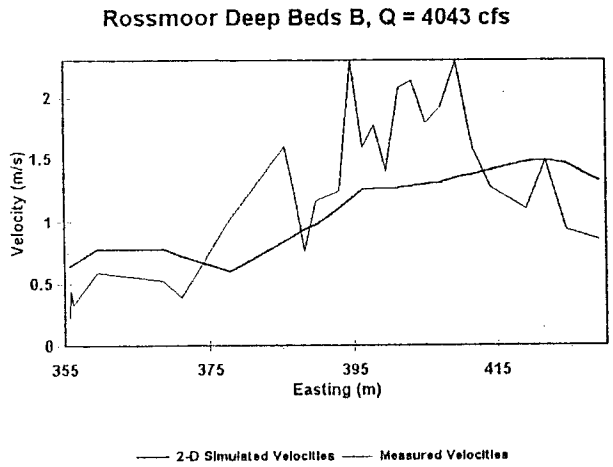
Rossmoor Deep Beds B, Q = 4043 cfs
Velocity (m/s)
0
0.5
1
1.5
2
355
375
395
415
Easting (m)
2-D Simulated Velocities
Measured Velocities

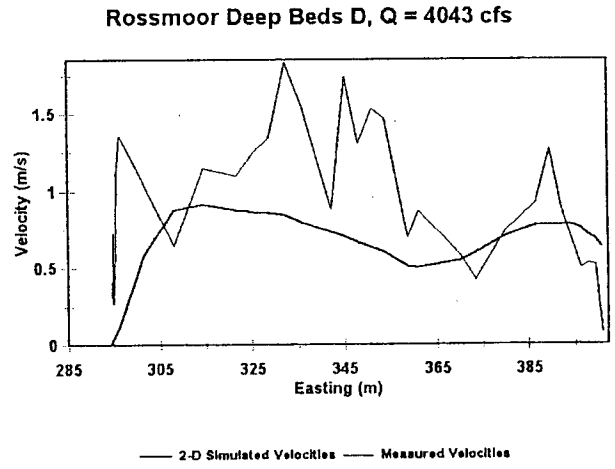
Rossmoor Deep Beds D, Q = 4043 cfs
Velocity (m/s)
0
0.5
1
1.5
285
305
325
345
365
385
Easting (m)
2-D Simulated Velocities
Measured Velocities

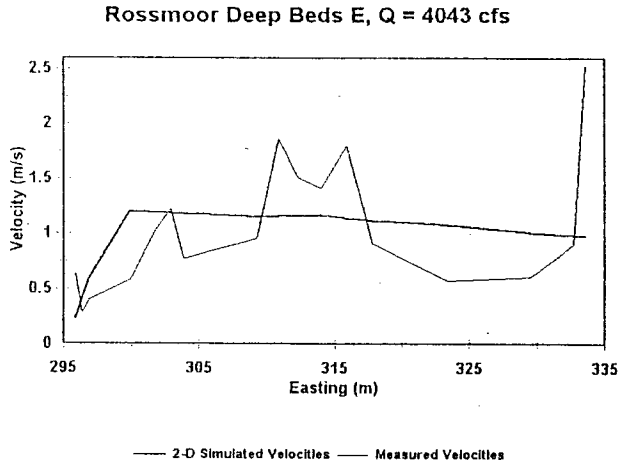
Rossmoor Deep Beds E, Q = 4043 cfs
Velocity (m/s)
2.5
2
1.5
1
0.5
0
295
305
315
325
335
Easting (m)
2-D Simulated Velocities
Measured Velocities

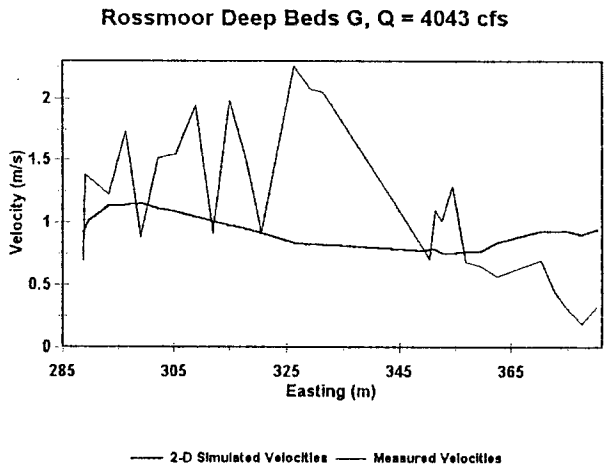
Rossmoor Deep Beds G, Q = 4043 cfs
Velocity (m/s)
2
1.5
1
0.5
0
285
305
325
345
365
Easting (m)
2-D Simulated Velocities
Measured Velocities

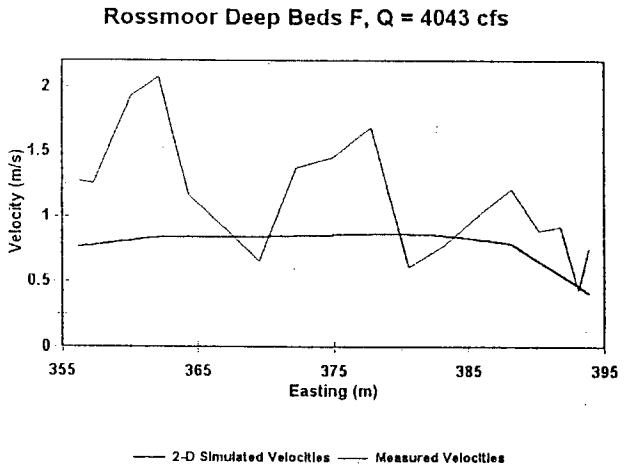
Rossmoor Deep Beds F, Q = 4043 cfs
Velocity (m/s)
2
1.5
1
0.5
0
355
365
375
385
395
Easting (m)
2-D Simulated Velocities
Measured Velocities

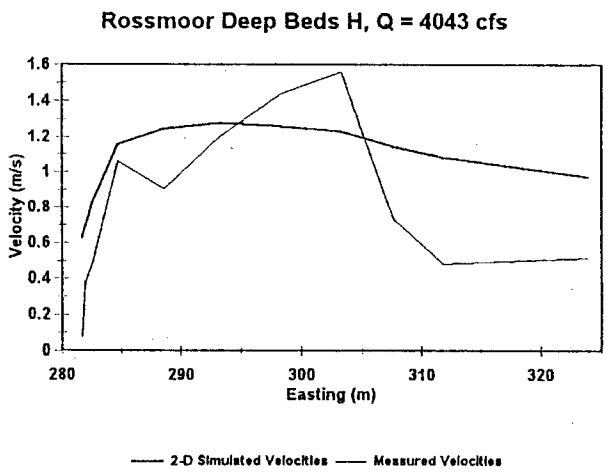
Rossmoor Deep Beds H, Q = 4043 cfs
Velocity (m/s)
1.6
1.4
1.2
1
0.8
0.6
0.4
0.2
0
280
290
300
310
320
Easting (m)
2-D Simulated Velocities
Measured Velocities

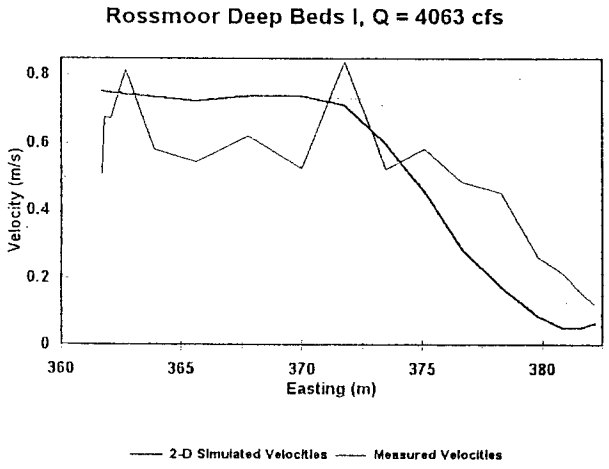
Rossmoor Deep Beds I, Q = 4063 cfs
Velocity (m/s)
0
0.2
0.4
0.6
0.8
360
365
370
375
380
Easting (m)
2-D Simulated Velocities
Measured Velocities

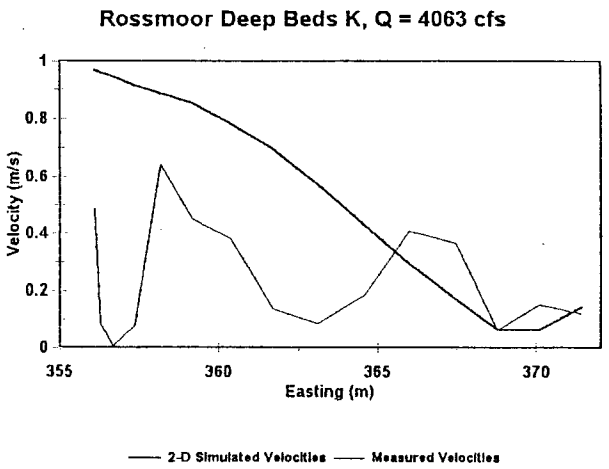
Rossmoor Deep Beds K, Q = 4063 cfs
Velocity (m/s)
0
0.2
0.4
0.6
0.8
1
355
360
365
370
Easting (m)
2-D Simulated Velocities
Measured Velocities

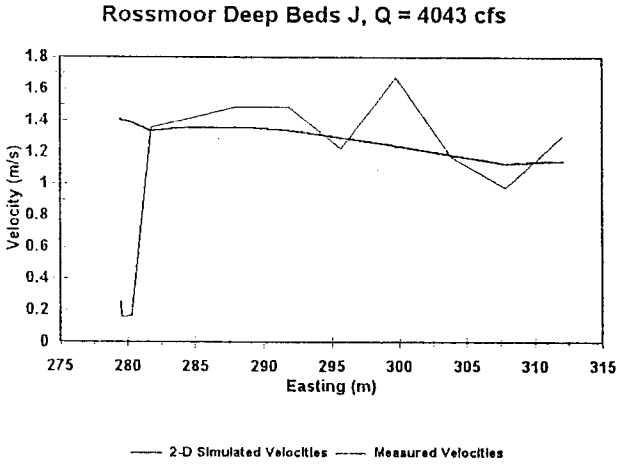
Rossmoor Deep Beds J, Q = 4043 cfs
Velocity (m/s)
0
0.2
0.4
0.6
0.8
1
1.2
1.4
1.6
1.8
275
280
285
290
295
300
305
310
315
Easting (m)
2-D Simulated Velocities
Measured Velocities

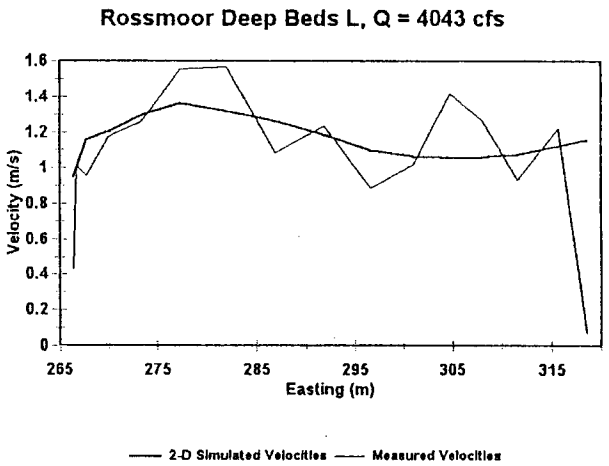
Rossmoor Deep Beds L, Q = 4043 cfs
Velocity (m/s)
0
0.2
0.4
0.6
0.8
1
1.2
1.4
1.6
265
275
285
295
305
315
Easting (m)
2-D Simulated Velocities
Measured Velocities

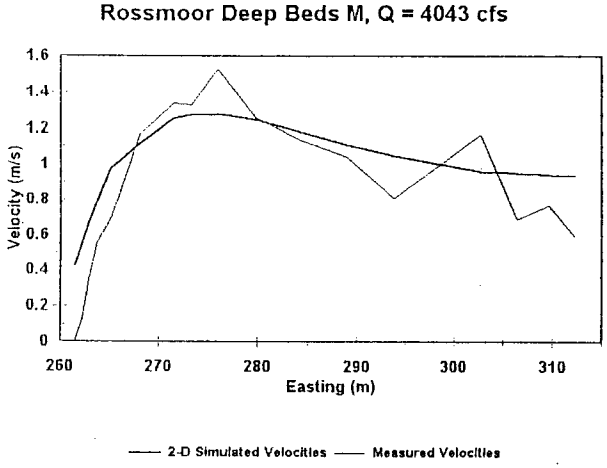
Rossmoor Deep Beds M, Q = 4043 cfs
Velocity (m/s)
1.6
1.4
1.2
1
0.8
0.6
0.4
0.2
0
260
270
280
290
300
310
Easting (m)
2-D Simulated Velocities
Measured Velocities

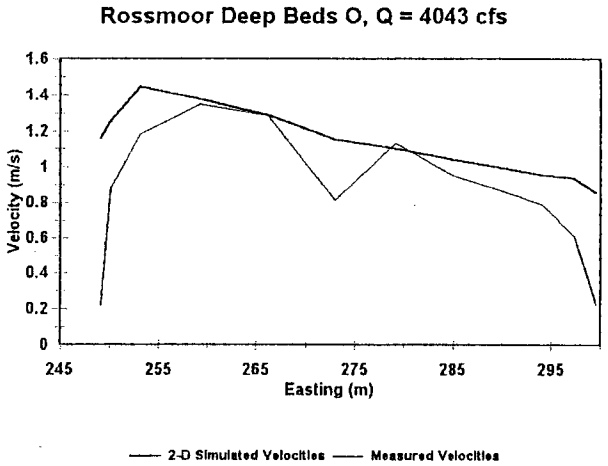
Rossmoor Deep Beds O, Q = 4043 cfs
Velocity (m/s)
1.6
1.4
1.2
1
0.8
0.6
0.4
0.2
0
245
255
265
275
285
295
Easting (m)
2-D Simulated Velocities
Measured Velocities

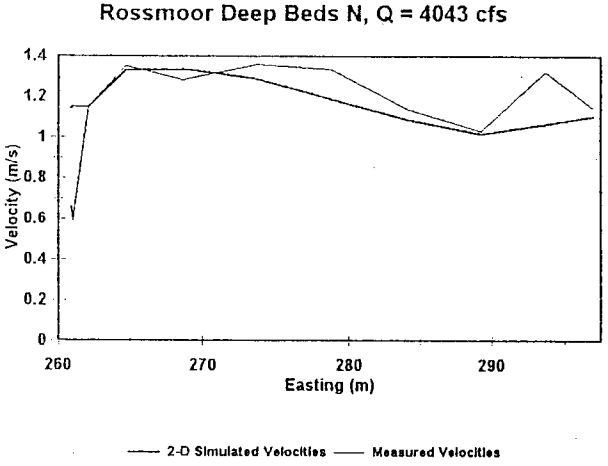
Rossmoor Deep Beds N, Q = 4043 cfs
Velocity (m/s)
1.4
1.2
1
0.8
0.6
0.4
0.2
0
260
270
280
290
Easting (m)
2-D Simulated Velocities
Measured Velocities

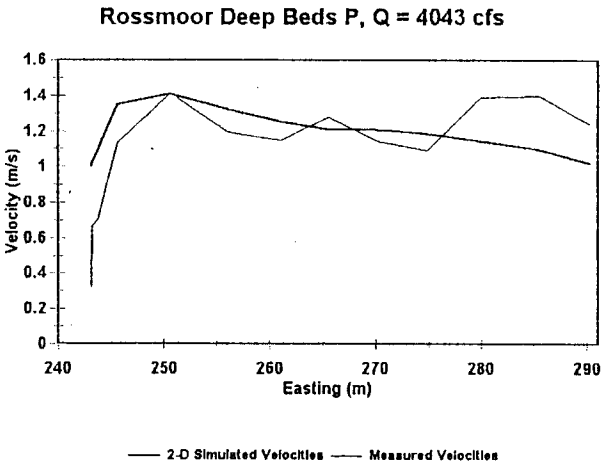
Rossmoor Deep Beds P, Q = 4043 cfs
Velocity (m/s)
1.6
1.4
1.2
1
0.8
0.6
0.4
0.2
0
240
250
260
270
280
290
Easting (m)
2-D Simulated Velocities
Measured Velocities

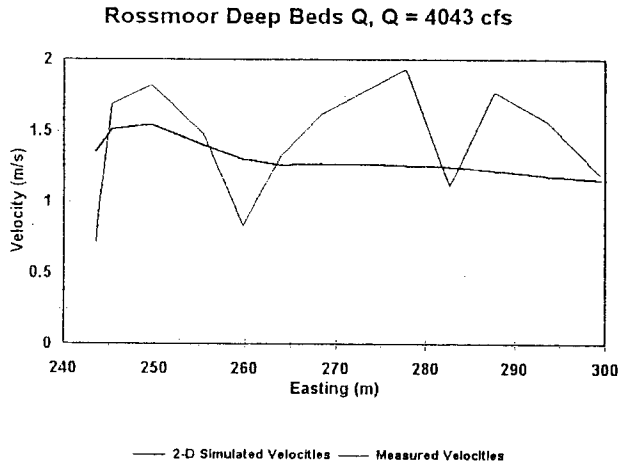
Rossmoor Deep Beds Q, Q = 4043 cfs
Velocity (m/s)
Easting (m)
2-D Simulated Velocities
Measured Velocities

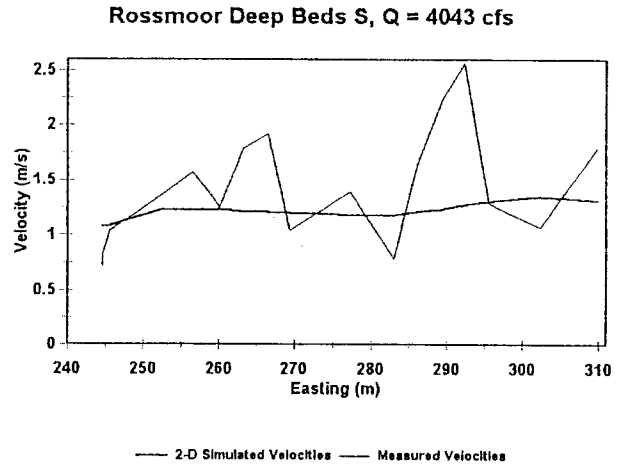
Rossmoor Deep Beds S, Q = 4043 cfs
Velocity (m/s)
Easting (m)
2-D Simulated Velocities
Measured Velocities

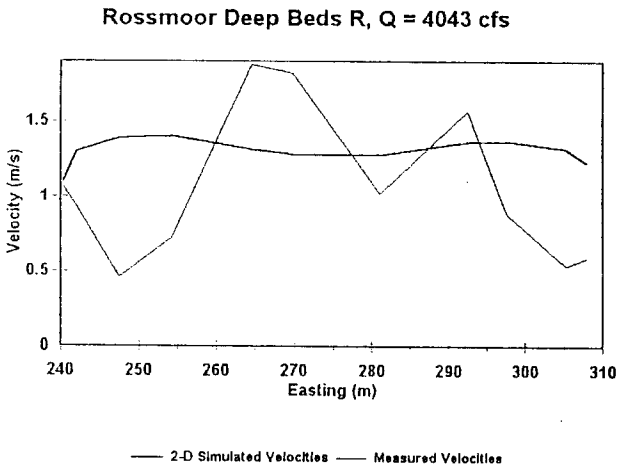
Rossmoor Deep Beds R, Q = 4043 cfs
Velocity (m/s)
Easting (m)
2-D Simulated Velocities
Measured Velocities

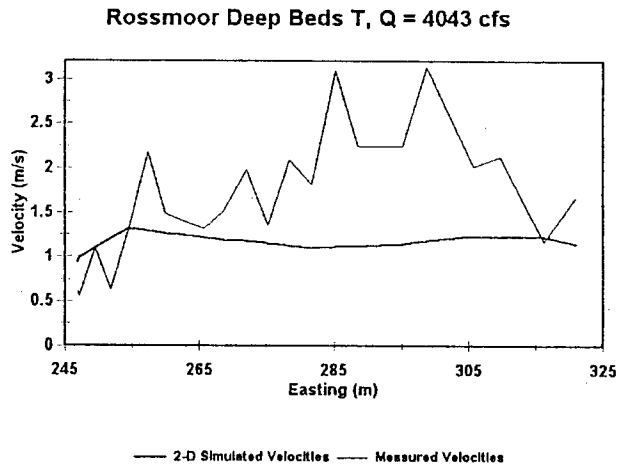
Rossmoor Deep Beds T, Q = 4043 cfs
Velocity (m/s)
Easting (m)
2-D Simulated Velocities
Measured Velocities

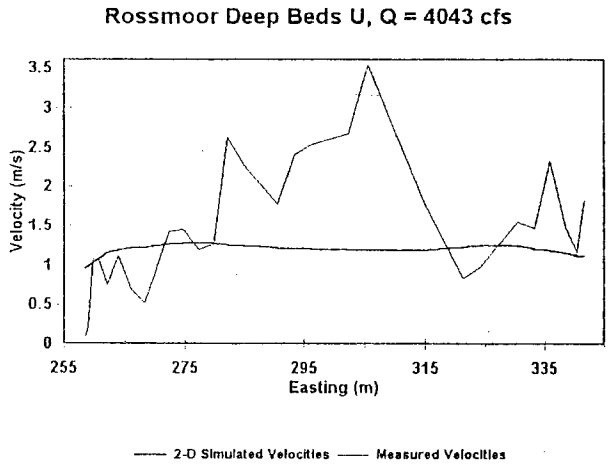
Rossmoor Deep Beds U, Q = 4043 cfs
Velocity (m/s)
3.5
3
2.5
2
1.5
1
0.5
0
255
275
295
315
335
Easting (m)
2-D Simulated Velocities
Measured Velocities

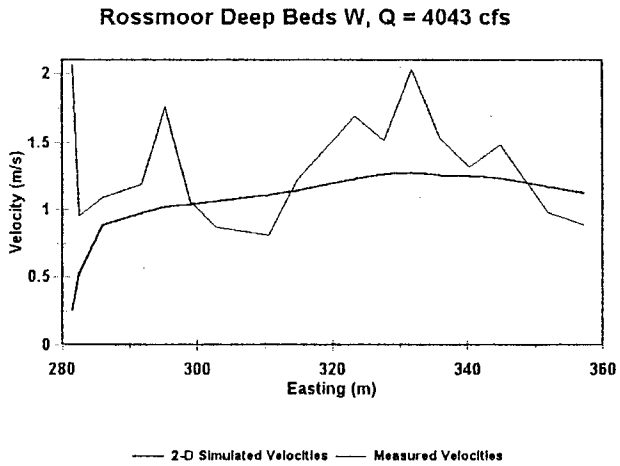
Rossmoor Deep Beds W, Q = 4043 cfs
Velocity (m/s)
2
1.5
1
0.5
0
280
300
320
340
360
Easting (m)
2-D Simulated Velocities
Measured Velocities

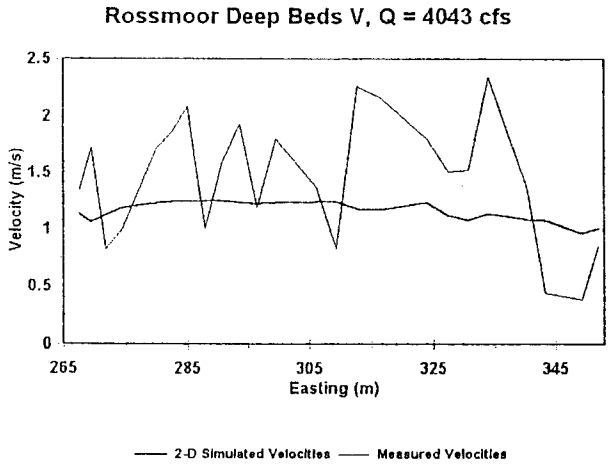
Rossmoor Deep Beds V, Q = 4043 cfs
Velocity (m/s)
2.5
2
1.5
1
0.5
0
265
285
305
325
345
Easting (m)
2-D Simulated Velocities
Measured Velocities

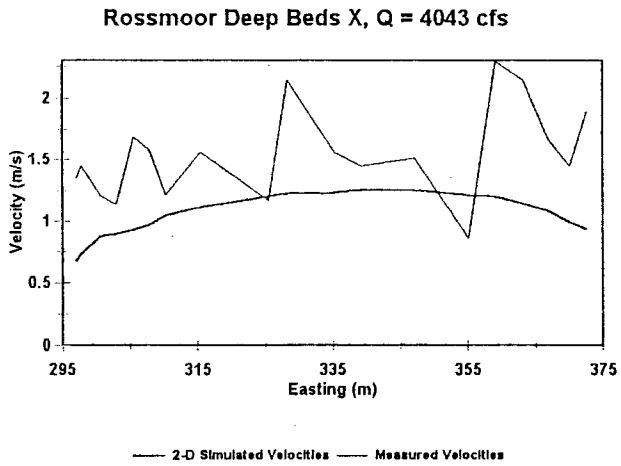
Rossmoor Deep Beds X, Q = 4043 cfs
Velocity (m/s)
2
1.5
1
0.5
0
295
315
335
355
375
Easting (m)
2-D Simulated Velocities
Measured Velocities

Rossmoor

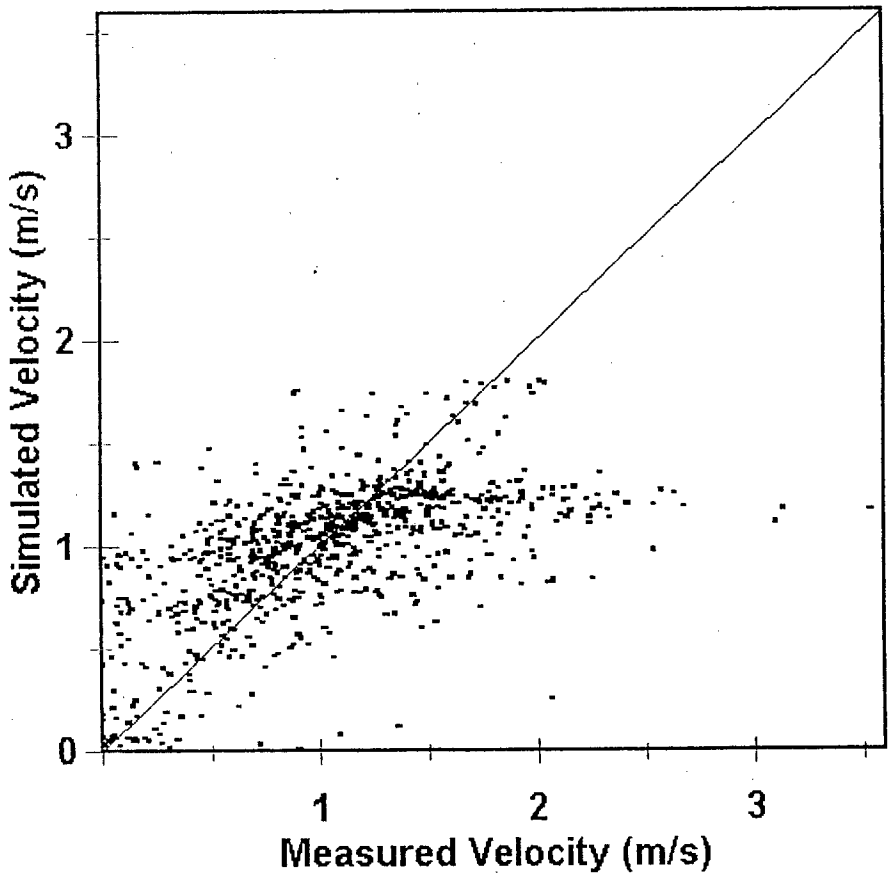

APPENDIX D
SIMULATION STATISTICS

Sailor Bar Site

Flow (cfs)	Net Q	Sol Δ	Max F
1000	0.7%	.000006	2.24
1200	5.1%	.000003	1.96
1400	3.3%	.000003	2.06
1600	1.3%	.000002	1.78
1800	0.8%	.000002	1.83
2000	0.7%	.000001	1.61
2200	0.3%	.000009	1.54
2400	1.1%	.000009	1.54
2600	0.6%	.000001	1.49
2800	0.6%	.000005	1.44
3000	0.8%	.000007	1.68
3400	4.2%	.000003	1.98
3800	0.8%	.000002	1.94
4200	0.5%	.000007	1.82
4600	1.3%	.000007	1.66
5000	0.7%	.000003	4.78
5400	3.2%	.000008	1.93
5800	0.2%	< .000001	1.57
6200	3.0%	< .000001	1.47
6600	2.3%	.000005	1.36
7000	1.7%	.000005	1.38
7400	0.7%	< .000001	1.48
7800	0.6%	< .000001	1.33
8200	0.4%	.000003	1.32
8600	0.4%	.000005	1.35
9000	0.3%	< .000001	1.32
9400	0.3%	.000009	1.26
9800	0.03%	< .000001	1.28
10400	0.02%	.000002	1.24
11000	0.001%	< .000001	1.32

Above Sunrise Site

Flow (cfs)	Net Q	Sol Δ	Max F
1000	0.3%	.000001	2.94
1200	1.3%	.000001	1.15
1400	0.9%	.000003	1.16
1600	0.3%	.000009	1.87
1800	0.1%	.000006	1.70
2000	0.04%	.000007	2.38
2200	0.03%	.000009	1.74
2400	0.5%	.000001	1.88
2600	0.08%	.000009	2.40
2800	0.01%	.000007	2.34
3000	0.2%	.000009	2.31
3400	0.3%	.000008	2.88
3800	0.2%	.000003	3.29
4200	0.2%	.000002	3.32
4600	0.04%	.000001	2.44
5000	0.06%	.000004	1.81
5400	0.1%	.000001	2.19
5800	0.07%	< .000001	1.75
6200	0.06%	< .000001	1.51
6600	0.04%	< .000001	1.47
7000	0.02%	< .000001	1.49
7400	0.01%	< .000001	1.51
7800	0.02%	< .000001	1.13
8200	0.03%	< .000001	1.15
8600	0.04%	< .000001	1.10
9000	0.06%	< .000001	0.79
9400	0.13%	.000009	0.82
9800	0.17%	.000006	0.73
10400	0.21%	< .000001	0.81
11000	0.23%	< .000001	0.93

Sunrise Site

Flow (cfs)	Net Q	Sol Δ	Max F
1000	0.9%	.000004	1.41
1200	0.99%	.000002	1.04
1400	1.0%	.000001	1.08
1600	0.9%	.000004	1.12
1800	1.2%	.000001	1.31
2000	1.0%	.000002	1.53
2200	1.1%	.000001	1.39
2400	1.8%	.000005	1.39
2600	0.9%	.000003	1.21
2800	1.0%	.000004	0.96
3000	1.2%	.000004	0.88
3400	0.9%	.000006	0.72
3800	0.9%	.000001	0.77
4200	0.95%	.000001	2.12
4600	0.9%	.000008	0.80
5000	0.9%	.000002	0.97
5400	0.98%	.000008	1.83
5800	0.97%	.000003	1.87
6200	0.6%	.000009	2.07
6600	0.7%	.000002	2.48
7000	0.7%	.000002	1.98
7400	0.8%	.000003	2.26
7800	0.7%	.000008	2.01
8200	0.7%	.000003	2.86
8600	0.8%	.000002	1.33
9000	0.9%	.000004	1.24
9400	0.9%	.000002	1.21
9800	0.9%	.000004	1.14
10400	0.9%	.000002	1.45
11000	0.9%	.000003	1.42

El Manto Site

Flow (cfs)	Net Q	Sol Δ	Max F
1000	0.7%	.000003	0.56
1200	0.4%	.000006	0.75
1400	0.3%	.000006	0.78
1600	0.3%	<.000001	0.71
1800	0.3%	.000003	0.67
2000	0.4%	.000010	0.63
2200	0.3%	.000003	0.72
2400	0.3%	.000003	0.69
2600	0.3%	.000003	0.68
2800	0.2%	.000003	0.68
3000	0.1%	.000004	0.67
3400	0.1%	.000003	0.71
3800	0.2%	.000002	0.75
4200	0.3%	.000004	0.74
4600	0.3%	.000002	0.69
5000	0.3%	<.000001	0.69
5400	0.3%	<.000001	0.69
5800	0.3%	.000017	0.69
6200	0.4%	.000004	0.75
6600	0.4%	.000003	0.75
7000	0.5%	.000002	0.74
7400	0.5%	.000001	0.74
7800	0.5%	.000001	0.74
8200	0.5%	.000001	0.74
8600	0.5%	< .000001	0.74
9000	0.5%	< .000001	0.74
9400	0.6%	< .000001	0.74
9800	0.6%	< .000001	0.74
10400	0.7%	< .000001	0.74
11000	0.7%	< .000001	0.74

Rossmoor Site

Flow (cfs)	Net Q	Sol Δ	Max F
1000	0.6%	.000007	1.19
1200	0.8%	.000002	1.68
1400	0.96%	.000006	1.76
1600	1.1%	.000007	1.06
1800	0.9%	.000005	0.74
2000	0.6%	.000004	0.71
2200	0.5%	< .000001	1.31
2400	0.6%	.000004	1.42
2600	0.5%	.000001	1.37
2800	0.6%	.000003	1.23
3000	0.6%	.000004	1.27
3400	0.5%	.000002	1.03
3800	0.5%	.000003	1.13
4200	0.5%	.000002	1.34
4600	0.4%	.000002	1.30
5000	0.4%	.000001	1.63
5400	0.3%	.000005	3.25
5800	0.2%	.000002	3.62
6200	0.03%	< .000001	4.40
6600	0.1%	< .000001	2.56
7000	0.3%	.000001	1.14
7400	0.4%	< .000001	0.93
7800	0.6%	< .000001	0.87
8200	0.8%	< .000001	0.86
8600	1.0%	.000007	1.36
9000	1.1%	< .000001	1.50
9400	1.3%	< .000001	1.53
9800	1.5%	< .000001	1.58
10400	1.6%	.000002	1.23
11000	1.7%	< .000001	1.00

APPENDIX E
HABITAT MODELING RESULTS

Fall-run chinook salmon spawning WUA (ft^2)

Flow (cfs)	Sailor Bar	Above Sunrise	Sunrise	El Manto	Rossmoor
1000	56543	99501	218840	36533	349944
1200	64971	108102	239302	33885	370772
1400	73636	116164	251831	31786	379631
1600	81752	123978	260959	30397	374873
1800	88888	129780	267945	29310	361881
2000	96660	133547	277977	28546	344799
2200	101794	135991	289311	28008	326802
2400	102913	138596	290280	27437	307179
2600	101353	139790	284026	26824	288956
2800	101223	140070	273542	25995	269721
3000	103096	140329	261551	24897	250109
3400	105863	139263	263650	22087	214309
3800	106455	135603	234448	19214	177184
4200	106627	129392	209454	16436	145474
4600	101611	123731	184654	14703	117703
5000	105271	116508	163901	13444	95788
5400	105529	110502	148972	12529	78361
5800	106013	103527	142158	11829	67597
6200	102203	96401	131491	11291	54519
6600	97478	90858	125754	10947	44724
7000	93581	87672	118725	10775	36145
7400	86617	83635	114065	10624	29245
7800	81956	80664	107962	10549	23928
8200	77478	76929	104216	10484	19902
8600	74034	73291	97650	10409	17125
9000	70611	70837	92203	10258	14940
9400	69868	68254	87779	10161	13067
9800	71838	65939	86089	10129	11937
10400	65466	62624	76316	9827	10947
11000	63227	59836	68437	9623	9849

Steelhead trout spawning WUA (ft^2)

Flow (cfs)	Sailor Bar	Above Sunrise	Sunrise	El Manto	Rossmoor
1000	38545	61160	91956	13272	99598
1200	42130	62506	90266	13498	106745
1400	45262	64002	91342	13110	109318
1600	48297	64895	92343	12260	109253
1800	49159	65724	94668	11151	110362
2000	49438	66510	97790	10366	110330
2200	49578	66413	99663	9903	109565
2400	50310	65347	100481	9548	107854
2600	50762	63797	102407	9042	105346
2800	50870	62861	103688	8568	102031
3000	51667	62129	104840	8202	98145
3400	54476	61236	107865	7556	90104
3800	55466	59169	106885	6997	79653
4200	54885	56693	104517	6200	70234
4600	52452	54906	99878	5791	61569
5000	55412	53163	94582	5360	54874
5400	54724	50978	90255	4865	48513
5800	52442	48965	84281	4564	44821
6200	53798	46877	77091	4284	39396
6600	51957	45090	72032	4069	34369
7000	50256	43023	66370	3875	29708
7400	48642	41538	59600	3746	25274
7800	47630	40138	54465	3660	21162
8200	46855	38718	49804	3531	17933
8600	45929	37544	45908	3401	15371
9000	44896	36231	43680	3326	13186
9400	44810	35198	40817	3401	11205
9800	36102	34455	39310	3358	10032
10400	33594	33809	35510	3251	7911
11000	32528	33346	33626	3154	6631

Sailor Bar, chinook salmon spawning

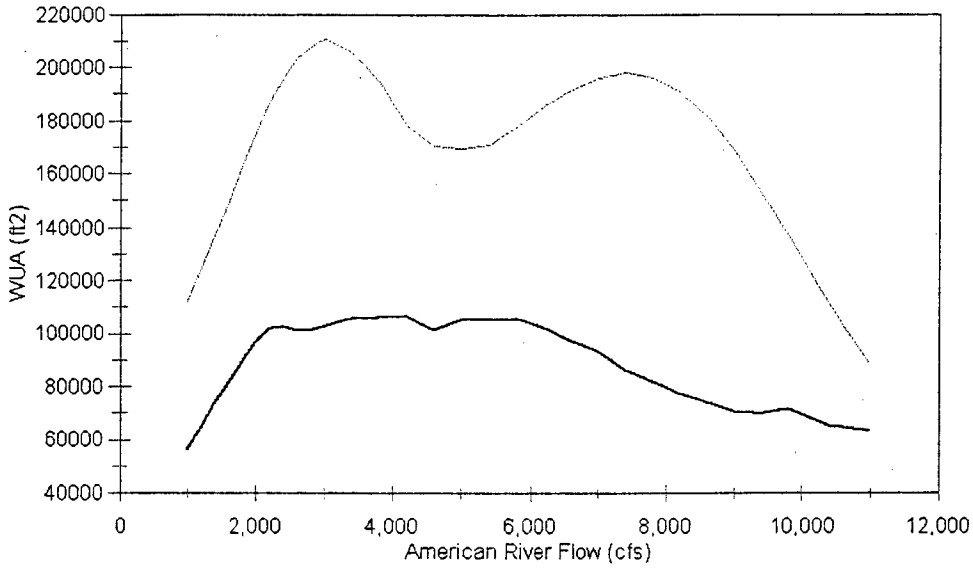

Sailor Bar, Steelhead spawning

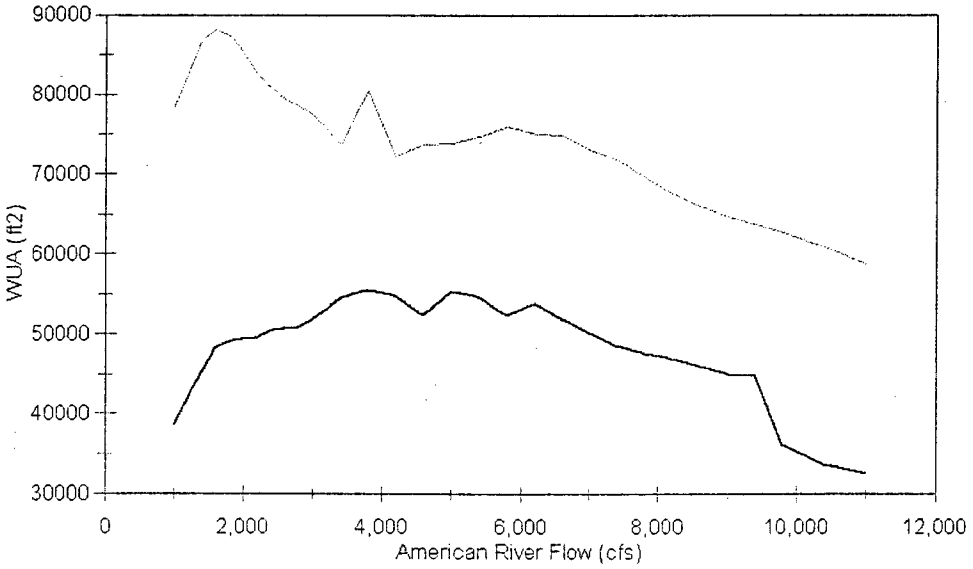

Above Sunrise, chinook salmon spawning

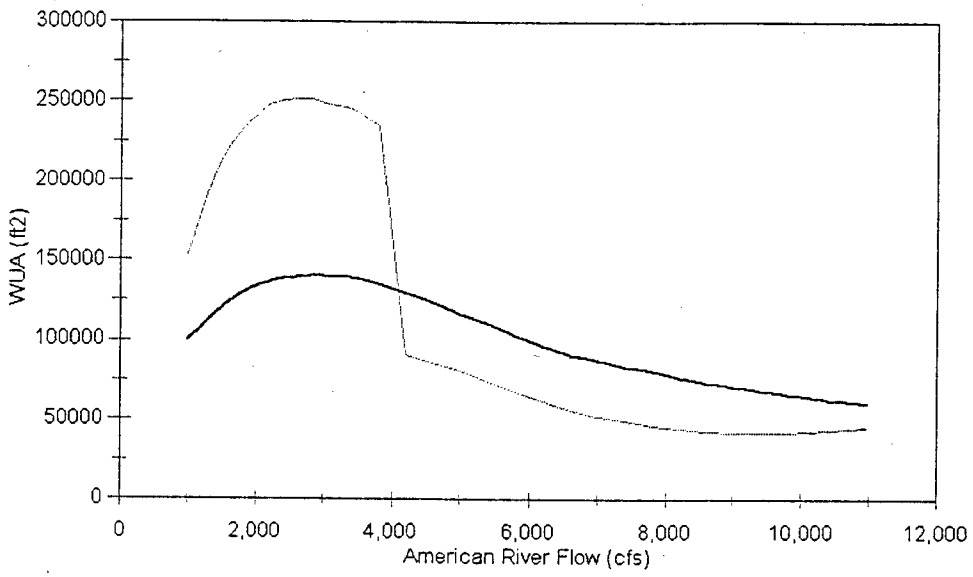

Above Sunrise, Steelhead spawning

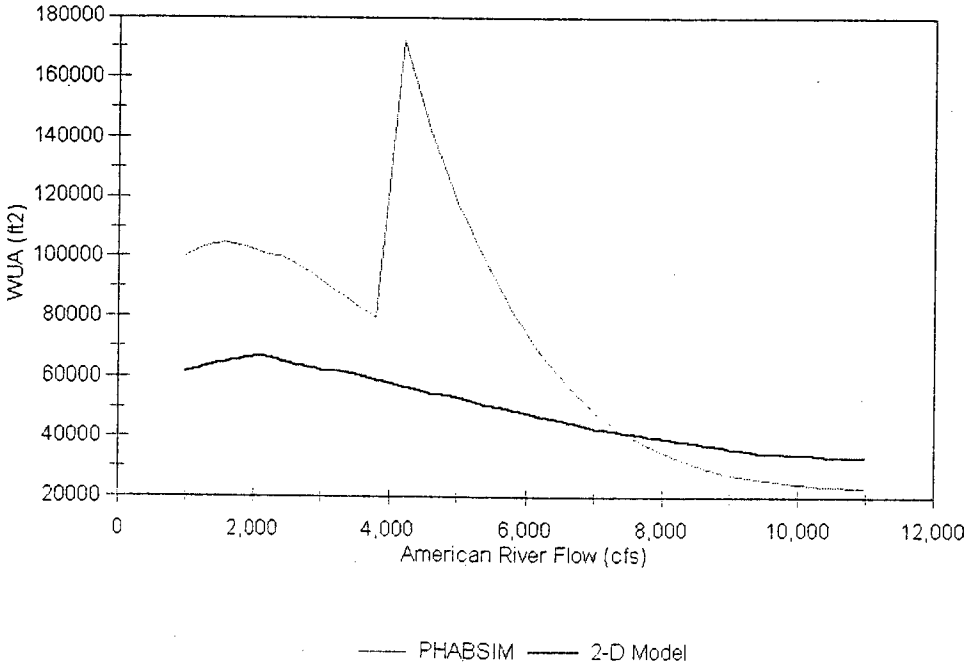

Sunrise, chinook salmon spawning

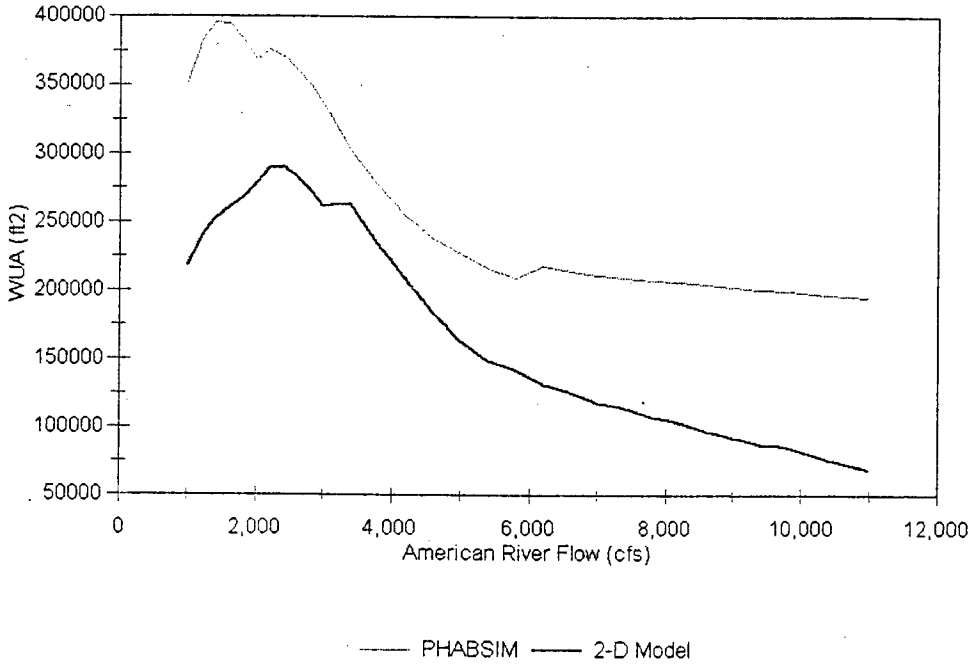

Sunrise, Steelhead spawning

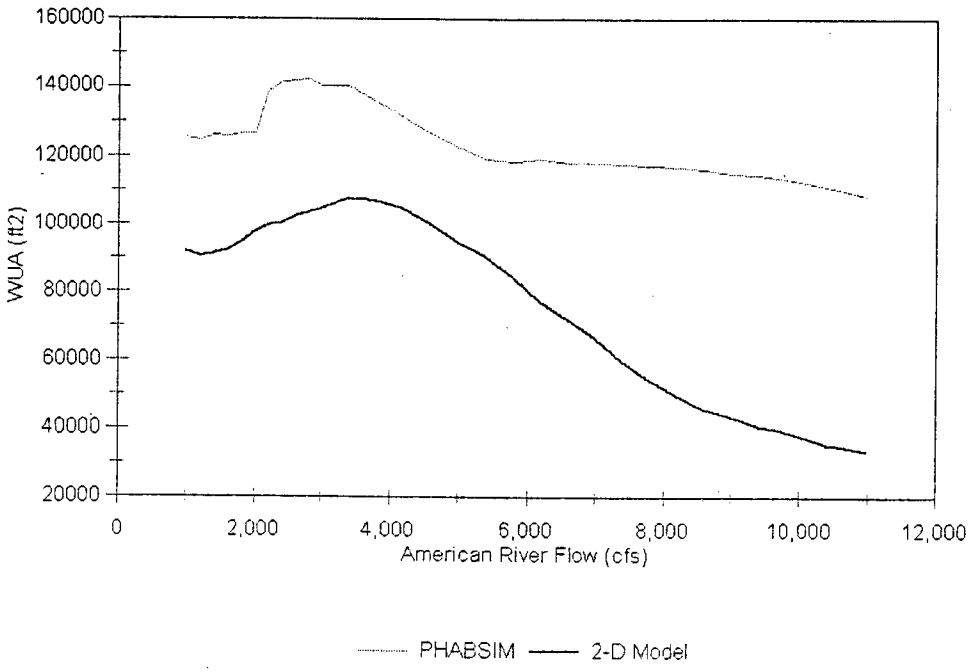

El Manto, Chinook Salmon spawning

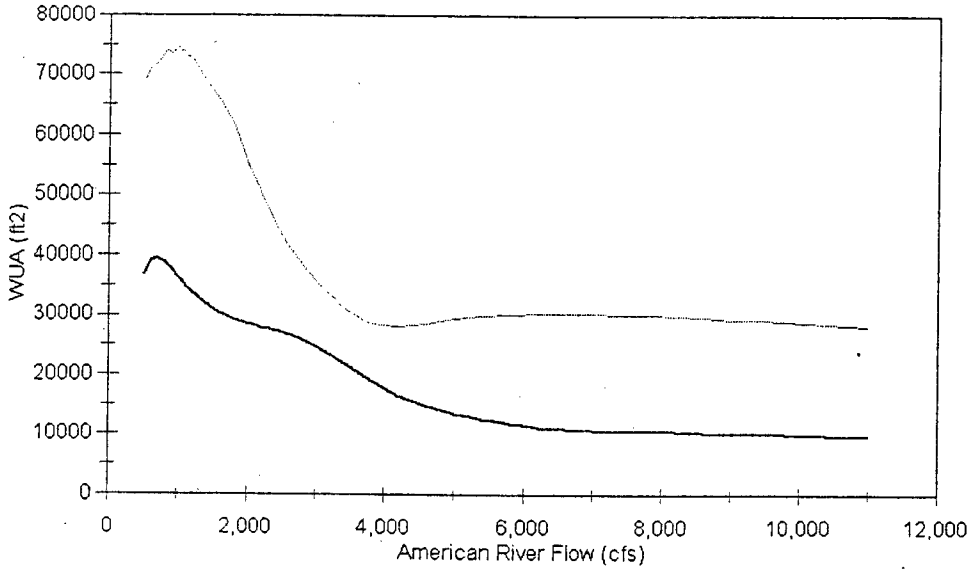

PHABSIM —— 2-D Model

El Manto, Steelhead spawning

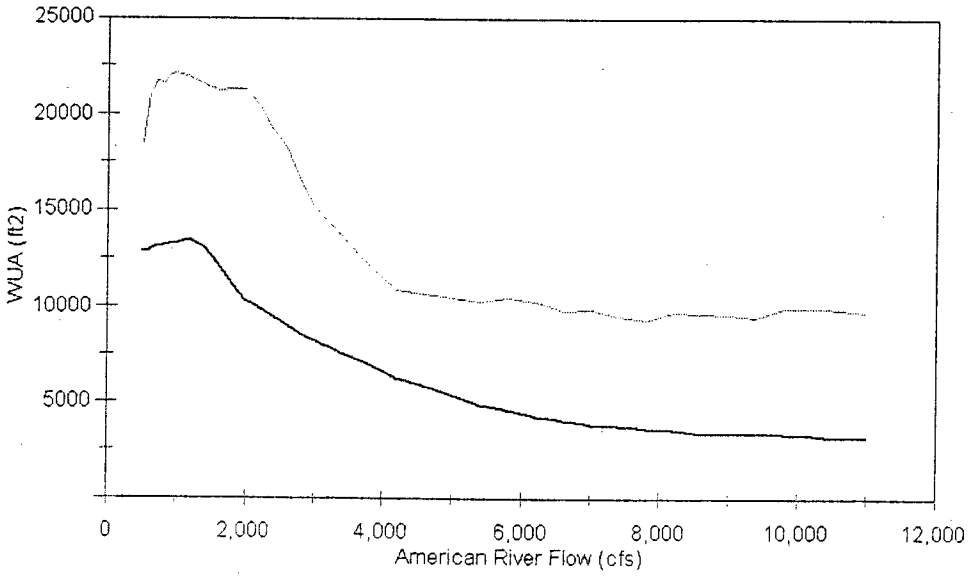

PHABSIM —— 2-D Model

Rossmoor, chinook salmon spawning

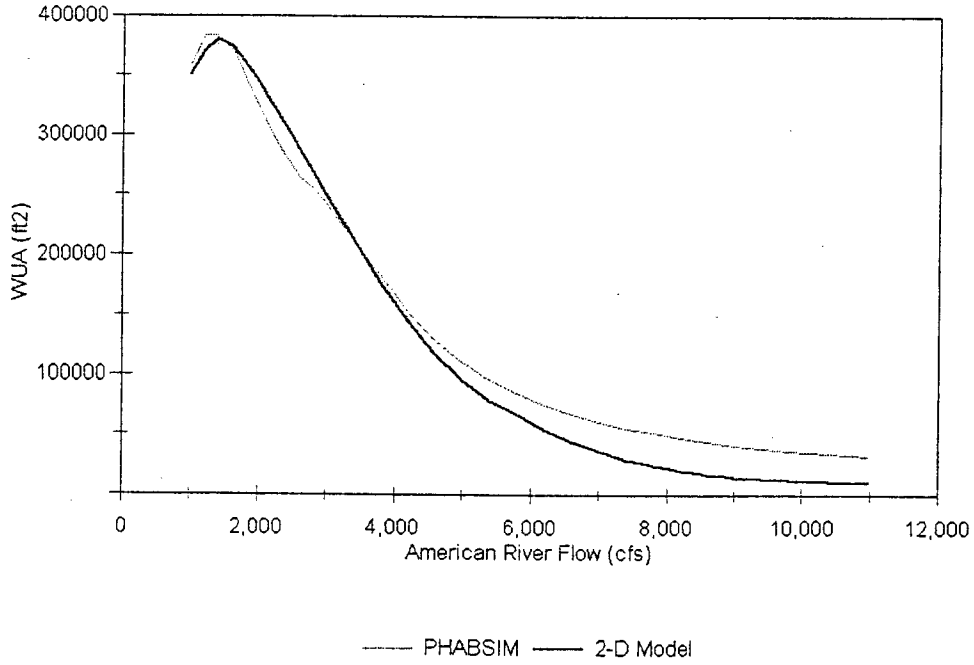

Rossmoor, Steelhead spawning

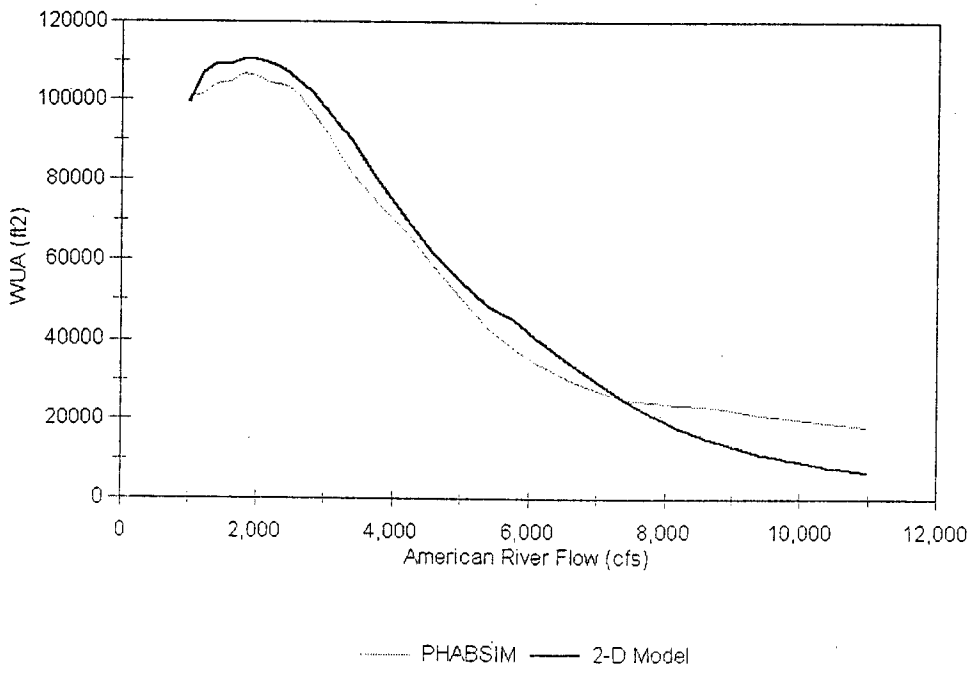

APPENDIX F
RIVER2D COMBINED SUITABILITY OF REDD LOCATIONS

SAILOR BAR STUDY SITE

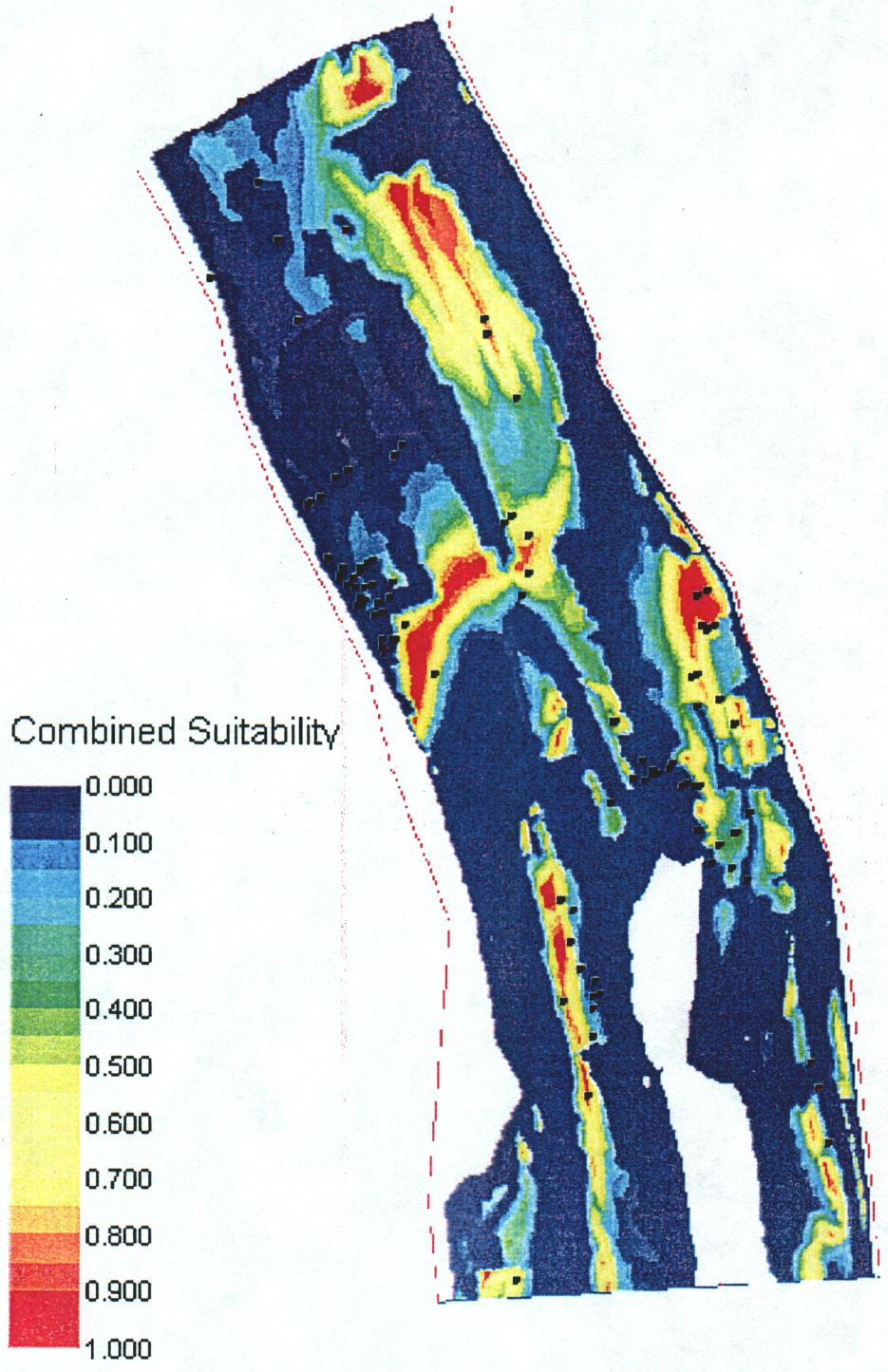

Redd locations: ●

ABOVE SUNRISE STUDY SITE

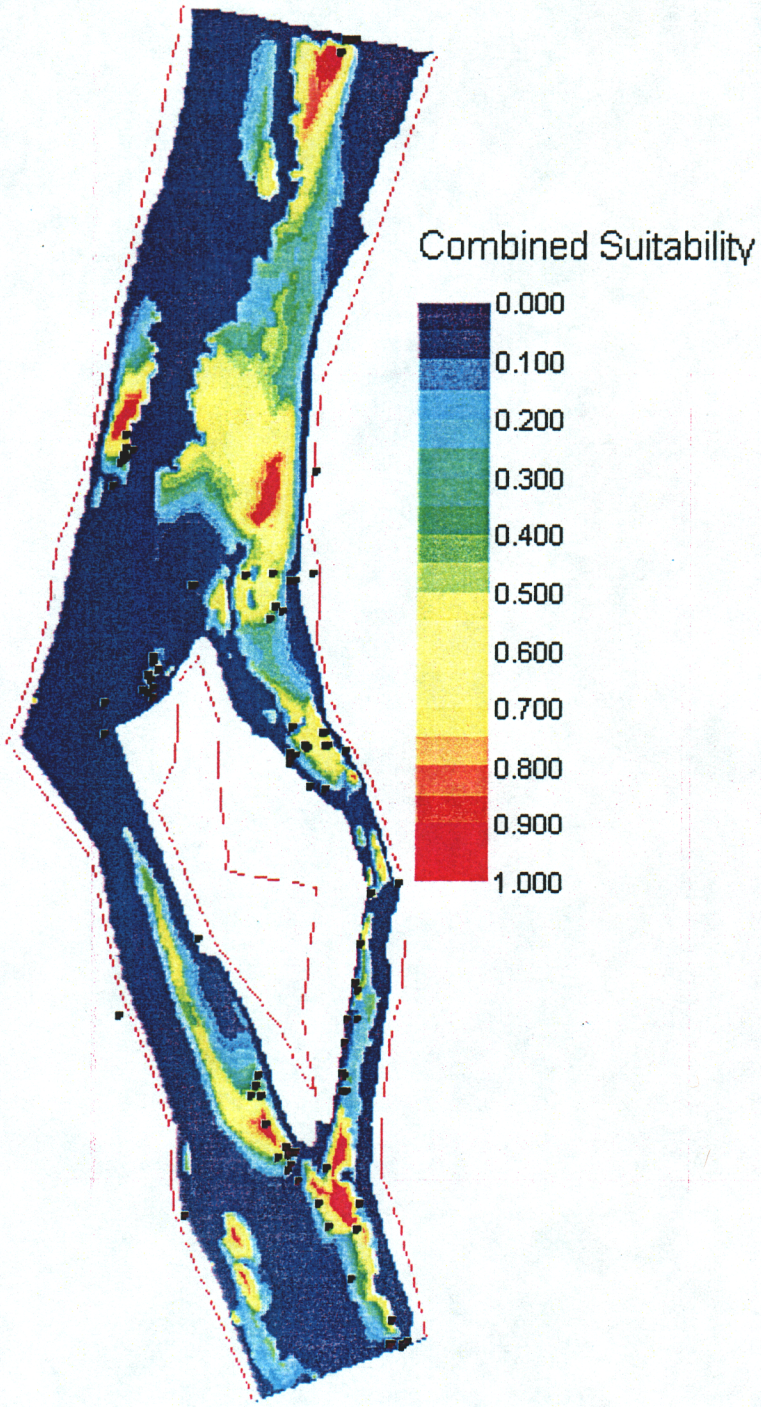

Redd locations: ●